2017

Characterization of Quorum-Quenching Lactonases and Plp-Dependent Aminotransferases: Structure, Mechanism and Alternative Turnover

Romila Nina Mascarenhas
Loyola University Chicago

LOYOLA UNIVERSITY CHICAGO

CHARACTERIZATION OF QUORUM-QUENCHING LACTONASES AND PLP-DEPENDENT AMINOTRANSFERASES: STRUCTURE, MECHANISM AND ALTERNATIVE TURNOVER

A DISSERTATION SUBMITTED TO

THE FACULTY OF THE GRADUATE SCHOOL

IN CANDIDACY FOR THE DEGREE OF

DOCTOR OF PHILOSOPHY

PROGRAM IN CHEMISTRY AND BIOCHEMISTRY

BY

ROMILA NINA MASCARENHAS

CHICAGO, IL

AUGUST 2017

ACKNOWDLEDGMENTS

I would like to thank my advisor, Dr. Dali Liu, for his guidance and support in research. He has always made time to teach me techniques, discuss project ideas and provide life lessons. I could not have asked for a more patient and adaptable mentor.

I would also like to thank Dr. Miguel Ballicora, Dr. Walter Fast, Dr. Richard Silverman and Dr. Daniel Becker for their collaborations on a large part of this dissertation. Their expertise allowed me to explore new techniques and take a diverse approach when solving a scientific question. At different points in graduate work, I have consulted with them and received valuable advice on experimental design and data interpretation. Additionally, working with their graduate students and post doc's has been a valuable learning experience. Some of the data in this thesis was collected in collaboration with Dr. Hoang Le, Dr. Pei Thomas, Dr. Ken Clevenger, and Cory Reidl. I would also like to thank my dissertation committee members for their valuable feedback during graduate school.

Doing research in the Liu lab was certainly a fun experience thanks to Yuanzhang Zheng, Daniel Catlin and all the undergraduate members. I'd also like to thank the faculty and staff of the Chemistry department for making graduate school at Loyola a pleasant experience.

On a more personal note I am indebted to a long list of family and friends, and particularly to Leela Desouza Bransten, in helping with my application to graduate school, transition into Chicago, and for the constant encouragement and guidance. Lastly, I'd like to thank my parents

Francis and Angella, and my siblings Rohit and Rohini for their unconditional love, support and prayers, which have enabled me to complete this dissertation.

TABLE OF CONTENTS

LIST OF FIGURES

LIST OF TABLES

SCHEMES

ABBREVIATIONS

Abbreviation	
AHL	*N*-acyl-L-homoserine lactone
AidC	autoinducer degrading gene isolated from a *Chryseobacterium* sp
AiiA	autoinducer inactivator A from *Bacillus* sp
AiiB	autoinducer inactivator B from *Agrobacterium tumefaciens*
Asp-AT	Aspartate aminotransferase
DEAE	Diethylethanolamine
DNA	Deoxyribonucleic acid
FCP	(1R,3S,4S)-3amino-4-fluorocyclopentane-1-carboxylic acid
FPLC	Fast protein liquid chromatography
GABA-AT	4-aminobutyrate transaminase
GABA	γ-Aminobutyric acid
GBL	γ-Butyrolactone
HSL	homoserine lactone
MBP	Maltose binding protein
OAT	Ornithine aminotransferase
PEG	Polyethylene glycol
PLP	Pyridoxal-5'-phosphate

PMP	Pyridoxamine phosphate
SEC MALS	Size exclusion chromatography multi angle light scattering
SDSPAGE	Sodium dodecyl sulfate polyacrylamide gel electrophoresis
TEV	Tobacco etch virus

ABSTRACT

Cell-to-cell communication by bacteria is essential for the regulation of gene expression important in colonization, biofilm formation, virulence and other processes. This communication is called "quorum-sensing" and is mediated by small molecules called autoinducers. One major class of autoinducers used by gram-negative bacteria is *N*-acyl homoserine lactones (AHL's). Enzymes capable of disrupting this communication are called "quorum-quenching" catalysts and have proven to be invaluable biochemical tools for understanding quorum-sensing pathways. Quorum-quenching enzymes hold promise for application in anti-biofouling, agriculture, aquaculture, bioremediation and other synthetic biology settings. However, the mechanisms that these enzymes use to recognize and process their substrates are not well characterized. A better understanding of selectivity and catalysis would enable the production of variant enzymes to recognize specific quorum-sensing signals to serve as catalysts for various applications.

Aminotransferases are a class of pyridoxal-5'-phosphate (PLP)-dependent enzymes that catalyze a myriad of biochemical reactions involved in several metabolic processes. The importance of these enzymes is further underscored because some of them have been identified as drug targets. For example, inhibition of γ-aminobutyric acid aminotransferase (GABA-AT) was proven effective in the treatment of many neurological disorders, and inhibition of ornithine aminotransferase (OAT) was shown to suppress the growth of hepatocellular carcinoma (HCC). Potent mechanism-based inactivators can be rationally designed against these PLP-dependent drug targets, but one of the remaining challenges is the lack of selectivity against other PLP-

dependent off-target enzymes such as aspartate aminotransferase. A better understanding of enzyme selectivity and mechanism would enable the design of molecules capable of displaying desirable specificity of inactivation discerning drug-targets and off-targets.

The goal of this dissertation is to provide better understanding of selectivity and catalysis in quorum-quenching enzymes, and selectivity and mechanisms of PLP-dependent aminotransferases. The structural and biochemical characterization of AidC, an *N*-acyl homoserine lactone lactonase, was carried out using X-ray crystallography and other biochemical techniques. The selectivity of a mechanism-based inactivator was tested in a PLP-dependent aminotransferase drug-target (OAT) and off-target (Asp-AT) using X-ray crystallography and enzyme assays. The proposed mechanism was confirmed by high-resolution mass spectrometry.

CHAPTER ONE

INTRODUCTION

Structural and Biochemical Characterization of AidC

Quorum-sensing

Cell-to-cell communication by bacteria is essential for coordinating the regulation of numerous genes important in colonization, biofilm formation, virulence, survival in competitive environments, and other processes. Such communication is called 'quorum-sensing'. Quorum sensing bacteria regulate gene expression using chemical signal molecules called autoinducers (AI). These autoinducers are produced within the cell and can diffuse across the cell membrane. Once the concentration outside the cell has reached a threshold, they bind cytoplasmic receptors and regulate gene expression in the QS regulon.[1,2]

The first described quorum-sensing system is that of bioluminescent gram-negative bacterium *Vibrio fischeri*[3]. Expression of the luciferase operon (*luxICDABE*) is controlled by two proteins, LuxI and LuxR. LuxI is the autoinducer synthase, which produces the acyl-homoserine lactone (AHL) and LuxR is the cytoplasmic autoinducer receptor/DNA-binding transcription activator.[4] A large number of other gram-negative bacteria possess LuxIR-type proteins and communicate with AHL signals[5] (Figure 1). These systems are used predominately for intraspecies communication and extreme specificity is known to exist between the LuxR proteins and their AHL signals.

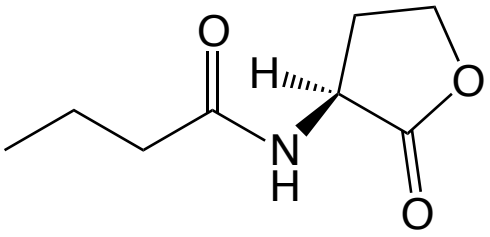

Figure 1. C4-*N*-acyl-L-homoserine lactone (AHL)

Gram-positive bacteria communicate using modified oligopeptides as signals and membrane-bound sensor histidine kinases as receptors[1]. Each gram-positive bacterium uses a signal different from other bacterium and has receptors that are extremely specific. Thus, like in gram-negative LuxIR systems, these peptide quorum-sensing systems are understood to be involved in intraspecies communication.

Quorum-quenching

The role of quorum-sensing in bacteria appears to be control of gene expression. In environments where bacteria compete for limited resources, the ability to disrupt this quorum-sensing may give some bacteria an advantage over another bacterial species that relies on quorum-sensing. Or, a host's ability to interfere with bacterial quorum-sensing may be crucial to prevent virulence caused by colonization of the pathogen[1]. Therefore, it is not surprising that mechanisms have evolved that have the ability to disrupt this bacterial cell-to-cell communication, called quorum-quenching. Enzymes capable of blocking these signaling pathways are referred to as quorum-quenching enzymes or quorum-quenching catalysts. Several quorum-quenching strategies have been identified in nature, and one of them includes the use of AHL degrading enzymes.

Quorum-quenching enzymes

Based on the chemical structure of AHLs, reports suggests that four different ways of degrading an AHL may occur by lactonase, decarboxylase, acylase and deaminase[6]. Of these only two types of quorum-quenching enzymes have been reported, namely lactonase and acylase[7]. The AHL lactonases, are very specific in recognizing the lactone ring and catalyzing a ring-opening reaction by hydrolyzing the lactones to their corresponding γ-hydroxy acid, a product that can no longer be used for signaling[8,9]. AHL acylases are very specific for the N–acyl substituent and catalyze amide hydrolysis[10]. These reactions are shown in Scheme 1. The research work in this dissertation will focus only on AHL lactonases.

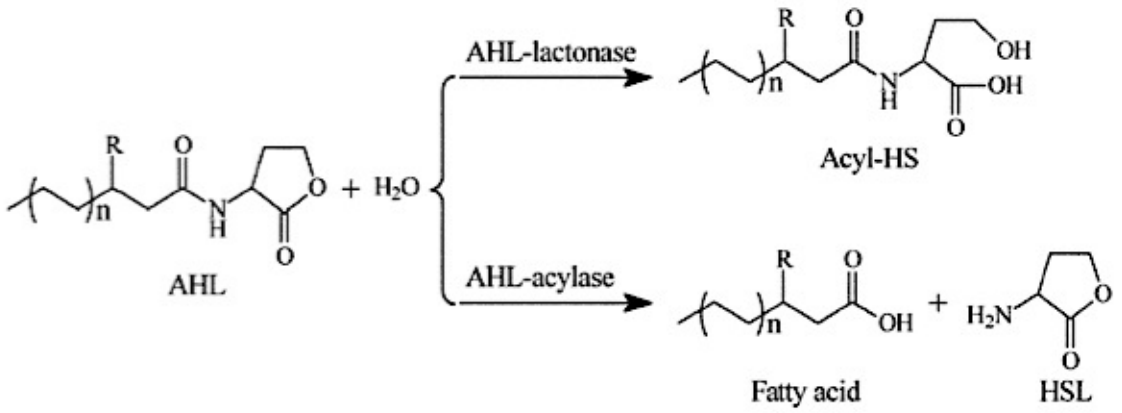

Scheme1: General reaction scheme for the conversion of N-acylhomoserine lactones by an acylase or lactonase to their corresponding homoserine lactone and γ-hydroxy acid respectively.

_N_-Acyl-L-homoserine lactone (AHL) Lactonases

The first reported quorum-quenching enzyme was AiiA (autoinducer inactivating protein A) from a *Bacillus sp.* strain 240B1 and is an AHL hydrolase[9]. The amino acid sequence shows a conserved sequence motif of HXHXDH H, similar to the metal binding motif in the metallo-β-lactamase superfamily of proteins[9]. Initial reports suggested that AHL lactonases were metal independent[11]; however, subsequent work proved AiiA contains two equivalents of tightly-bound zinc ions that are found in a dinuclear zinc cluster at the active site, and the metal ions play an essential role in catalysis[12,13]. A series of papers have been published, using product-bound structures, molecular modeling and site-directed mutagenesis which support the role of each zinc ion that is consistent with the rest of the super family[14,15].

Substrate specificity in AiiA

AiiA is specific for the ring structure in N-acyl-HSLs, but can process various lengths and substitutions on the acyl chain[11,12]. Figure 2 represents a list of substrates that can be processed by AiiA.

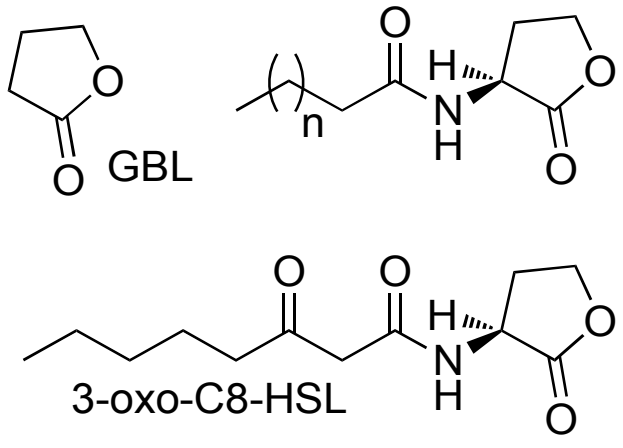

AHL	n
C4-HSL	1
C5-HSL	2
C6-HSL	3
C7-HSL	4
C8-HSL	5
C10-HSL	7
C12-HSL	9

Figure 2. AiiA substrates

AiiA is not very selective for the length or substitution of AHL's, although longer alkyl chains ($n \geq 4$) are preferred[11,15]. The promiscuity of AiiA is proposed to be derived from the wide, shallow, hydrophobic groove in which the N-acyl substituent of the product is observed to bind[14,15] (Figure 3). Initially, AiiA did not appear to have any substrate-binding loops that facilitate ligand binding. However, the structure of an AiiA mutant (F107W) bound to a ring-opened product of a longer AHL substrate[16] (C10-HSL) shows, the hydrophobic N-acyl substituent does not bind to the same groove as the shorter C6-HSL product, but rather extends through a different channel that is formed by closure of a loop that was previously disordered[17], making a 'phenylalanine-clamp' that is proposed to hold longer ligands. (Figure3)

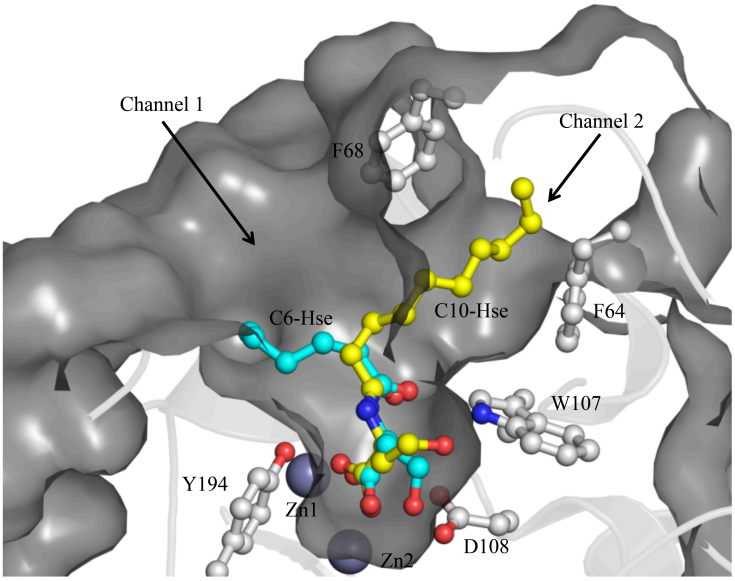

Figure 3. Substrate binding pocket in AiiA. Channel 1 represents the wide, shallow groove used by AiiA to process shorter acyl tails (from PDB:3DHB). Channel 2 represents the alternate binding site for the N-alkyl substituent in a phenylalanine-clamp (from PDB:4J5H)

A proposed catalytic mechanism of AiiA

Based on structural and functional studies, a catalytic mechanism has been proposed for AiiA (Figure 4).[14,15] The crystal structures of AiiA (Figure 4: I)[13] and AiiA bound to product (Figure 4:V)[14,15] represent two states in the catalytic cycle. One unusual feature of the proposed mechanism is the use of Zn2 as a superacid to stabilize the anionic charge that develops on the leaving group oxygen (Figure 4: IV). In AiiA studies using different metalloforms, a strong thio-effect is reported on K_{cat} when thiolactones are used as substrates[18]. This finding supports a kinetically significant interaction of the leaving group, which is consistent with the intermediate IV in Figure 4. Structural data supports three states of the enzyme represented as I, IV and V in the proposed mechanism in Figure 4.

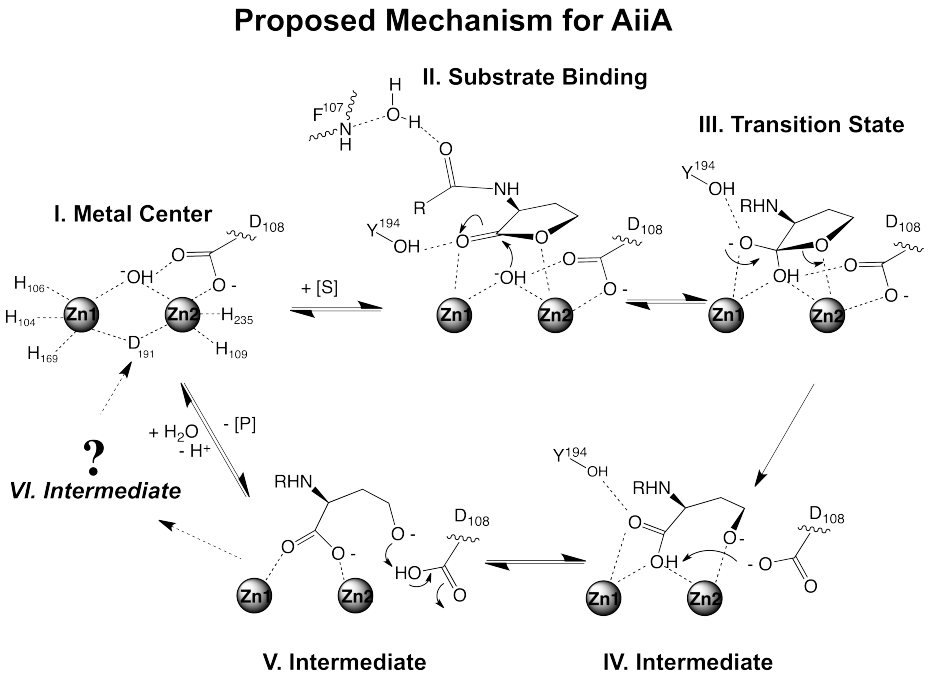

Figure 4. Proposed catalytic mechanism of dizinc AiiA. Structural data supports the species represented in I, IV and V.

AidC a quorum-quencing AHL lactonase from *Chryseobacterium sp.*

Recently, AidC was reported as a quorum-quenching enzyme because of its ability to catalyzes the hydrolytic ring opening of multiple *N*-acyl homoserine lactone (AHL) substrates[19]. Analysis of protein sequence alignments revealed that AidC is homologous to other AHL lactonases found in the metallo-hydrolase / oxidoreductase superfamily, and shares a conserved dinuclear metal binding motif. The most striking feature of AidC is its reported K_M values. All previously characterized wild-type AHL lactonases have K_M values $\geq$ 1.4 mM[14-16], with the exception of MomL (440 μM; *Muricauda olearia* marine AHL lactonase).[17] In contrast, the reported K_M values for AidC are approximately $\geq$ 24-fold lower: 46 - 72 μM[19]. The lower K_M values of AidC are of interest since a better understanding of how quorum-quenching enzymes recognize and process their substrates can enable their appropriate selection and optimization as biochemical tools and help in the proposed development of this class of enzymes as therapeutic, anti-infective, and anti-biofouling proteins.[3-7]

Limitations of quorum-quenching lactonases and objectives for this dissertation

The current quorum-quenching lactonases are not well understood. Their broad substrate specificity limits their potential applications, and their impact on survival in competitive environments is not well understood. A better understanding of the basis of selectivity and catalysis would enable the production of variant enzymes tuned to recognize specific quorum-sensing signals to serve as more precise biochemical probes, and as catalysts for other applications. The work in my dissertation directly addresses gaps in our knowledge of quorum-quenching AHL lactonases.

In the first part of this thesis I have worked on the structural and biochemical characterization of AidC. Structural studies reveal a novel structure of AidC, and a complex structure of AidC bound to its product. Steady-state kinetic experiments provide information about substrate specificity and show AidC is the most efficient quorum-quenching enzyme characterized to date. Implications on the catalytic mechanism of quorum-quenching enzymes are discussed.

Selective targeting by a mechanism-based inactivator against PLP-dependent aminotransferases

Aminotransferases

Pyridoxal-5'-phosphate (PLP), the active form of vitamin B_6, is an important coenzyme in many enzymatic reactions[20]. Aminotransferases are a class of PLP-dependent enzymes that catalyze myriad biochemical reactions involving amino acid metabolism, amino acid-derived metabolites, and the biosynthesis of amine-containing compounds. Aminotransferases catalyze the reversible transfer of an amino group from a substrate to an α-keto acid acceptor[21]. All aminotransferases undergo a similar catalytic mechanism, in which two coupled half-reactions are required for one transamination cycle. This is commonly referred to as a "ping-pong" mechanism. Both reactions are often catalyzed by a basic lysine residue and involve the tautomerization of an aldimine formed between the substrate and PLP. In the first half-reaction, the cofactor PLP accepts the amino group from the substrate and is converted to the pyridoxamine 5'-phosphate (PMP) form, and the substrate becomes the corresponding carbonyl compound. The second half-reaction involves the reactivation of the enzyme in a similar manner, by transferring the amino group from PMP to a suitable carbonyl-containing acceptor compound[20](Scheme 2).

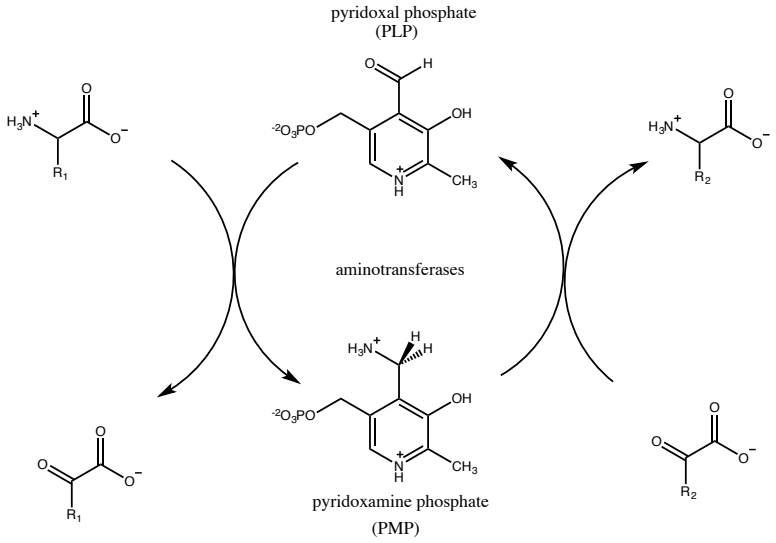

Scheme 2. General aminotransferase reaction. The scheme represents two coupled half reactions required for one complete transamination cycle.

Aminotransferase as drug-targets

Aminotransferases are vital for because they catalyze biochemical processes involving amino acid metabolism[20]. Their importance is further highlighted because they are important drug-targets for the treatment of diseases. The work in this thesis focuses on two of these drug-targets γ-aminobutyric acid aminotransferase (GABA-AT) and ornithine aminotransferase (OAT).

γ-Aminobutyric acid aminotransferase (GABA-AT; EC 2.6.1.19) is a PLP-dependent enzyme, found in many organs, including brain, liver, kidney, and pancreas; however, it is present at higher specific activity in glial cells and presynaptic neurons[22]. It catalyzes the transfer of an amino group of GABA to α-ketoglutarate, producing succinic semi aldehyde and L-glutamate (Scheme 3). Abnormally low levels of GABA in the brain have been associated with neurological disorders including epilepsy, Parkinson's disease, Huntington's disease and Alzheimer's diseases[23]. Thus, inhibition of GABA-AT is considered as a drug target for developing treatments for these neurological diseases and has been studied in detail.

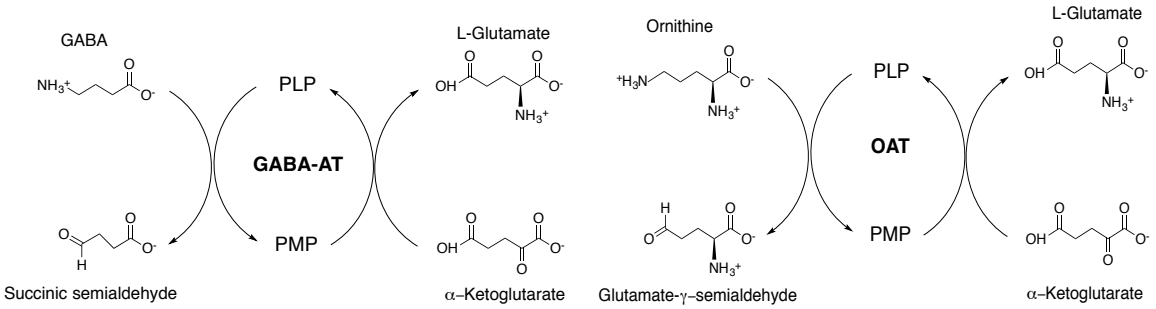

Scheme 3. General Mechanism of GABA-AT and OAT

Ornithine aminotransferase, OAT (L-ornithine 2-oxoacid d- aminotransferase, EC 2.6.1.13) is a pyridoxal 5-phosphate (PLP) dependent enzyme, found in the mitochondrial matrix of most human and animal tissues[24] and, catalyzes the transfer of the δ-amino group of L-ornithine to α-ketoglutarate, forming glutamate γ-semialdehyde and

L-glutamate (Scheme 3). It was recently discovered that ornithine aminotransferase (OAT), is highly upregulated in hepatocellular carcinoma (HCC), which is the second most common cause of death from cancer in men worldwide[25]. Inhibition of overexpressed OAT was shown to suppress the growth of HCC tumors[26]. Inhibition of OAT is proposed to also be beneficial in treating hyperornithinia[27] and, is being investigated as a target in chemotherapeutic drug development.

Aminotransferase as off-targets

The reactions catalyzed by PLP dependent aminotransferases appear diverse, but they all share a similar catalytic mechanism[28]. This makes it challenging to design specific inactivators of enzyme drug targets like GABA-AT and OAT without effecting off-target PLP dependent aminotransferases. For the purpose of this work we studied aspartate aminotransferase (Asp-AT) as a model off-target enzyme.

Aspartate aminotransferase is a PLP dependent enzyme that catalyzes a transamination reaction between aspartate and α-ketoglutarate to oxaloacetate and L-glutamate. (Scheme 4)[28] During the enzyme catalyzed reaction, the cofactor is interconverted between its PLP and pyridoxamine (PMP) form. The transfer of the amino group catalyzed by AspAT is crucial in both amino acid degradation and biosynthesis. Therefore, when designing an inactivator for PLP dependent drug-targets any molecule that also inhibits/inactivates Asp-AT irreversibly even at low concentrations may not be a promising molecule for further pharmacological development.

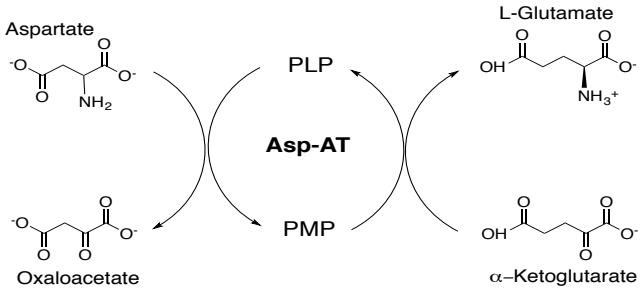

Scheme 4. General Mechanism of Aspartate aminotransferase

Similarities between Asp-AT, OAT and GABA-AT: General mechanism and structure

All aminotransferases follow the same initial catalytic mechanism, except for the structure of the substrate that is recognized and the resulting product. The specific steps of the first half of the reaction are shown in Scheme 5 and the second half proceeds in the reverse manner[20,28].

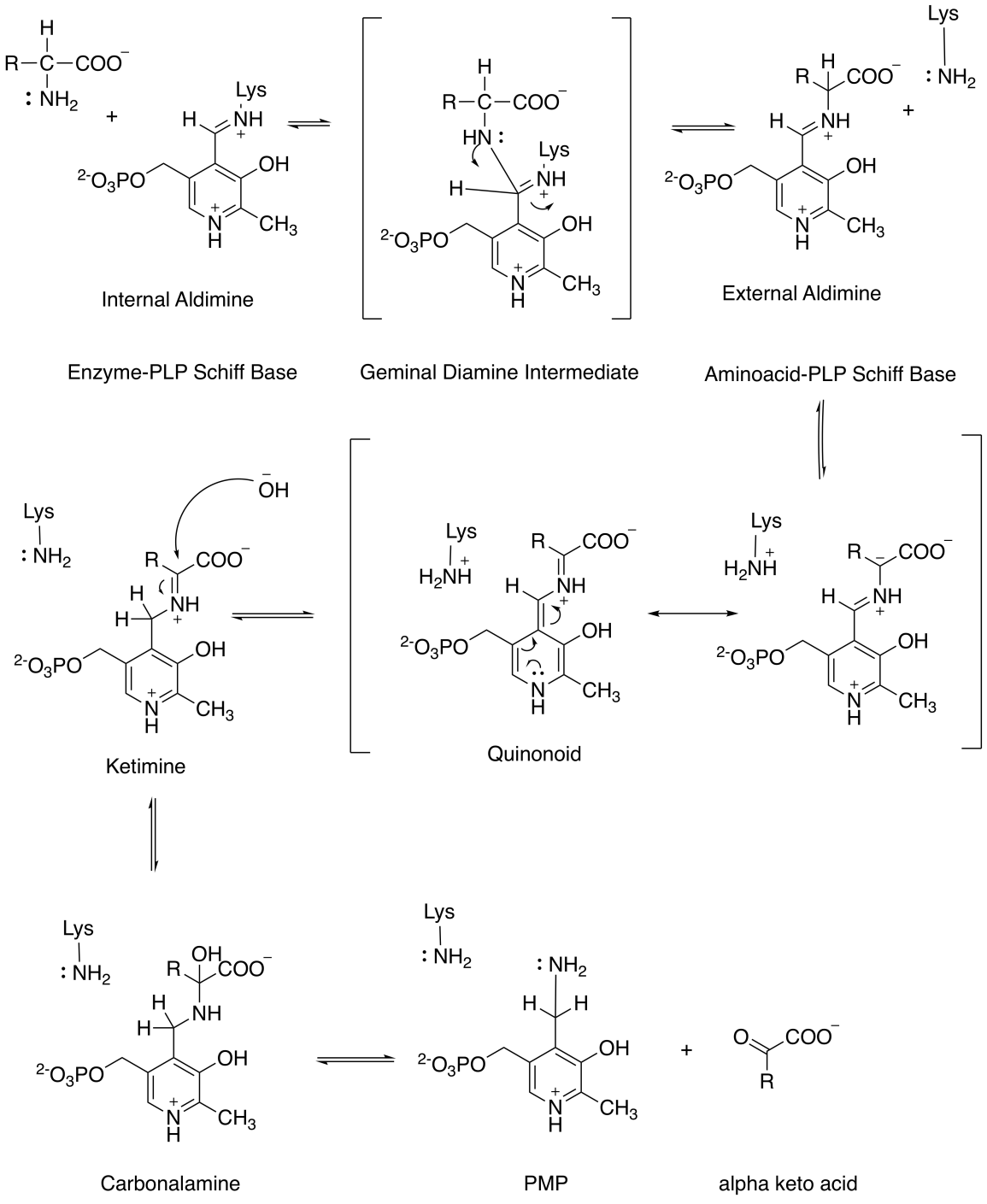

Scheme 5. General mechanism of aminotransferases

First, the amino group of the catalytic Lys forms a Schiff base with the aldehyde carbon to generate an internal aldimine. The amino group of Lys in displaced by the amino group of the

substrate via nucleophilic attack to form the external aldimine. The hydrogen attached to the alpha-carbon of the substrate in then abstracted (Lys is proposed as the proton acceptor) to form a quinonoid intermediate. The quinonoid is reprotonated, but now at the aldehyde carbon, to form the ketimine intermediate. Finally, the ketimine is hydrolyzed to form PMP and oxaloacetate. This reaction is proposed to have several rate-determining steps[29], however, it is shown substrate binding drives the catalytic reaction[30].

GABA-AT, OAT and, Asp-AT share the same initial catalytic mechanism. Therefore, it is not surprising that they share a significant amount of structural homology. Storici et al[31]. first reported the crystal structure of GABA-AT from pig liver, which is known to be 96% identical to human brain GABA-AT. The crystal structure of human recombinant OAT was first reported by Shen et al.[32] In its native form, the PLP cofactor is linked to a lysine residue in the active site, as shown in Scheme 5. An overlap of the crystal structures of OAT, GABA-AT, and Asp-AT show that they all share a similar Class I aminotransferase protein fold[33] and PLP interacts similarly with the conserved active-site residues (Figure 5). Also, the phosphate group of the cofactor provides a firm anchor to the region in the active site known as the "phosphate-binding cup."[34]

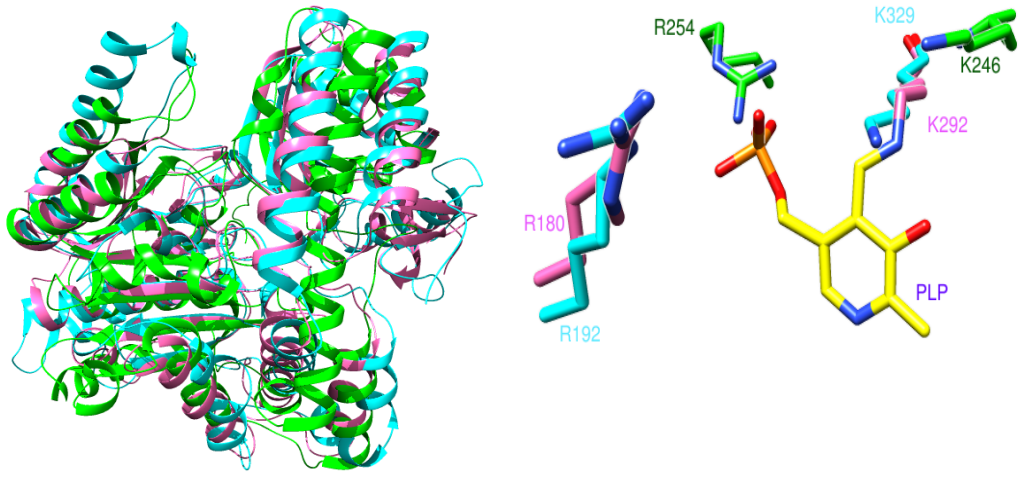

Figure 5. Comparison of the structure of Asp-AT(green), GABA-AT(blue) and OAT (pink). A. Overall secondary structure of GABA-AT (PDB accession code 1OHV), OAT (PDB accession code 1OHV) and, Asp-AT (PDB accession code 1ARG). B. The overlap of active sites shows similarities in the position of important catalytic residues Lys and Arg.

Mechanism-based enzyme inactivation

The similarities in the structure and mechanism of OAT, GABA-AT and Asp-AT make it challenging to design a drug molecule that can specifically inhibit only one drug-target without binding to other PLP dependent enzymes and off-targets. One way to overcome this difficulty is by designing mechanism-based inactivators. According to Silverman[35], a mechanism based inactivator is an unreactive compound who's structure resembles that of the substrate or product of the target enzyme and, undergoes a catalytic transformation by the enzyme to a species, that prior to release from the active site causes inactivation of the enzyme. Mechanism-based inactivators have a higher chance of being selective because they require the distinct catalytic mechanism of the enzyme to occur before inactivation. The Silverman group has designed a library of compounds (Figure 6) that are GABA analogs and mechanism-based inactivators for GABA-AT. For the purpose of this work we test (1R,3S,4S)-3amino-4-fluorocyclopentane-1-carboxylicacid (FCP) (Figure 6: 12) on OAT a drug-target and Asp-AT a model off-target.

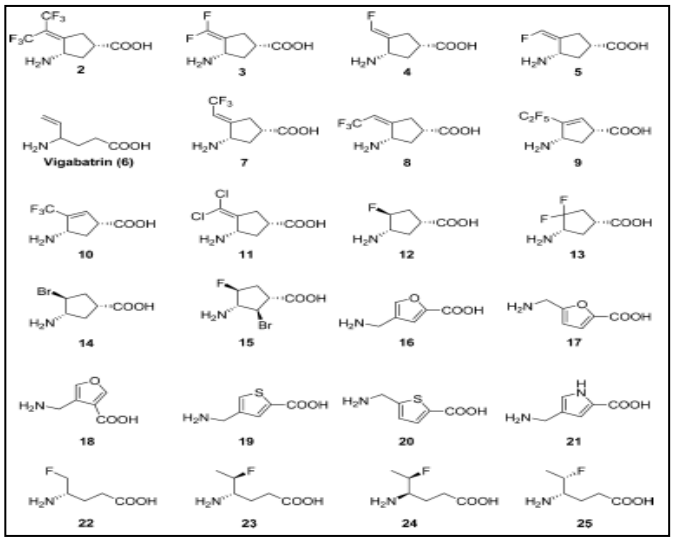

Figure 6. GABA analogs as mechanism-based enzyme inactivators

(1R,3S,4S)-3amino-4-fluorocyclopentane-1-carboxylicacid (FCP) as a mechanism based inactivator and objectives for this dissertation

GABA-AT and OAT share a similar catalytic mechanism, overall structure and, have similar catalytic residues in their active site[23]. Therefore, it is not surprising that some mechanism-based inactivators of GABA-AT also inactivate OAT. (1R,3S,4S)-3amino-4-fluorocyclopentane-1-carboxylicacid (FCP) is a known inactivator of GABA-AT. Previously Storici *et al*[36] reported the inactivation of GABA-AT by FCP with the crystal structure of the inactivated enzyme showing the adduct derived from the mechanism of inactivation. FCP is also reported as an inactivator of OAT[26], but no information is available about its detailed mechanism of inactivation. An understanding of the mechanistic differences between GABA-AT and OAT can help in the design of selective inhibitors of OAT over GABA-AT.

For the purpose of this dissertation I investigated the mechanism by which FCP inactivates OAT, and tested the effects of FCP on a PLP-dependent off-target Asp-AT. This study serves as a proof-of-principle that new OAT inactivators could be developed from GABA analogues,

without targeting other off-target PLP-dependent enzymes. In this study, we obtained the crystal structure of inactivated OAT by FCP and provide implications about the mechanism. We also report the crystal structures of the off-target Asp-AT in complex with FCP in the presence as well as in the absence of α-ketoglutarate. The crystal structures of Asp-AT in complex with FCP, along with inhibition assays and high resolution mass spectrometry, support the turnover of FCP by Asp-AT and the proposed mechanism.

CHAPTER TWO

STRUCTURAL AND BIOCHEMICAL CHARACTERIZATION OF AidC, A QUORUM-QUENCHING LACTONASE WITH ATYPICAL SELECTIVITY

Summary

Quorum-quenching catalysts are of interest for potential application as biochemical tools to interrogate interbacterial communication pathways, as anti-biofouling agents, and as anti-infective agents in plants and animals. Herein, the structure and function of AidC, an *N*-acyl-L-homoserine (AHL) lactonase from *Chryseobacterium*, is characterized. Steady-state kinetics show that zinc-supplemented AidC is one of the most efficient wild-type quorum-quenching enzymes characterized to date, with a k_{cat}/K_M value of approximately 2×10^6 $M^{-1}s^{-1}$ for *N*-heptanoyl-L-homoserine lactone. The enzyme has stricter substrate selectivity and significantly lower K_M values (ca. 50 μM for preferred substrates) than typical AHL lactonases (ca. > 1 mM). X-ray crystal structures of AidC alone, and with the product *N*-hexanoyl-L-homoserine were determined at resolutions of 1.09 and 1.67 Å, respectively. Each structure displays as a dimer, and dimeric oligiomerization was also observed in solution by size-exclusion chromatography coupled with multi-angle light scattering. The structures reveal two atypical features as compared to previously characterized AHL lactonases: a 'kinked' α-helix that forms part of a closed binding pocket which provides affinity and enforces selectivity for AHL substrates, and an active-site His substitution that is usually found in a homologous family of phosphodiesterases. Implications for the catalytic mechanism of AHL lactonases are discussed.

INTRODUCTION

One of the most prominent social behaviors displayed by bacteria is quorum-sensing, the ability to coordinate gene expression in response to population density through the production and detection of interbacterial signaling molecules such as the *N*-acyl-L-homoserine lactones (AHLs).[37] Enzymes capable of blocking these signaling pathways, called quorum-quenching enzymes, are important biochemical tools for probing quorum-sensing pathways.[38] They also hold considerable promise as reagents to prevent marine and membrane biofouling, as treatments to prevent costly infections of plants and fish, as potential protein therapeutics, and possibly as tools to manipulate interactions between diverse microbes.[7,39–42] Some of the quorum-quenching enzymes most widely used for such applications are AHL lactonases, which use a dinculear zinc center to hydrolyze a wide range of AHL substrates (Figure 7).[43]

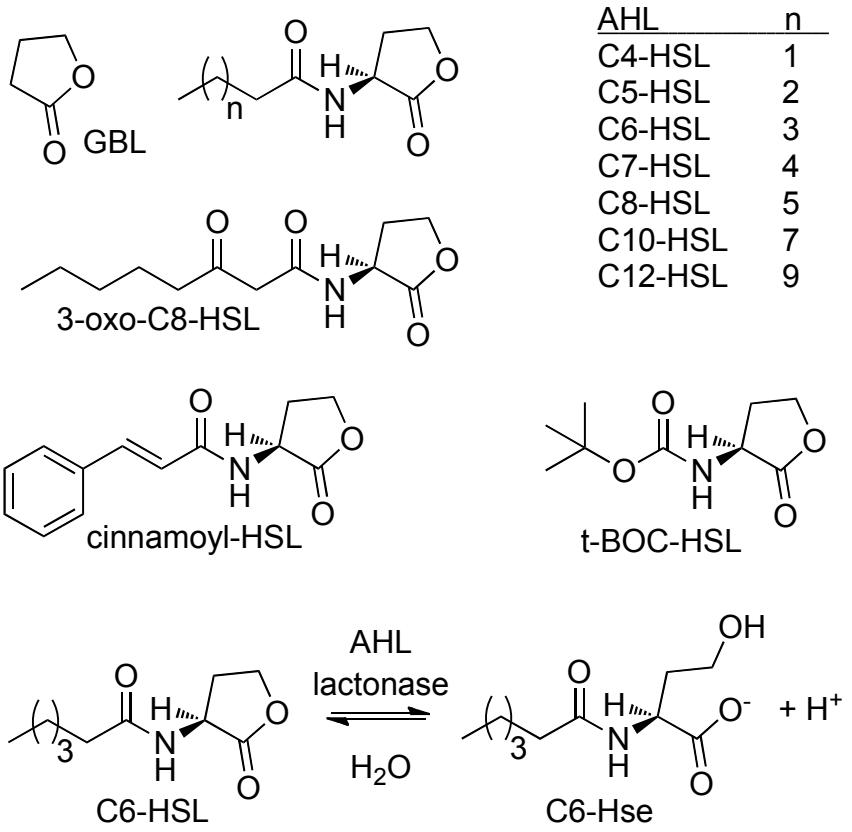

AHL	n
C4-HSL	1
C5-HSL	2
C6-HSL	3
C7-HSL	4
C8-HSL	5
C10-HSL	7
C12-HSL	9

Figure 7. Potential Substrates and the AHL Lactonase-Catalyzed Reaction. γ-Butyrolactone (GBL) and naturally-occurring and synthetic AHLs including C4-, C5-, C6-, C7-, C8-, 3-oxo-C8-, C10-, C12-, cinnamoyl-, and *t*-BOC-HSL are assayed as potential AidC substrates. The inset table assigns chain lengths in the neighboring structures to the matching abbreviations used throughout the text. The general reaction catalyzed by AHL lactonases is also shown with C6-HSL as an example, resulting in the C6-Hse and H^+ products.

The gene encoding an AHL lactonase with unusual properties has been previously identified: *aidC* an autoinducer degrading gene isolated from a *Chryseobacterium* sp. strain StRB126 originally associated with potato roots.[19] The encoded protein, AidC (Genbank Protein: BAM28988; EC: 3.1.1.81), catalyzes the hydrolytic ring opening of multiple *N*-acyl homoserine

lactone (AHL) substrates. Analysis of protein sequence alignments revealed that AidC is homologous to other AHL lactonases found in the metallo-hydrolase / oxidoreductase superfamily, and shares a conserved dinuclear metal binding motif. However, AidC is phylogenetically distant from the other AHL lactonase clusters.[19] For example, optimal global pairwise alignment[44] of AidC with two other homologous dizinc AHL lactonases, AiiA (autoinducer inactivator A from *Bacillus* sp. 240B1[9]) and AiiB (autoinducer inactivator B from *Agrobacterium tumefaciens* C58[45]) show only ~20% and ~17% amino acid identity, respectively. Additionally, these sequence alignments predict that active-site Asp and Tyr residues, conserved in other AHL lactonases due to their roles in zinc-binding and catalytic turnover, are possibly replaced in AidC by Leu and Ser, respectively.[14,15,19] However, the most striking feature of AidC is its reported K_M values. All previously characterized wild-type AHL lactonases have K_M values $\geq$ 1.4 mM[11,15,46],with the exception of MomL (440 μM; *Muricauda olearia* marine AHL lactonase).[47] In contrast, the reported K_M values for AidC are approximately $\geq$ 24-fold lower: 46 - 72 μM.[19] The lower K_M values of AidC are of interest since a better understanding of how quorum-quenching enzymes recognize and process their substrates can enable their appropriate selection and optimization as biochemical tools and help in the proposed development of this class of enzymes as therapeutic, anti-infective, and anti-biofouling proteins.[39-42] Toward these ends, we report here the characterization of purified AidC alone, and with a bound product. Two aspects of the active site are atypical compared to previously characterized AHL lactonases: a novel substrate-binding pocket defined, in part, by an unusual 'kinked' α-helix containing an internal proline residue, and an active site His substitution that is usually found in more distant superfamily members that belong to a different family, the phosphodiester hydrolases.

RESULTS AND DISCUSSION

Most AHL lactonases characterized to date have poor affinity for their substrates, as gauged by millimolar K_M values. However, unusually low micromolar K_M values were reported for AidC-catalyzed hydrolysis of AHLs.[19] To better understand the basis for substrate affinity, selectivity, and turnover in AidC, we cloned and purified this AHL lactonase for functional and structural studies.

Purification of AidC, determination of activity and zinc content.

Heterologous expression of AidC in *E. coli* using a codon-optimized coding sequence (Figure 8) led to good yields of purified protein (~ 10 mg / L culture).

```
gaa aac ctg tat ttt cag ggc ATG AAC CGG CGC GAG CTG CTG AAA AGC GGA CTG CTG GCG GGC ACT CTC TCA TTC ATG CCG  < 81
E   N   L   Y   F   Q   G   M   N   R   R   E   L   L   K   S   G   L   L   A   G   T   L   S   F   M   P
            10          20          30          40          50          60          70          80

TTC TCA AAC GTT TTC GCA GAA ACG AAA CTG TTC TCA GAG AAA ACC GAA GAT GAC CTC TCA GGG TTT AAG AAG ATT AAA CTT  < 162
F   S   N   V   F   A   E   T   K   L   F   S   E   K   T   E   D   D   L   S   G   F   K   K   I   K   L
          90          100         110         120         130         140         150         160

GGC GAG CTG GAA CTG TTT ATT CTG ACA GAT GGC TAC ATT CAC GAA GAG AAC TTA ATC AGT TTT GCC CCT CGC GGG AAT GTC  < 243
G   E   L   E   L   F   I   L   T   D   G   Y   I   H   E   E   N   L   I   S   F   A   P   R   G   N   V
        170         180         190         200         210         220         230         240

GCG GAA CTT AAA ACT ATT CTT AAA GAT AAC TTT CGT GCC GAC CAT TAC ATC GAC ATG GCG ATT AAC ATT CTT CTG GTG AAA  < 324
A   E   L   K   T   I   L   K   D   N   F   R   A   D   H   Y   I   D   M   A   I   N   I   L   L   V   K
        250         260         270         280         290         300         310         320

ACC AAG GAG AAA CTG ATT CTG ATG GAT ACC GGC ATG GGT ATC TTT GCA GAC GAG CGG ACC GGC TTT CTG TTG AAA TCA CTG  < 405
T   K   E   K   L   I   L   M   D   T   G   M   G   I   F   A   D   E   R   T   G   F   L   L   K   S   L
      330         340         350         360         370         380         390         400

CAG AAA GCC GGC TTT TCG GCA CAT GAT ATT ACC GAT ATT TTT TTA TCA CAT GCA CAT CCG GAT CAT ATT GGC GGT GTA GTA  < 486
Q   K   A   G   F   S   A   H   D   I   T   D   I   F   L   S   H   A   H   P   D   H   I   G   G   V   V
    410         420         430         440         450         460         470         480

GAC AAA CAG AAT AAG TTG GTC TTC CCG AAC GCG TCT ATT TTC ATC AGC AAA ATC GAG CAT GAT TTC TGG ATT AAT GCA AGC  < 567
D   K   Q   N   K   L   V   F   P   N   A   S   I   F   I   S   K   I   E   H   D   F   W   I   N   A   S
    490         500         510         520         530         540         550         560

ATT AAA GAC TTT AAC AAC AGT GCT CTG AAA GCC CAC CCG GAA CGT CTG AAC CAG ATC ATT CCA GCG CTG CAG AAC ATC CTG  < 648
I   K   D   F   N   N   S   A   L   K   A   H   P   E   R   L   N   Q   I   I   P   A   L   Q   N   I   L
  570         580         590         600         610         620         630         640

AAA GCC ATT CAA CCG AAA CTC AAG TTC TAT GAC CTT AAT AAA ACG CTG TAC TCC CAT TTC AAC TTC CAG CTG GCT CCA GGT  < 729
K   A   I   Q   P   K   L   K   F   Y   D   L   N   K   T   L   Y   S   H   F   N   F   Q   L   A   P   G
650         660         670         680         690         700         710         720

CAC ACC CCT GGG CTG ACT GTT ACA ACT ATT AGC AGC GGC AAT GAA AAA CTT ATG TAT GTG GCA GAT TTG ATC CAT AGC GAT  < 810
H   T   P   G   L   T   V   T   T   I   S   S   G   N   E   K   L   M   Y   V   A   D   L   I   H   S   D
730         740         750         760         770         780         790         800

GTA ATC CTG TTC CCA CAT CCG GAC TGG GGT TTC TCA GGT GAC ACA GAC TTA GAC ATT GCA ACG GCG AGT CGC AAA AAA TTT  < 891
V   I   L   F   P   H   P   D   W   G   F   S   G   D   T   D   L   D   I   A   T   A   S   R   K   K   F
          820         830         840         850         860         870         880         890

CTT AAG CAG CTG GCG GAT ACA AAG GCC CGT GCT TTC ACT TCA CAT CTG CCG TGG CCA GGC CTG GGC TTC ACC AAA GTA AAA  < 972
L   K   Q   L   A   D   T   K   A   R   A   F   T   S   H   L   P   W   P   G   L   G   F   T   K   V   K
        900         910         920         930         940         950         960         970

GCC CCG GGT TTC GAA TGG ATT CCC GAA AGC TTC ATG AAC TAA  < 1014
A   P   G   F   E   W   I   P   E   S   F   M   N   *
      980         990         1000        1010
```

Figure 8. Sequence of AidC. Top lines shows the DNA sequence, codon optimized for expression in E. coli, that was obtained from commercial gene synthesis (IDT), and contained within a shuttle vector. Bottom lines show the translated AidC protein sequence, including the N-terminal addition of a TEV protease cleavage site (ENLYFQ↓G, shown in blue). The * indicates a stop codon.

Kinetic characterization of the "as purified" form of untagged AidC gave K_M (65 ± 4 μM) and k_{cat} values (4.6 ± 0.1 s^{-1}) for lactone hydrolysis of C6-HSL, similar to values reported previously for AidC containing an *N*-terminal maltose binding protein affinity tag: 55 ± 4 μM and 2.3 ± 0.2 s^{-1}, respectively.[19] Although we used a purification procedure similar to that for other AHL lactonases,[48] we found that purified AidC does not contain the typical two equivalents of zinc ions. Instead, the "as purified" AidC preparation only contained 1.2 ± 0.1 equivalents of zinc ions per AidC monomer. We suspected that the protein may not have fully retained its zinc content throughout the purification protocol, and so monitored the observed rates for AidC-mediated hydrolysis of saturating concentrations of substrate upon supplementing the Assay Buffer with varying concentrations of $ZnSO_4$ (Figure 9).

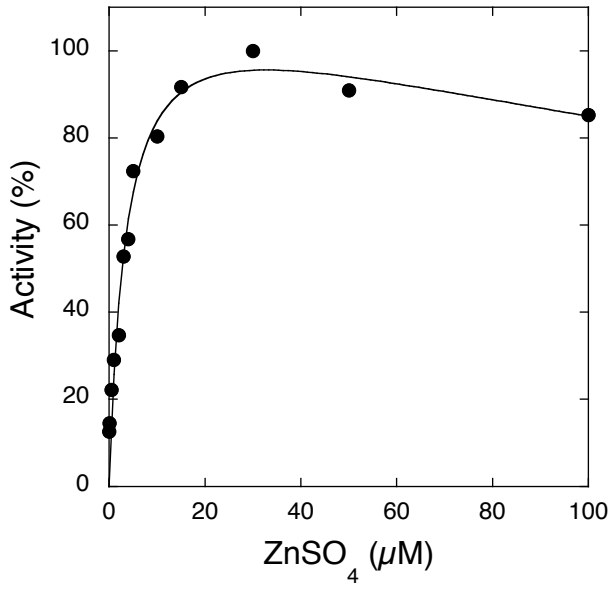

Figure 9. Optimization of Assay Zinc Concentration. The relative observed initial rates of AidC-catalyzed hydrolysis of C6-HSL under saturating conditions (1 mM) are graphed with respect to the concentrations of supplemental ZnSO4 added to the Assay Buffer. Maximum activity was

detected at 30 μM supplemental ZnSO4. Points are fitted to the equation: Activity (%) = Actmax×[Zn2+]/(EC50 + [Zn2+]×(1+[Zn2+]/Ki)) where Actmax is the maximum activity, EC50 is the half maximal concentration of activation, and Ki is the apparent inhibition constant, with fitted values of 120 ± 10 %, 3.6 ± 0.9 μM and 300 ± 180 μM, respectively.

A significant increase in rate is observed upon increasing the $ZnSO_4$ concentration, with a maximum activity at approximately 30 μM $ZnSO_4$, and a slight decrease at higher concentrations. Zinc supplementation leads to an increased k_{cat} (C6-HSL: 59 ± 1 s^{-1}), which is > 10-fold larger than the k_{cat} of the "as purified" form. If the 1.2 equivalents of zinc ions in the "as purified" AidC represent approximately half dizinc protein and half zinc-free protein, one might expect a two-fold increase in k_{cat} values, at most, upon reconstitution of the dizinc active site. However, since the observed increase in rate is much larger, it likely represents instead an increase in activity due to the transition between mono- and dizinc metalloforms. Further studies will be required to characterize zinc affinity in more detail. However, a supplement of 30 μM $ZnSO_4$ is used for the remaining kinetic experiments herein to maximize observed activity.

*Determination of kinetic parameters***.**

The previous characterization of AidC containing an *N*-terminal maltose-binding fusion protein reported unusually low K_M values (C6-HSL: 55 μM, C8-HSL: 64 μM), with very little selectivity for, or against, related substrates with 3-oxo substitutions.[19] The associated k_{cat} values (approximately 2 s^{-1}) are less than typically reported for AHL lactonases. To augment this previous study, we determined the steady-state kinetic parameters for purified, untagged AidC, now supplemented with exogenous $ZnSO_4$, using a broader set of substrates (Table 1).

Table 1. Steady-State Kinetic Parameters for Substrates of Dizinc AidC

Substrate	K_M (μM)	k_{cat} (s^{-1})	k_{cat}/K_M (M^{-1} s^{-1})
GBL	N.D.[a]	N.D.	16 ± 1
C4-HSL	470 ± 60	39 ± 2	8.3×10^4
C5-HSL	130 ± 20	57 ± 3	4.4×10^5
C6-HSL	61 ± 4	59 ± 1	9.7×10^5
C7-HSL	47 ± 5	80 ± 2	1.7×10^6
C8-HSL	83 ± 10	45 ± 3	5.4×10^5
C10-HSL	12 ± 4	5.2 ± 0.4	4.3×10^5
C12-HSL	7 ± 4	0.40 ± 0.05	5.7×10^4
3-oxo-C8-HSL	130 ± 20	28 ± 1	2.2×10^5
cinnamoyl-HSL	470 ± 80	25 ± 2	5.3×10^4
t-BOC-HSL	740 ± 70	44 ± 1	5.9×10^4

[a.] N.D.: not determined. The K_M value for GBL exceeds 700 mM, so only the k_{cat}/K_M value was determined.

In general, we confirm the low K_M values reported previously. The K_M values for zinc-supplemented AidC, "as purified" AidC, and AidC with an *N*-terminal maltose binding fusion

protein are all quite similar, independent of zinc content. However, zinc supplementation (but not cleavage of the *N*-terminal tag) greatly improves the k_{cat} values, which are all generally increased by > 20 fold. These results indicate that the differences in k_{cat} values between this and the prior report likely arise from differences in zinc content rather than the presence of the *N*-terminal fusion protein.

As compared to other quorum-quenching enzymes, AidC appears to be a much more efficient catalyst. If the k_{cat}/K_M value for hydrolysis of the best AHL substrate of AidC is compared with k_{cat}/K_M values for the best of the kinetically characterized substrates for other wild-type quorum-quenching enzymes (including non-homologous enzymes from different superfamilies), AidC ranks the highest (Table 2). Achieving the highest rank in this comparison is due to a combination of both a low K_M value and a high k_{cat} value, since AidC does not have the lowest or highest of either of these individual values with respect to the same set of enzyme/substrate pairs (Table 2). Therefore, to the best of our knowledge, AidC appears to have the highest k_{cat}/K_M reported for any wild-type quorum-quenching enzyme to date. Additionally, even when k_{cat}/K_M values are similar, the low K_M value of AidC may make this enzyme more suitable than homologs with higher K_M values for quorum-quenching applications at low AHL concentrations.[49]

Table 2. Steady-State Rate Constants for Selected Wild-Type Quorum-Quenching Enzymes And AHL Substrates With Highest Reported k_{cat}/K_M Values

Enzyme	Substrate	k_{cat} (s^{-1})	K_M (μM)	k_{cat}/K_M ($M^{-1}s^{-1}$)	Reference
AidC	C7-HSL	80	47	10^6	This work
MomL	3-oxo-C10-HSL	224	440	10^5	17
PvdQ[a]	C12-HSL	2.5	11	10^5	50
PON2[b]	3-oxo-C12-HSL	13	50	10^5	48
PONX_OCCAL[c]	3-oxo-C12-HSL	44	180	10^5	48
AiiA	C6-HSL	91	5600	10^4	14
AiiB	C6-HSL	25	1600	10^4	16
MCP[d]	C12-HSL	0.3	23	10^4	51
*Vmo*Lac[e]	C8-HSL	0.6	260	10^3	52
GKL[f]	C8-HSL	0.5	1200	430	53

[a] Pyoverdine biosynthetic protein Q from *Pseudomonas aeruginosa*. Enzyme belongs to the metal-independent NTN-hydrolase superfamily.
[b] Paraoxonase-2 from human. Enzyme belongs to the dicalcium-binding paraoxonase family with a six-bladed β-propeller fold.
[c] Paraoxonase X from *Oceanicaulis alexandrii*. Enzyme belongs to the same family as PON-2.
[d] Lactonase from *Mycobacterium avium* subsp. *paratuberculosis* K-10. Enzyme belongs to the phosphotriesterase-like lactonase group of enzymes within the amidohydrolase superfamily.
[e] Lactonase from the hyperthermophile *Vulcanisaeta moutnovskia*. Enzyme belongs to the same group as MCP.
[f] Lactonase from the thermophile *Geobacillus kaustophilus*. Enzyme belongs to the same group as MCP.

Substrate selectivity

As gauged by k_{cat}/K_M values, the most efficiently processed substrates of AidC are C6- and C7-HSL (approx 10^6 $M^{-1}s^{-1}$) (Table 1). AHL substrates that differ in length by one methylene

have a > 2-fold decrease in their specificity constant (k_{cat}/K_M). Commonly occurring AHLs with more extreme size differences, C4- and C12-HSL, are more significantly disfavored by 20- and 30-fold, respectively. The previous characterization of AidC indicated no preference for or against 3-oxo substitutions,[19] and here we find consistent results in which the 3-oxo substitution only mildly perturbs both K_M and k_{cat} values, resulting in a 2.5 fold decrease in k_{cat}/K_M. The most significantly disfavored substrates we assayed were the bulky cinnamoyl-HSL[50] and the synthetic t-BOC-HSL compound, which had specificity constants approximately 30-fold less than the best substrate. Interestingly, the mechanism used to disfavor substrates with sterically bulky substituents appears to differ from that used to disfavor substrates with long unsubstituted n-alkyl substituents (see below).

Structure determination and model building.

To better understand the structural basis of substrate recognition and catalysis, we determined the X-ray crystal structure of AidC, and the structure of AidC in complex with the reaction product C6-homoserine (C6-Hse) through co-crystallization with the substrate C6-HSL. Data processing and refinement statistics are shown in Table 3.

Table 3. Crystallographic Data for AidC and AidC:C6-Hse complexes

	AidC	AidC:C6-Hse
PDB Code	4ZO2	4ZO3
	Data Processing	
Space group	$P2_12_12_1$	$P2_12_12_1$
Cell dimension		
α, β, γ (°)	90, 90, 90	90,90,90
a, b, c (Å)	51.7, 97.30, 110.64	47.09, 47.87, 249.15
Resolution (Å)	1.09	1.67
[a]R_{merge} (%)	4.9 (100)[b]	9.3 (75.4)
I/σ (I)	23.6 (1.1)	20.3 (3.3)
[c]$CC_{1/2}$	0.997 (0.539)	0.992 (0.767)
[d]R_{pim}(%)	3.00 (60.8)	5.0 (41.8)
Completeness (%)	99.6 (99.2)	99.3 (99.9)
Multiplicity	6.6 (3.4)	4.4 (3.9)
No. Reflections	1580815	295571
No. Unique Reflections	239792	67109
	Refinement	
Average B factor (Å^2)	23.6	28.8
[e]R_{work}/[f]R_{free} (%)	13.08/16.20	18.44/22.83
No. of Atoms		
Protein	4810	4714
Ligand	N/A[g]	30
Metal	4	4
Water	955	585
B-factors		
Protein	21.5	27.4
Ligand	N/A	32.69 - 47.58
[g]RMSD		
Bond length (Å)	0.015	0.018
Bond angle (°)	1.401	1.164
Ramachandran plot		
Most Favored (%)	97.70	97.29
Allowed (%)	2.20	2.54
Outliers (%)	0.00	0.17

[a] $R_{merge} = \Sigma|I_{obs}-I_{avg}|/ \Sigma I_{avg}$

[b] The values for the highest resolution bin are in parentheses.

[c] $CC_{1/2}$, Pearson correlation coefficient of two "half" data sets.

[d] R_{pim}, the precision-indicating merging R

[e] $R_{work} = \Sigma|F_{obs}-F_{calc}|/ \Sigma F_{obs}$

[f] Five percent of the reflection data were selected at random as a test set and only these data were used to calculate R_{free}.
[g] RMSD, root mean square deviation; N/A, Not Applicable

The unliganded AidC crystal diffracted to a resolution of 1.09 Å. The 2Fo-Fc omit map for the active site zinc ions and coordinating residues is shown in Figure 10. The "substrate-treated" AidC co-crystal diffracted to a resolution of 1.67 Å and contained the ring-opened product, C6-Hse. The final R_{work}/R_{free} values for AidC and AidC:C6-Hse are 13.08 / 16.20 % and 18.23 / 23.07 %, respectively. The occupancies of the zinc ions are refined to values between 0.6 and 0.8, as assessed by occupancy refinement in Phenix. During crystallization, the concentration of enzyme is higher, and the solution pH values lower, than during the functional studies discussed above. So, these occupancies may not reflect zinc binding during kinetic studies, and will be a topic for future experiments.

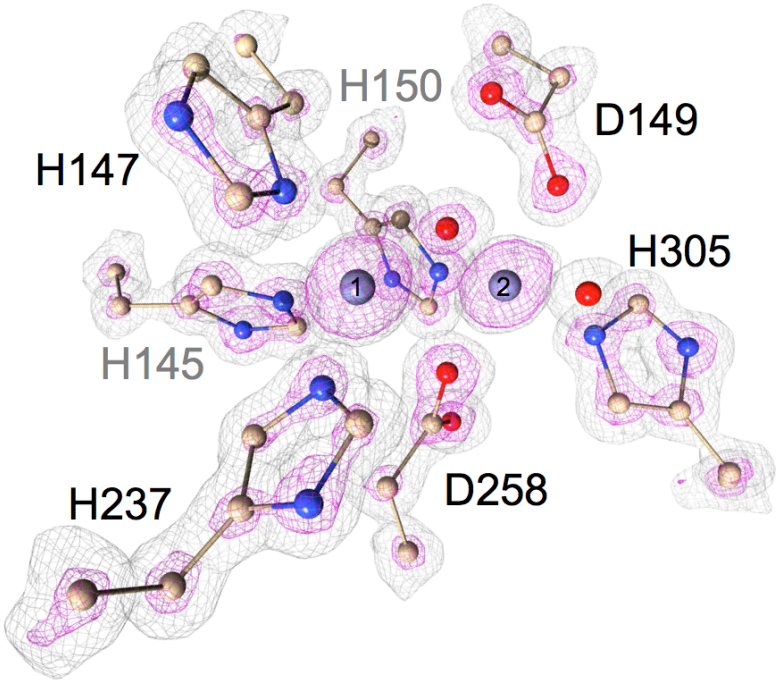

Figure 10**.** 2Fo-Fc omit map for the unliganded AidC dizinc site and coordinating residues. The map is shown at two different σ levels, with the grey mesh at 1.5 σ and the magenta mesh at 4.0 σ. The protein and zinc atoms are shown in ball-and-stick form, and colored with tan for carbon, blue for nitrogen, red for oxygen and grey for zinc. The 4σ map can be seen to indicate individual atom positions, characteristic of an ultra high resolution map.

AidC core structure, 'kinked' helix and dimerization

The AidC monomer structure displays a characteristic pseudosymmetrical core of two mixed β-sheets flanked by α-helixes to form the αββα protein fold conserved throughout the entire metallo-hydrolase / oxidoreductase superfamily, as cataloged in the Structural Classifications of Proteins (SCOP) database.[51] A dinuclear zinc ion cluster is found at one edge of where the two central β-sheets meet and is described below in more detail as part of the active site. A structural overlay of AidC with two related AHL lactonases, AiiA[13] and AiiB[46], highlights their conserved αββα cores, and shows the most significant structural divergence occurs in loops and helixes, adjacent to the dizinc active site, which serve to connect the core secondary structural elements (Figure 11A). Parts of these regions interact closely with active-site ligands.

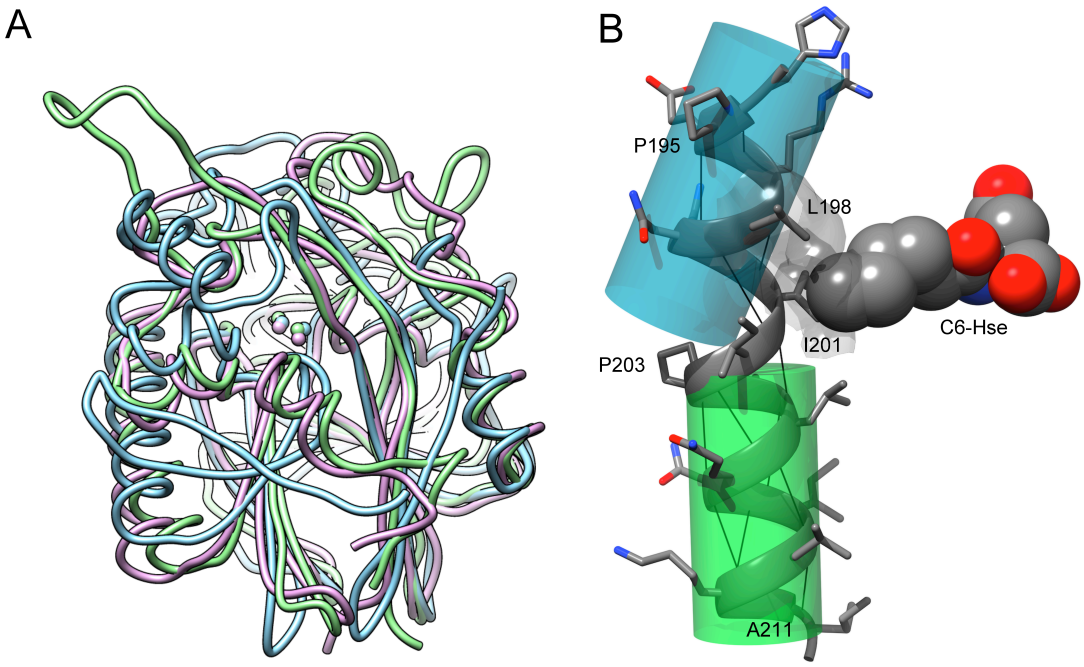

Figure 11. Structure of AidC Monomer. A. Superimposition of AidC (blue), AiiA (pink), and AiiB (green) structural models. Proteins backbones are depicted as 'licorice' strands. Structural conservation is higher in the zinc-binding site and the αββα core scaffold of the protein, but diverges more significantly in the connecting elements surrounding the active site. B. Ribbon diagram of a 'kinked' α-helix in AidC containing an internal proline residue. The regular H-bonding pattern (in black thin lines) of the α-helix backbone from residues P195 – A211 is interrupted by an internal P203 residue. The two ends of the α-helix, defined as P195-Q200 (blue) and A204-A211 (green) are offset by approximately 25°. Hydrophobic side chains near the bend, I201and L198 (surface in grey), contribute to the binding site for the *N*-acyl substituent of the bound product (C6-Hse, shown in space-fill form).

The AidC structure contains an unusual feature. One of the major helices H11 containing residues P195-A211 has an internal proline residue (P203) that disrupts the regular H-bonding of the α-helix. It results in a 'kinked' structure where one segment of the α-helix is found at an approximate 25° angle from the other (Figure 11B). Most soluble proteins do not contain α-helixes with internal proline residues, but this feature is not unprecedented.[52] A survey of 291 helices found that approximately 3% contain an internal proline, and the associated helix 'kinks' typically measure 26° ± 5°, tilting away from the proline sidechain, consistent with what is found in AidC.[53] Kinked α-helices typically place the hydrophobic side chain of the internal proline residue toward the solvent, and the kink aids in packing long helices around globular proteins;[54] both of these attributes are observed in AidC. Proline residues responsible for inducing kinks are typically highly conserved,[53] but P203 is not a conserved residue in this superfamily. However, several side chains of residues near the P203-induced kink do form part of the AidC substrate-binding cavity, suggesting a functional implication for this unusual structural element.

In our structural determination, AidC displays as a crystallographic dimer in the spacegroup $P2_12_12_1$ (Figure 12A). The protein-protein interface is heterogeneous and comprised of hydrophobic interactions as well as direct and through-water hydrogen bonds. The Proteins Interfaces Structures and Assemblies (PISA) algorithm[55] was used to calculate 2440 $Å^2$ buried surface area, and predicts a ΔG^{diss} of 6.1 kcal / mol.

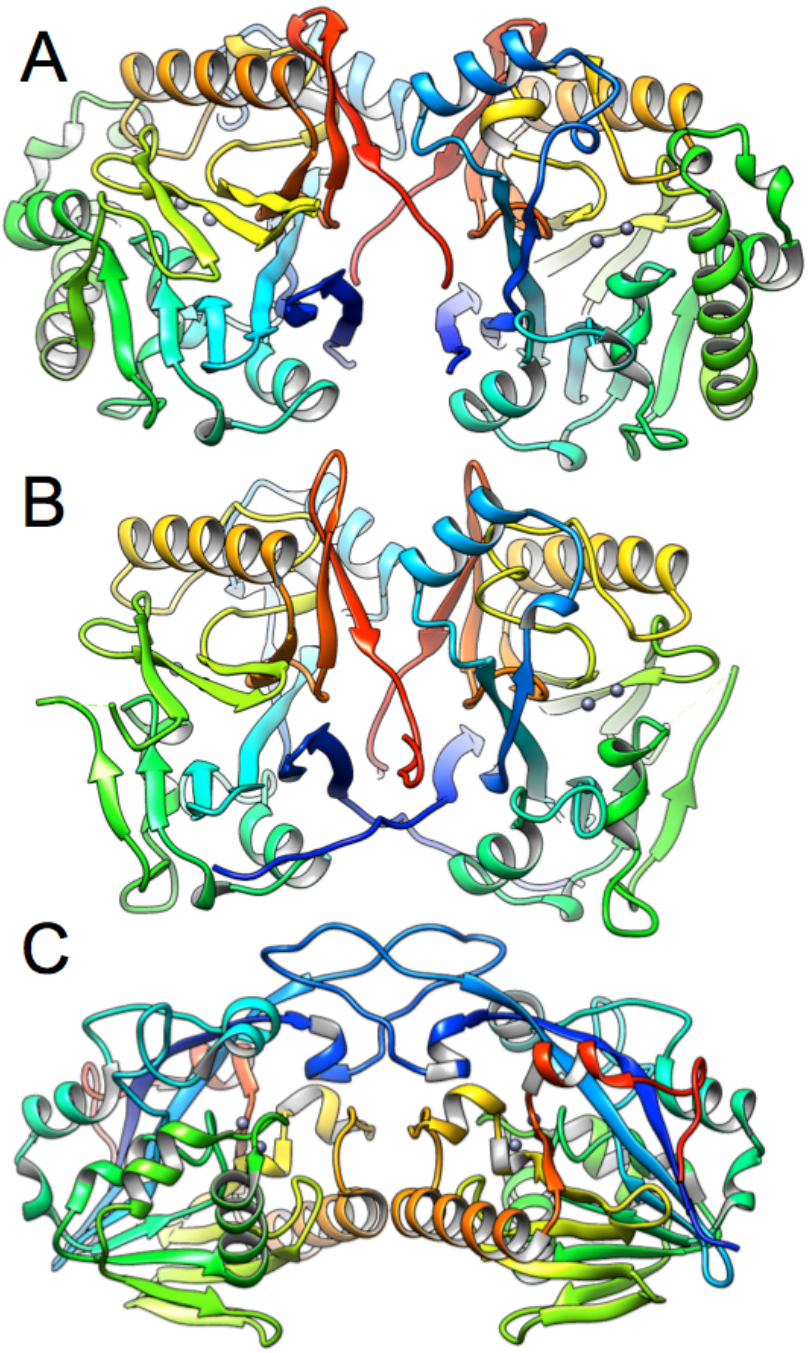

Figure 12**.** The Dimer Structure of AidC and Homologs. Each monomer is shown in ribbon form, with rainbow coloring from each *N*-terminus (blue) to the corresponding C-terminus (red). Rainbow coloring is used here to facilitate chain tracing and to emphasize similarities and

differences between the oligomeric interfaces. Zinc ions are shown as grey spheres. A. Depiction of the AidC dimer. B. Depiction of the OPHC2 dimer (from PDB: 4LE6). C. Depiction of the AiiB dimer (from PDB: 2R2D). The dimers of AidC and OPHC2 are very similar, but that of AiiB is divergent and uses different protein-protein interfaces

To determine if oligomerization is relevant in solution, size-exclusion chromatography – multiple angle light scattering (SEC-MALS) was used to assay for AidC oligomers (Figure 13). First, AiiA was used as a control since this homologous AHL lactonase was previously shown by analytical ultracentrifugation to be monomeric in solution.[13] Purified AiiA elutes from the size exclusion column as a single peak (detected by $Abs_{280\ nm}$), and light scattering is used to determine a molecular weight of 28 ± 2 kDa for this peak, which matches the mass calculated from the expected sequence (28,635 Da). Purified AidC elutes from the size exclusion column as one major peak preceded by a small second peak. The molecular weight determined for the major peak, 72.1 ± 0.9 kDa, matches reasonably well with that calculated for the dimer (36979 × 2 = 73,958 kDa). The molecular weight calculated for AidC oligomers in the small minor peak is 148 ± 4 kDa, which matches that calculated for the tetramer (36979 × 4 = 147,916 kDa). Therefore, at least when high protein concentrations are used, AidC forms a dimer in solution. Further studies will be required to determine if the dimer interface observed crystallographically is conserved in solution. Under the dilute assay conditions used to determine steady-state kinetic parameters, the activity of the enzyme varies linearly with concentration (Figure 14). So, either the dimer K_d value does not occur within the tested concentration range, or there is no change in activity upon change in oligomeric state.

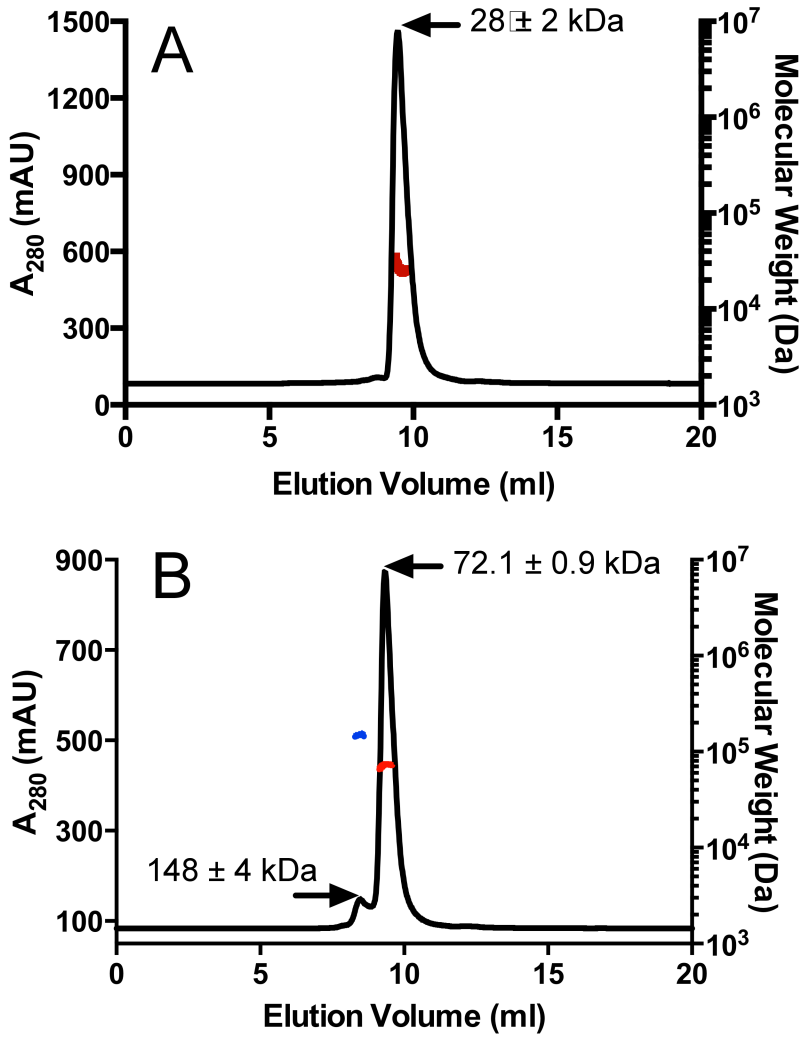

Figure 13. Molecular Weight Determinations of AidC and AiiA in Solution. SEC-MALS profiles are shown for AiiA and AidC. Absorbance at 280 nm is shown as a black line and calculated molecular weight for protein in the eluent at a particular time is shown in color, as noted. A) AiiA (molecular weight in red) gives a single peak with a molecular weight of 28 ± 2 kDa. B). AidC gives two peaks with the major peak containing an oligomer with the molecular weight (in red) of 72.1 ± 0.9 Da, and a minor preceding shoulder containing an oligomer with the molecular weight (in blue) of 148 ± 8 Da.

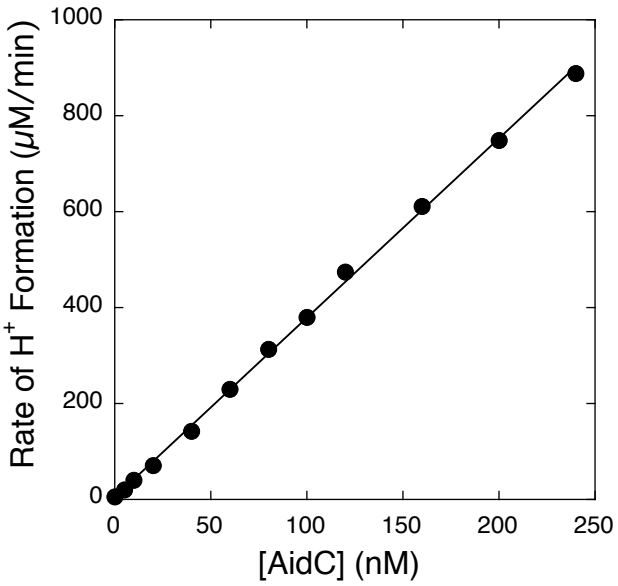

Figure 14. Correlation of observed rate with enzyme concentration. The relative rates of AidC-catalyzed hydrolysis of *t*-BOC-HSL (5 mM) at varying concentrations of "as purified" AidC, with Assay Buffer supplemented with $ZnSO_4$ (30 μM). AidC concentrations are those calculated using the monomer molecular weight

Previously, various AHL lactonases have been characterized as monomers[13] and dimers,[46] and the superfamily has examples of higher oligomers. When the AidC dimer structure is compared with that of AiiB (Figure 12C), which has been observed as a dimer in a crystal,[46] and in solution (unpublished observations), it is clear that the protein-protein interfaces are actually very divergent and involve different sides of the protein. However, when the AidC dimer structure is compared to the crystallographic dimer structure of the organophosphotriesterase OPHC2 (Figure 12B),[56] the protein-protein interfaces that comprise each dimer interface appear to be structurally conserved. In fact, the overall structural similarity of AidC ranked higher with

OPHC2 than with any other AHL lactonase, as gauged by the Dali server for structural comparison of proteins.[57] The active sites for each AidC monomer are distant from each other, and none of the structural or functional evidence presented here suggests that they are interdependent. Interestingly, AidC appears to also conserve other features besides this dimerization interface, with superfamily members outside of the immediate AHL lactonase family as will be described below.

AidC active site

The dinculear zinc active site of AidC is highly conserved with other AHL lactonases and other members in the superfamily. As can be seen in the comparison of dinuclear zinc sites in AidC, the AHL lactonase AiiA,[13] the organic phosphotriesterase OPHC2,[56] and the phosphodiesterase ZipD,[38] all the zinc-1 (Zn1) ions are coordinated by three histidines, and all the zinc-2 (Zn2) ions by two histidines and an aspartate, with both zinc ions sharing a monodentate bridge by an aspartate residue and most sharing a bridging water. Although a bridging water is not modeled into the ZipD structure, its presence may be obscured by the resolution of the diffraction (2.9 Å). Due to its proximity to both zinc ions, this conserved bridging water is likely bound as a hydroxide ion, which is proposed to be the hydrolytic nucleophile (Figure 15),[43] similar to its function in other superfamily members.[58] The Zn1 and Zn2 of AidC also each coordinate to their own apical water molecules, illustrating the proposed coordination sites for the lactone carbonyl oxygen and ring oxygen in AHL substrates, respectively. In all cases, the Zn-to-Zn distances are all very similar (see Figure 15 legend for relevant distances).

There is one notable difference in AidC immediately adjacent to the dinculear zinc cluster. All of the AHL lactonases previously characterized have a Tyr (Y194 in AiiA; Figure 15B) that we previously proposed as a H-bond donor to help stabilize a tetrahedral adduct formed in the hydrolysis reaction.[43] However, this position in AidC is instead occupied by His261 (Figure 15A). Although, the related organic phosphotriesterase OPHC2 has a Leu at this position (Figure 15C), and likely does not use this residue during catalysis, the homologous phosphodiesterase ZipD does places a His side chain in the same structural position (Figure 15D), with the residue coming from a position later in the primary sequence.

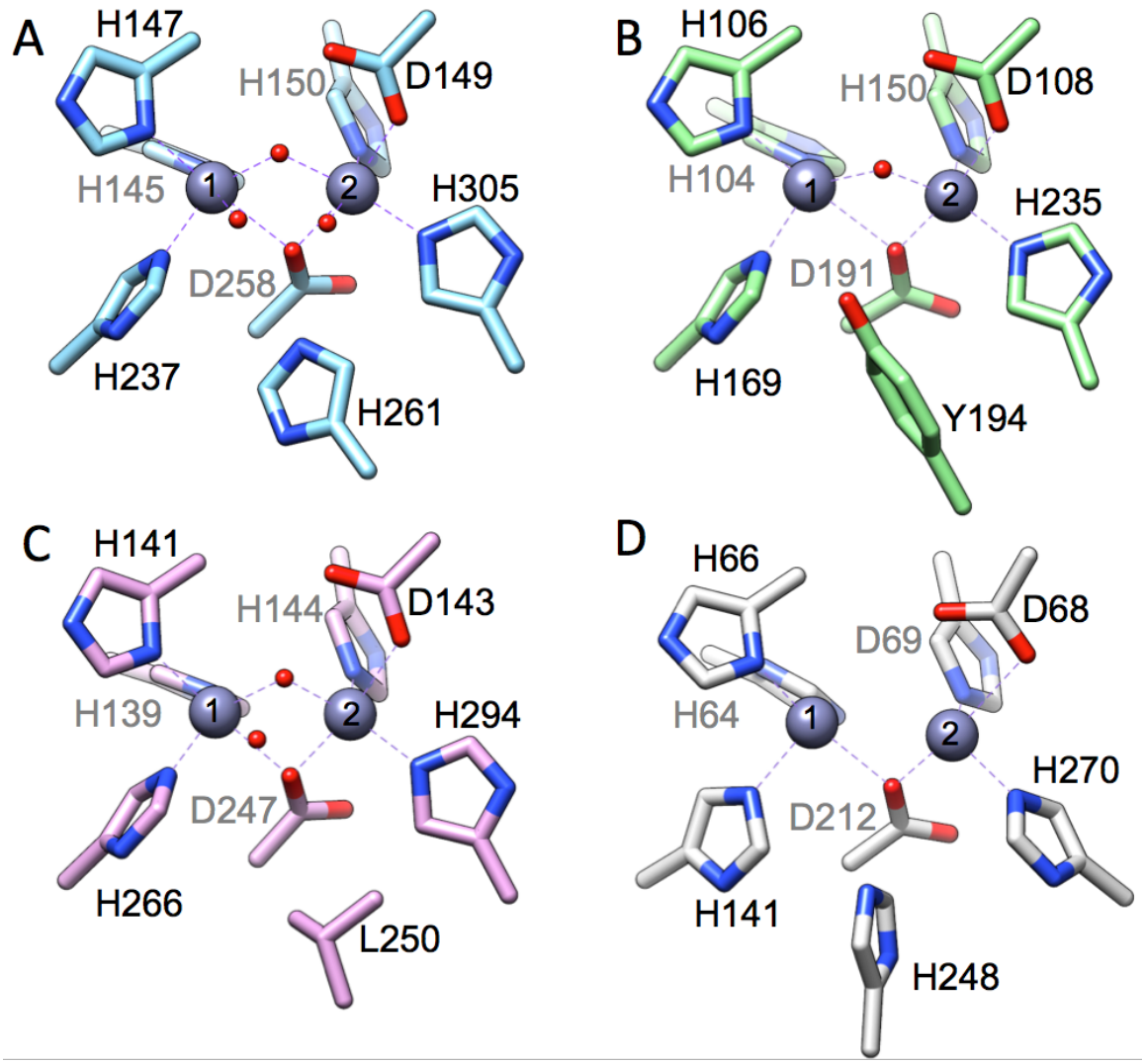

Figure 15. Unliganded Active-Site Structures. A. Active-site structure of AidC (blue). Protein residues are shown as sticks, and zinc ions (grey) and water molecules (red) as spheres, with oxygens in red and nitrogens in blue. The Zn-to-Zn distance is 3.3 Å; the Zn-O distances to the bridging hydroxide are 1.9 and 2.0 Å; The distance from Zn1 to its apical water is 2.7 Å, and Zn2 to its apical water is 2.5 Å; The distance from the bridging hydroxide to the non-chelating O of D149 is 2.7 Å; and the distance from His261 $^{\varepsilon}$N to the Zn1 and Zn2 apical waters is 3.4 and 3.0 Å, respectively. B. Active site structure of AiiA (green, from PDB: 2A7M). The Zn-to-Zn

distance is 3.3 Å; The Zn-O distances to the bridging hydroxide are 2.1 and 2.0 Å; and the distance from the bridging hydroxide to the non-chelating O of D108 is 2.8 Å. C. Active site structure of OPHC2 (pink, from PDB: 4LE6). The Zn-to-Zn distance is 3.2 Å; The Zn-O distances to the bridging hydroxide are both 2.2 Å; and the distance from the bridging hydroxide to the non-chelating O of D143 is 2.7 Å. D. Active site structure of ZipD (grey, from PDB: 2CBN). The Zn-to-Zn distance is 3.3 Å. No bridging or apical waters were modeled into the structure, possibly due to the limited diffraction resolution (2.9 Å).

Our determination of the AidC structure allows a structural alignment to be constructed that helps to correct some prior predictions based on primary sequence alignments (Figure 16). Leu259 was predicted to replace the zinc-bridging Asp residue,[19] but Asp258 is seen here to retain this role. Also Ser262 was predicted to replace the Tyr adjacent to the active site, but, as discussed above,[19] the His261 side chain is shown to occupy this position.

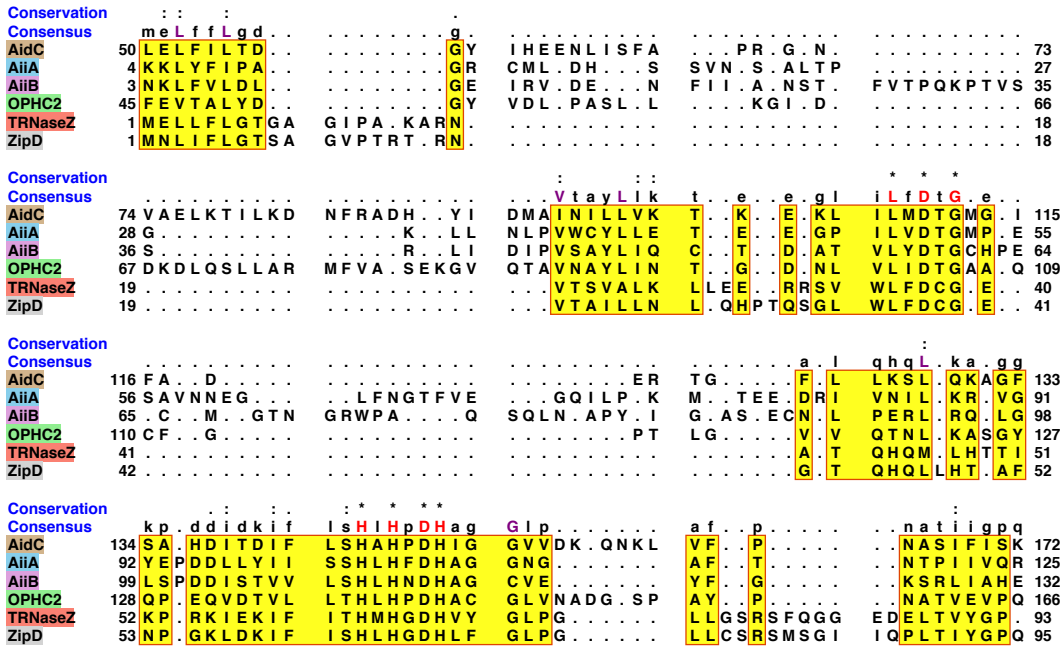

A

B

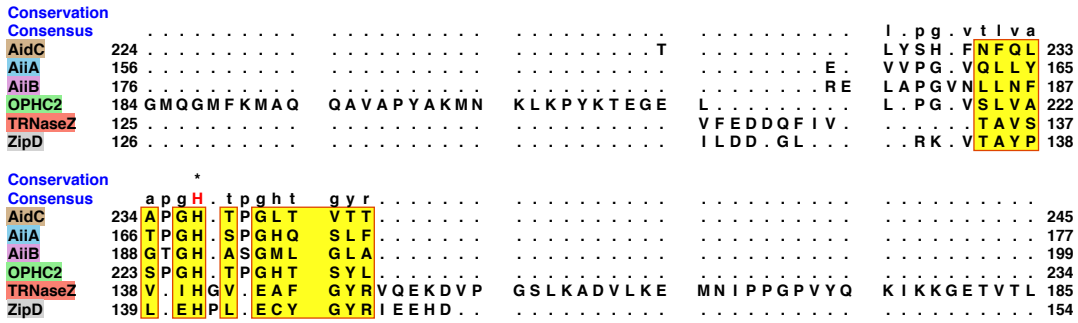

C

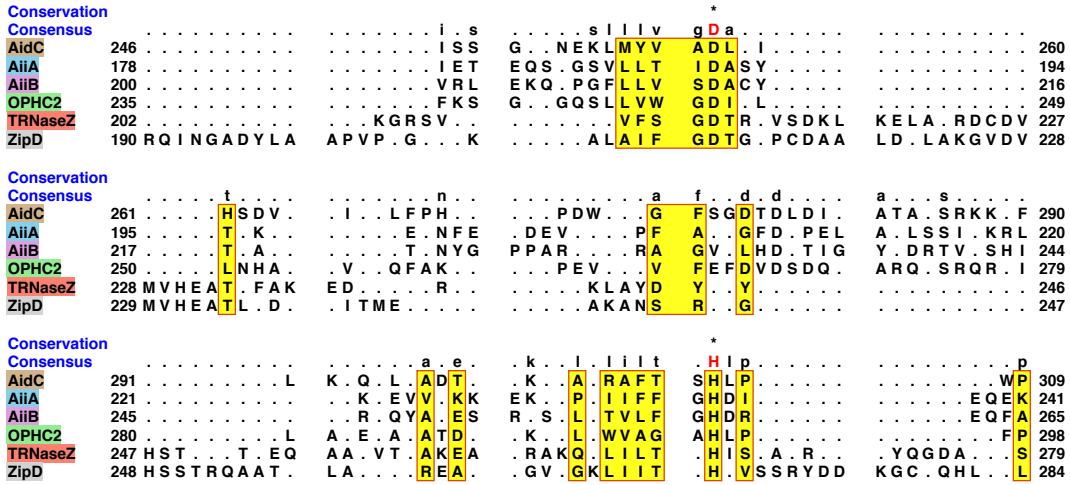

Figure 16. Structure-Based Sequence Alignment of AHL lactonases and Homlogs: AidC, AiiA, AiiB, OPHC2, tRNAseZ, and ZipD. The structural models of AidC, AiiA (PDB: 2A7M), AiiB (PDB: 2R2D), OPHC2 (PDB: 4LE6), tRNaseZ (PDB: 1Y44), and ZipD (PDB: 2CBN) are superimposed and a structure-based sequence alignment calculated using the program UCSF Chimera (Pettersen, EF, Goddard, TD, Huang, CC, Couch, GS, Greenblatt, DM, Meng, EC, Ferrin, TE. UCSF Chimera: A visualization system for exploratory research and analysis. *J. Comput. Chem.* **2004**, *25*, 1605-1612). Only three separate regions of the entire alignment have

significant structural overlap, and are presented above as A, B and C, with the fully populated columns highlighted in yellow. Primary references for the PDB entries are as follows: AidC (this work); AiiA (2A7M); AiiB (2R2D); OPHC2 (4LE6); tRNaseZ (1Y44); and ZipD (2CBN).

AidC product complex

Addition of the substrate C6-HSL to the crystallization mixture allowed us to characterize the interactions of product with the AidC active site (Figure 17A). Although technically this experiment could be classified as co-crystallization, the substrate and enzyme were incubated together for three days before the mixture was "seeded" with unliganded AidC crystals. Therefore this procedure may be more akin to co-crystallization with product, or if the unliganded AidC seeding biases the resulting conformation, crystal soaking with the product. Regardless, the experiment resulted in a structure in which product was bound at the active site of AidC.

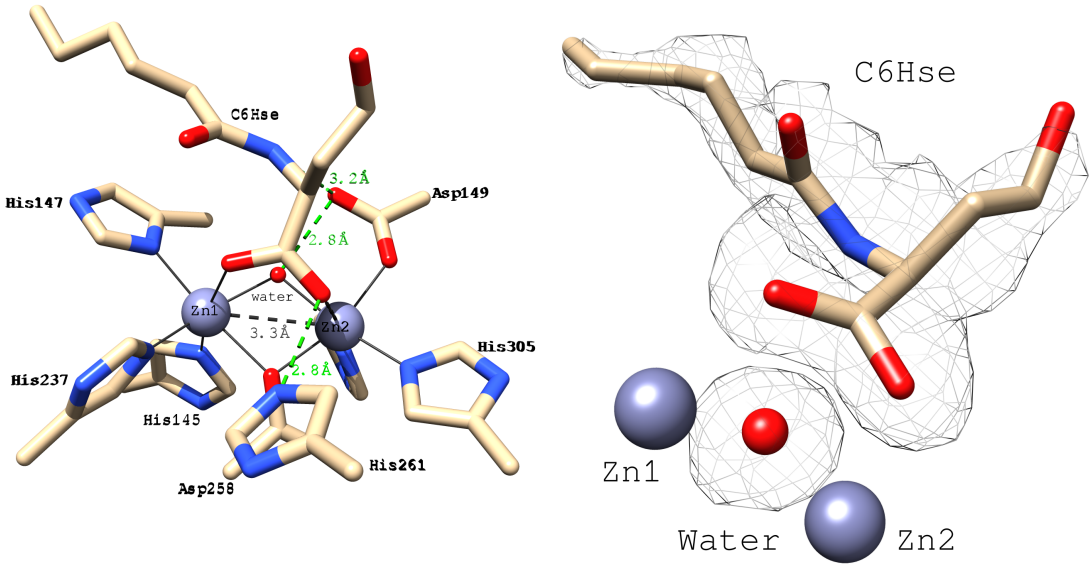

Figure 17. C6-Hse Product Bound Structure of AidC. A. Active site of AidC bound to product C6-Hse. Carbon atoms are in light blue, oxygen in red, nitrogen in dark blue, and zinc in grey. The green dotted line represents the hydrogen bonds formed between the C6-Hse and AidC. Zn-Zn distance is shown as a grey dotted line. B. Simulated Annealing Omit Map (Fo-Fc) for Product. The omit map is shown as a grey mesh at 2.2 σ. The omit map was generated with both the C6-Hse and bridging hydroxide omitted from the coordinates. Carbon atoms are in light blue, oxygen in red, nitrogen in dark blue, and zinc in grey.

The simulated annealing omit map (Fo-Fc) electron density found at the active site of AidC monomer A is very well defined and matches with the ring-opened product C6-Hse (Figure 17 B). The density at the same relative position in monomer B is also consistent with fitting C6-Hse, but is less well defined. The newly-formed product carboxylate coordinates both zinc ions, bridging the site in a bidentate fashion (A). The positioning of the amide and alcohol substituents are generally similar to that seen in the product complex with the homologous AHL lactonase AiiA (Figure 17),[14] however there are some differences. In AidC, the product carboxylate oxygens are farther from the zinc ions (~ 2.5 Å) than those in product-bound AiiA (~ 2.1 Å). Also, the AidC product complex has a closer Zn-to-Zn distance (3.2 Å) and retains a bridging hydroxide, but the AiiA product complex has a longer Zn-to-Zn distance (3.7 Å) and is missing the bridging hydroxide. If AidC and AiiA use the same catalytic mechanism, these two structures may represent different steps along the reaction coordinate. The AiiA structure shows that the product closely associates with the zinc ions after ring opening, and the AidC structure may illustrate how the product is then displaced by reforming the hydroxide bridge, reducing the Zn-to-Zn distance and lengthening the bonds between the product and the zinc ions. The

product-bound AidC complex may also shed light on the relative positioning of substrate at the active site. The bridging hydroxide is only 2.6 Å from the carbonyl carbon of the product; this close positioning may mimic the substrate bound complex in which hydroxide attacks this substrate carbonyl. However, the $^{-}$OH-C4-O2 angle is only 78°, so the product is likely angled differently than substrate, for which a larger, more typical Bürgi-Dunitz angle[59] would be predicted.

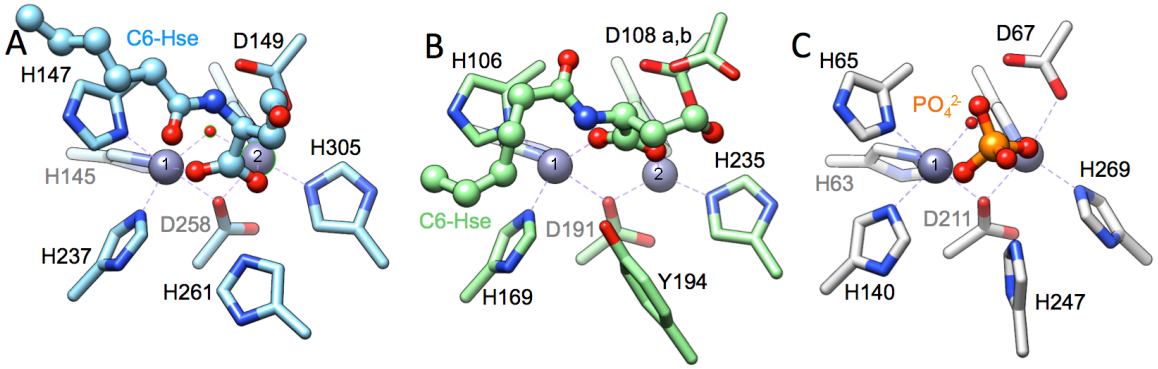

Figure 18. Product-Bound Active-Site Structures. In all cases the liganded product is shown as ball and stick, and the binding site consisting of protein residues is shown as sticks, with heteroatom coloring as above. A. Active-site structure of AidC bound to C6-Hse (blue). Measurements are given for monomer A. The Zn-to-Zn distance is 3.3 Å; the Zn-O distances to product are each 2.5 Å, and the Zn-O distances to the bridging hydroxide are each 2.0 Å. The H261 N^{ε} is 3.6 and 2.7 Å from the product carboxylate oxygens. B. Active site structure of AiiA bound to product (green, from 3DHB). The Zn-to-Zn distance is 3.7 Å; the Zn-O distances to product are 2.0 and 2.1 Å; and the distance of the leaving group alcohol to the closest O of the unchelated conformer of D108 is 2.6 Å. The Y194 phenol O is 3.8 and 4.0 Å from the product carboxylate oxygens. C. Active site structure of tRNase Z bound to phosphate (grey, from

1Y44). tRNase Z and ZipD (Figure 15D) are different proteins, but both are colored grey to indicate that they are both phosphodiesterases. The Zn-to-Zn distance is 3.3 Å; the Zn-O distances to the bridging hydroxide are 2.0 and 2.3 Å; the Zn-O distances to product are 2.3 and 2.5 Å; the distance from the closest O of D67 and PO_4^{2-} is 3.6 Å, and the other non-chelating O of PO_4^{2-} is 3.1 Å from the N^{ε} of His247.

One particular amino acid substitution raises the possibility that the AidC mechanism might diverge from that of AiiA. In AiiA, the Y194 residue was proposed to help stabilize the tetrahedral adduct formed upon initial hydroxide attack.[15] However the H261 residue in AidC, which occupies the same relative position, has a lower predicted pK_a value. Additionally, the H261 N^{ε} is more distant (3.6 Å) from the product oxygen that is placed where the carbonyl of the substrate is predicted to occupy than it is to the product oxygen that placed where the leaving group of the substrate is predicted to occupy (2.7 Å). This arrangement suggests a possible participation in ring opening through general acid / base catalysis, a mechanism reminiscent of that proposed for the homologous phosphodiesterase tRNAse Z in which a structurally conserved histidine is proposed to act as a general acid during hydrolysis.[60] In the phosphate bound structure of tRNAse Z, the structurally analogous histidine (His247) can be seen within H-bonding distance (3.1 Å) to one of the phosphate oxygens (Figure 18C).[61] (Since a product-bound ZipD structure is not available, we consider instead the homologous phosphodiesterase tRNAse Z, which also contains this active-site His substitution.) Further studies will be required to see if AidC uses His261 as a mimic of Y194 in AiiA, or if it instead uses this residue for general acid / base catalysis or a different function.

The N-alkyl substituent binding pocket and a mechanism for selectivity

The most striking difference between the product-bound AidC and AiiA structures are the binding pockets for the *N*-acyl substituents of the products (Figure 19). AidC contains a hydrophobic pocket, formed in part by the 'kinked' α-helix that completely surrounds the terminal part of the *N*-acyl substituent, which is buried below the surface of the protein (Figure 19A, 20B, 11B). In contrast, AiiA instead only cradles the *N*-acyl substituent of C6-Hse along a wide and shallow hydrophobic trough found on the surface of the enzyme (Figure 19C, 20D).[14] Products with longer *N*-acyl substituents can also bind to AiiA in an alternative orientation (not shown) in which they receive some additional stabilization by a "phenylalanine-clamp."[16] However, in contrast to the relatively open *N*-acyl binding site in AiiA, AidC instead contains a closed, well-defined *N*-acyl binding pocket that is unlike the substrate binding pockets in all previously characterized AHL lactonases in the superfamily, and this pocket is likely the major contributor to the uniquely low K_M values observed for substrates of this enzyme.

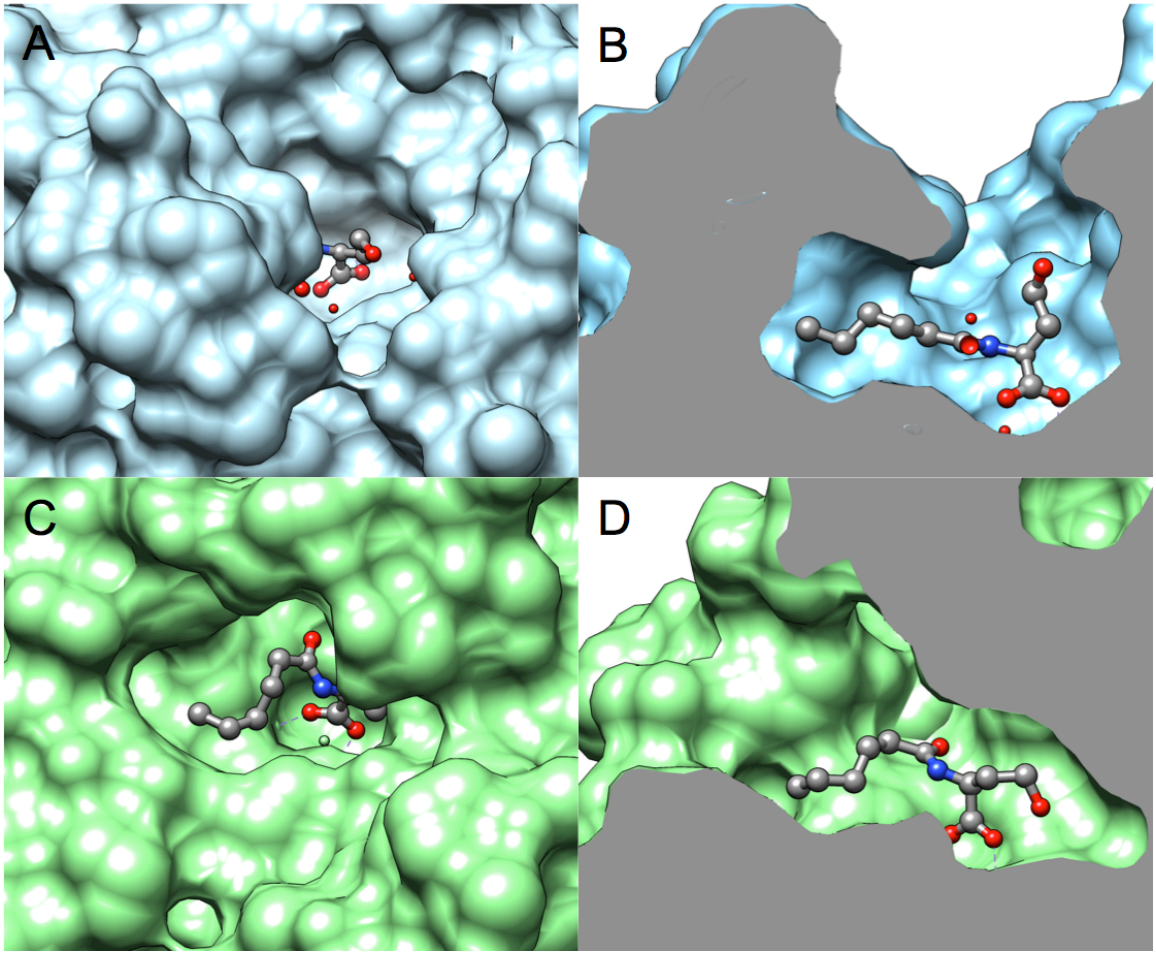

Figure 19. *N*-Acyl Chain Binding Pockets. A. A surface coated AidC (blue) is shown with the C6-Hse product as ball and stick (carbons in grey, heteroatoms as above). The *N*-acyl chain of the product is buried below the surface. B. A rotated, cut-away view of Figure 19A, showing a defined pocket for binding the *N*-acyl chain of the product, while the opened ring is pointing toward solvent. C. A surface coated AiiA (green, from PDB: 3DHB) is shown with the C6-Hse product as ball and stick (coloring as above). The *N*-acyl chain lies in a shallow groove of the enzyme and is visible from the surface. D. A rotated, cut-away view of Figure 19C, showing the *N*-acyl chain of the product extending toward the solvent and the opened ring enclosed in a more defined pocket.

This binding pocket suggests a mechanism whereby AidC can impose substrate selectivity. Substrates with short *N*-acyl substituents would not be able to reach as deeply into the pocket and bury as much hydrophobic surface as longer, more favored substrates, and a resulting difference in K_M values would ensue. For example C4-HSL has a 10-fold higher K_M value than C7-HSL, but the differences in k_{cat} values are more minor. The same effect is seen with substrates containing very bulky *N*-acyl substituents that can not easily enter the buried pocket, such as cinnamoyl- and t-BOC-HSL, which have K_M values 10- and 16-fold higher than C7-HSL, again with lesser effects on k_{cat} values. In contrast, substrates with longer *N*-acyl substituents would be disfavored by a different mechanism. The long alkyl substitutions on these substrates could easily enter and fully occupy the binding pocket, but as the length of this substituent increases, the attached lactone group would be held farther away from the catalytic dinuclear zinc center, for which a difference in k_{cat} values would be predicted. For example, C12-HSL actually has a 7-fold lower K_M value than C7-HSL, but catalysis is more significantly impaired, as seen in the 200-fold lower k_{cat} value. This selectivity mechanism is different than that used by other AHL lactonases characterized to date. However, we have shown that the nonhomologous, metal-independent *N*-terminal nucleophile hydrolase PvdQ uses a similar strategy to discriminate between *N*-acyl-HSL substrates of different lengths.[62]

CONCLUSIONS

The quorum-quenching AHL lactonase from the potato root-associated *Chryseobacterium* sp. strain StRB126, AidC, has an unusually low K_M value for AHL substrates and displays a stricter substrate selectivity than any other related AHL lactonase characterized to date. At the time of writing, AidC also has the highest reported k_{cat}/K_M value for any characterized wild-type

quorum-quenching enzyme, regardless of superfamily. Structural determination of AidC alone, and with bound product, reveals an unusual 'kinked' helix and suggests a structural-basis for the enhanced selectivity. Further studies will be required to determine how and if this selectivity impacts the chemical ecology of *Chryseobacterium* sp., but we note that *Erwinia carotovora*, a phytopathogen relevant to potatoes, produces AHLs within the optimal range for AidC substrates[63], and that AHL lactonases have been shown to impact rhizosphere competence.[64] Intriguingly, AidC shows some structural similarities that more closely match families more distant from AHL lactonases, sharing a dimeric structure similar to an organic phosphotriesterase and an active-site histidine residue similar to that found in related phosphodiesterases. Tawfik and co-workers have identified an entirely different superfamily in which both paraoxonase and lactonase activities have evolved,[65–67] and may, by comparison, provide insight into the relationship of the various activities found in AHL lactonase homologs. AidC serves as an example for understanding how quorum-quenching enzymes can achieve selectivity between structurally similar AHL substrates, and may serve as an efficient catalytic template amenable to further optimization for a broad array of quorum-quenching applications.

MATERIALS AND METHODS

Materials

Unless otherwise noted, all chemicals were purchased from Sigma-Aldrich Chemical Co. (St. Louis, MO), and all enzymes used for cloning were purchased from New England BioLabs (Beverly, MA). The lactones assayed as substrates, γ-butyrolactone (GBL) and *tert*-butyl(tetrahydro-2-oxo-3-furanyl)carbamate (t-BOC-HSL), were purchased from Sigma-Aldrich Chemical Co. (St. Louis, MO). *N*-Butyryl-L-homoserine lactone (C4-HSL) and *N*-3-oxo-octanoyl-L-homoserine lactone (3-oxo-C8-HSL) were from Cayman Chemical Co. (Ann Arbor, MI). *N*-Pentanoyl-(*S*)-homoserine lactone (C5-HSL), *N*-hexanoyl-(*S*)-homoserine lactone (C6-HSL), *N*-heptanoyl-(*S*)-homoserine lactone (C7-HSL), *N*-octanoyl-(*S*)-homoserine lactone (C8-HSL), *N*-decanoyl-(*S*)-homoserine lactone (C10-HSL), *N*-dodecanoyl-(*S*)-homoserine lactone (C12-HSL), and *N*-cinnamoyl-(*S*)-HSL (C-HSL) were synthesized from (*S*)-α-amino-γ-butyrolactone hydrochloride and the corresponding acyl chloride similar to the methods described previously.[15,18] Substrate stock solutions were prepared in methanol, with the final assay mixtures containing 1% methanol cosolvent.

Cloning, expression and purification of AidC

The coding sequence for AidC from *Chryseobacterium* sp. Strain StRB126, was codon optimized for expression in *Escherichia coli*; a sequence encoding the cleavage site for tobacco etch virus (TEV) protease (ENLYFQG) was inserted at the 5' end of the AidC coding region; restriction sites *Eco*R1 and *Nde*1 were added to the 5' and 3' ends, respectively; and the resulting sequence was ordered from Integrated DNA Technologies, Inc. (Figure 8). A shuttle vector

carrying the synthesized gene and a commercial protein expression vector, pMAL-C5X (New England Biolabs, Beverly, MA), were both digested using restriction enzymes EcoR1 and Nde1, and the resulting insert containing *aid*C was ligated into the expression vector using T4 DNA Ligase (New England Biolabs, Beverly, MA) to yield a protein expression plasmid encoding an *N*-terminal maltose binding protein (MBP) linked through a TEV cleavage sequence to the full length AidC enzyme. The resulting vector (pMAL-t-AidC) was used to transform *E.coli* DH5α cells for plasmid storage and amplification. The entire coding region in pMAL-t-AidC was verified by DNA sequencing to determine that there were no unintended mutations (CRC DNA Sequencing, University of Chicago).

For protein production and purification, pMAL-t-AidC was used to transform *E. coli* BL21(DE3) cells. The resulting *E. coli* BL21(DE3)(pMAL-t-AidC) cells were incubated at 37 °C while shaking in Luria-Bertani (LB) medium supplemented with 100 μg/mL ampicillin. When the culture OD_{600} value reached 0.6-0.8 absorbance units, expression of the MBP-t-AidC fusion protein was induced by addition of 0.3 mM IPTG. The LB medium was supplemented with 0.5 mM $ZnSO_4$, and expression was continued for an additional 16-18 h at 25 °C after induction. Cells were harvested by centrifugation at 12400 × *g*, washed with Wash Buffer (20 mM Tris-HCl buffer with 200 mM NaCl at pH 7.4), and stored at -80 °C after flash freezing in liquid nitrogen. The frozen cell pellet was thawed, sonicated in Wash Buffer, and centrifuged at 40000 × *g* to pellet cell debris, which was discarded. The resulting supernatant was loaded onto an amylose affinity column (16 × 25 mm Dextrin Sepharose – MBL Trap HP, GE LifeSciences, preequilibrated with Wash Buffer). The column was washed with Wash Buffer and the MBP-t-AidC fusion protein was eluted from the column using Wash Buffer supplemented with maltose

(10 mM). Fractions were evaluated using coomassie-stained SDS-PAGE, and those fractions containing MBP-t-AidC were combined and treated batch-wise with TEV protease, following previously published protocols.[48] The resulting cleaved proteins were exchanged into Ion Exchange Buffer (20mM Tris-HCl, 5mM NaCl at pH 7.5) and loaded onto a column (XK 16/20 GE LifeSciences) loaded with diethylaminoethanol (DEAE)-sepharose ion exchange resin to separate MBP, TEV protease and the untagged AidC. The column was equilibrated with Ion Exchange Buffer (20 mM Tris-HCl, 5 mM NaCl at pH 7.5) and after loading, the protein eluted by a linear gradient between Ion Exchange Buffer and the same buffer supplemented by 1 M NaCl. Fractions containing untagged AidC protein were pooled, concentrated using a 10,000 molecular weight cut off (MWCO) Amicon-Ultra centrifugal filter device (Millipore, MA), and further purified by size exclusion chromatography using a HiLoad Superdex-200PG column, 16 × 600 mm (GE Lifesciences, CA). The column was equilibrated and the protein was purified using Size Exclusion Buffer (50 mM HEPES buffer, 300 mM NaCl, pH 7.5). During the purification, fractions were assayed for the presence of MBP-t-AidC or AidC at each step by using 12% SDS-PAGE, followed by staining with EX-Run Gel Staining Solution (Fisher BioReagents) to detect bands at ~ 75 or ~ 32 kDa, respectively. The final purified untagged AidC protein appeared homogenous when characterized on a Coomassie-stained 12% SDS-PAGE gel. Protein concentrations in solution were measured using bovine serum albumin (BSA) standards and the Bradford assay (BioRad). This purification procedure typically results in a yield of 10 mg of purified untagged AidC / L culture media.

Determining the zinc dependence, steady-state kinetic parameters, and zinc content of purified AidC

Substrate hydrolysis rates were monitored using a previously described continuous spectrophotometric assay in which the pH indicator phenol red acts as part of the Assay Buffer (1 mM Hepes at pH 7.5), and results in a change in colorimetric signal upon protonation by the net release of a proton upon lactone hydrolysis.[48] The optimal Assay Buffer zinc concentration was determined by monitoring hydrolysis of saturating concentrations of C6-HSL (1 mM) as catalyzed by AidC (27 nM) to determine the maximum observed initial rates upon varying the zinc concentration (0 – 100 μM). To determine the relationship between AidC concentration and k_{cat}, the substrate *t*-BOC-HSL (5 mM) was used at saturating concentrations while the enzyme concentration was varied (0 – 250 nM). The concentration of AidC was determined using a calculated[20] extinction coefficient (ε_{280} = 29160 $M^{-1}cm^{-1}$). The stoichiometry of bound zinc ions to protein in purified AidC was determined by dividing the total zinc concentration determined using the colorimetric chelator 4-(2-pyridylazo)resorcinol under denaturing conditions, as described previously,[68] by the concentration of AidC.

Crystallization

Purified AidC was concentrated to 20 mg/mL using a 10,000 molecular weight cut off (MWCO) Amicon-Ultra centrifugal filter device (Millipore, MA), and the concentrated protein was buffer exchanged into Crystallization Screening Buffer (50mM HEPES, pH 7.0). Crystallization screens (Crystal Screen 1 & 2, Crystal Screen Cryo 1 & 2, PEG Ion 1 & 2 and Index1 & 2 from Hampton Research and Wizard 1 & 2 from Emerald BioSystems) were prepared using a Crystal Gryphon (ArtRobbins) crystallization robot using a ratio of 1:1 for Well Solution: AidC stock solution (20 mg/mL). Crystals appeared in the well solution containing $MgCl_2.6H_2O$ (0.2 M), Bis-Tris (0.1 M), pH 6.5, 25 % (w/v) PEG 3350 after a week when

incubated at room temperature. Crystallization was repeated and optimized using a 1:2 ratio of Well Solution:AidC (20 mg/mL) in sitting drops, and seeded on day 3 with AidC crystals obtained from previous trials. Crystallization was done in 24 well Cryschem Plates (Hampton Research). For co-crystallization of AidC and substrate, 4 μL of AidC (20 mg/mL) was mixed with 1 μL of Well Solution and 1 μL of 10 mM C6-HSL (dissolved in 50 % methanol). Crystals formed within a week after seeding, during which C6-HSL likely hydrolyzed to the ring-opened product *N*-hexanoyl-L-homoserine (C6-Hse). AidC and AidC:C6-Hse crystals with the best morphology were transferred into a cryo-protecting solution (Well Solution supplemented with 25 % (v/v) glycerol) and then into liquid nitrogen.

Data collection and processing

Monochromatic data sets were collected at the 19-BM beamline at the Structural Biology Center (SBC), Advanced Photon Source (APS) at Argonne National Laboratory (ANL). Diffraction data was collected at a wavelength of 0.98 Å at 100 °K using a Quantum 210r Charge Coupled Device (CCD) detector from Area Detector Systems Corporation (ADSC). All collected data sets were indexed and integrated using iMosflm[69] and scaled using Scala in the CCP4 program suite.[70] The best data sets were processed at resolutions of 1.09 Å and 1.67 Å for AidC and AidC:C6Hse, respectively. Data collection statistics are summarized in Table 1.

Structure determination, model building and refinement

The AidC structure was solved by molecular replacement using PHASER in the Phenix software suit.[71] The initial search model was a poly-alanine model created based on a previously published structure of the organic phosphotriesterase OPHC2 (PDB Code: 4LE6;

Organophosphate hydrolase C2 from *Pseudomonas pseudoalcaligenes*),[56] because this enzyme shares 26 % amino acid sequence identity with AidC. The program Phenix.Autobuild was used to build the residue side chains based on the phases obtained from running PHASER; Phenix.Autobuild uses iterative cycles of model building and refinement until no more side chains can be built in automatically.[71] The AidC:C6Hse structure was solved by molecular replacement using PHASER in the CCP4 software suit; the search model was the unliganded AidC structure.[70] Both models were rebuilt and refined using the program Phenix[24] and analyzed using the programs COOT[72] and UCSF Chimera.[73] Final refinement statistics are presented in Table 1. Structural figures were made using UCSF Chimera.

Determining oligomeric states of AidC and AiiA

To determine the molecular mass of AidC oligomers in solution, we used size-exclusion chromatography coupled with multi-angle light scattering (SEC-MALS). Our experimental setup included an AKTA FPLC (GE Healthcare Biosciences) with a silica-based size-exclusion chromatography column (WTC-030S5; Wyatt Technology) as a liquid chromatography unit. Downstream of the column is a refractive index detector (Optilab T-rEX; Wyatt Technology), followed by a multi-angle light scattering detector (Dawn Heleos II; Wyatt Technology) used for determining protein concentration and particle size, respectively. As a control sample, we analyzed the related AHL lactonase AiiA, which is of similar monomeric size and has previously been demonstrated by analytical ultracentrifugation to be a monomer in solution.[13] Each sample injection consisted of approximately 0.5 to 1 mg (injection volume 95 μL) of purified protein (either AiiA or AidC) in buffer containing 50 mM HEPES, 300 mM NaCl at pH 7.5. Flow rate

was set at 0.4 mL / min, and data were collected at 2 second intervals. Data processing and analysis were performed using the ASTRA software (Wyatt Technology).

CHAPTER THREE

N-(2-OXOCYCLOBUTYL) DECANAMIDE AS A TRANSITION STATE MIMETIC FOR AN AHL LACTONASE AiiA FROM *Bacillus Thuringiensis*

INTRODUCTION

Enzymes capable of hydrolyzing *N*-acyl-L-homoserine (AHL) lactones are of important significance because they disrupt the signal molecule used in cell-to-cell communication in bacteria[1]. Studying the mechanism of these enzymes provides insight into bacterial quorum sensing and is useful when designing more efficient quorum quenching enzymes. AiiA, a metalloenzyme enzyme from *Bacillus sp.* is the best characterized AHL-lactonase to date. Based on structural and functional studies, a catalytic mechanism has been proposed for AiiA (Figure 20).[12,13,14] The crystal structures of AiiA (Figure 20:I)[13] and AiiA bound to product (Figure 20:V)[13,14] represents two states in the catalytic cycle. Structural data supports three states of the enzyme represented as I, IV and V in the proposed mechanism in Figure 20.

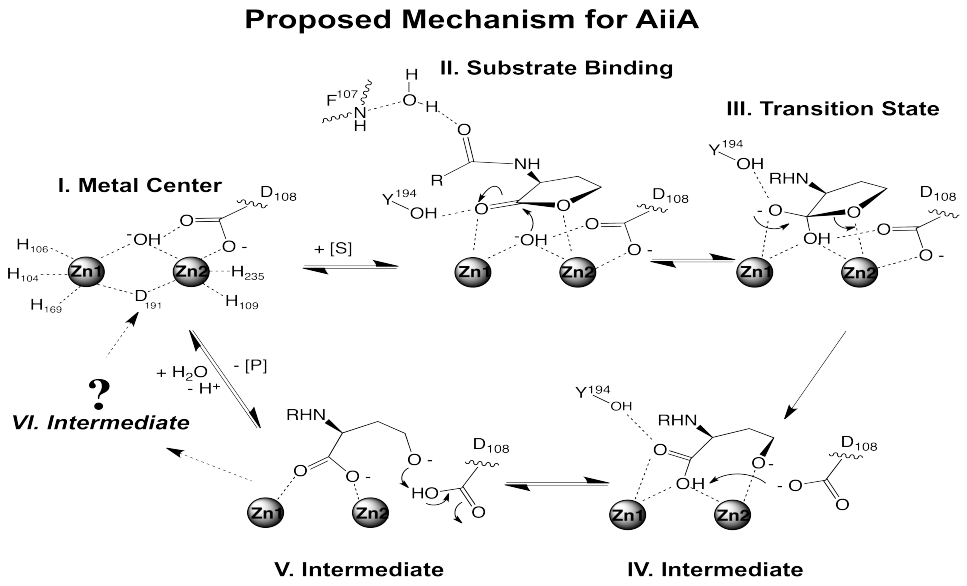

Figure 20**:** Proposed mechanism for AiiA

To gain further insight into the mechanism of AiiA lactonase, we collaborated with the Becker group at Loyola University, Chicago to study N-(2-oxocyclobutyl) decanamide (**2**) as an analog to trap the proposed tetrahedral transition-state in the mechanism of AiiA. Inhibition assays were performed at varying concentrations of (**2)**. Co-crystallization of AiiA-Co with (**2**) revealed the structure of a ring-opened byproduct —4-decanamideobutanoic acid (**3**). Experiments were performed to determine if the ring-opened byproduct (**3**) was formed by enzyme mediated catalysis or as a result of exposure to X-ray radiation during data collection.

RESULTS AND DISCUSSION

Kinetic assays were conducted to test the effects of **(2)** on the activity of AiiA-Co and crystallography experiments were conducted to gain structural insight into the mechanism of AiiA.

Inhibition Assay of AiiA-Co with N-(2-oxocyclobutyl) decanamide (**2**)

A previously published continuous assay with details described in methods was used to test the effects of (**2**) on the activity of AiiA by plotting activity versus concentration of N-(2-oxocyclobutyl) decanamide (**2**).

Inhibition assays were carried out at substrate (C7-HSL) concentrations of 0.5, 1.0 and, 2.5mM. The IC_{50} values at these 3 concentrations were 0.06 ±0.02, 0.10±0.03 and, 0.38±0.04, respectively. Figure 21 shows the plots of activity (Au/s) versus concentrations of the inhibitor **(2)**.

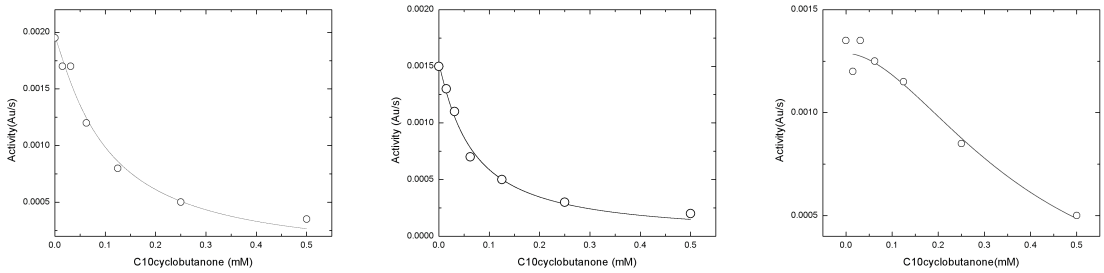

Figure 21: The plots show inhibition (C10 cyclobutanone) curves at substrate (c7homoserine lactone) concentrations of 0.5, 1.0, 2.5mM, respectively.

The plots show the IC_{50} value increases with increase in concentration of substrate. From this data we can conclude that N-(2-oxocyclobutyl) decanamide is a competitive inhibitor of AiiA.

Crystal Structure of AiiA-N-(2-oxocyclobutyl) decanamide (AiiA-C10CBO)

The structure of AiiA-C10CBO was solved by molecular replacement using a monomer of a known AiiA-Zn structure as a search model (PDB: 2A7M) after deleting all water and ligand molecules in the space group $P2_12_12_1$. Multiple cycles of model building and refinement were conducted and the final model was refined to a resolution of 1.6 Å with R_{free}/R_{work} values of 20.64/17.72. Final refinement statistics are shown in Table 4.

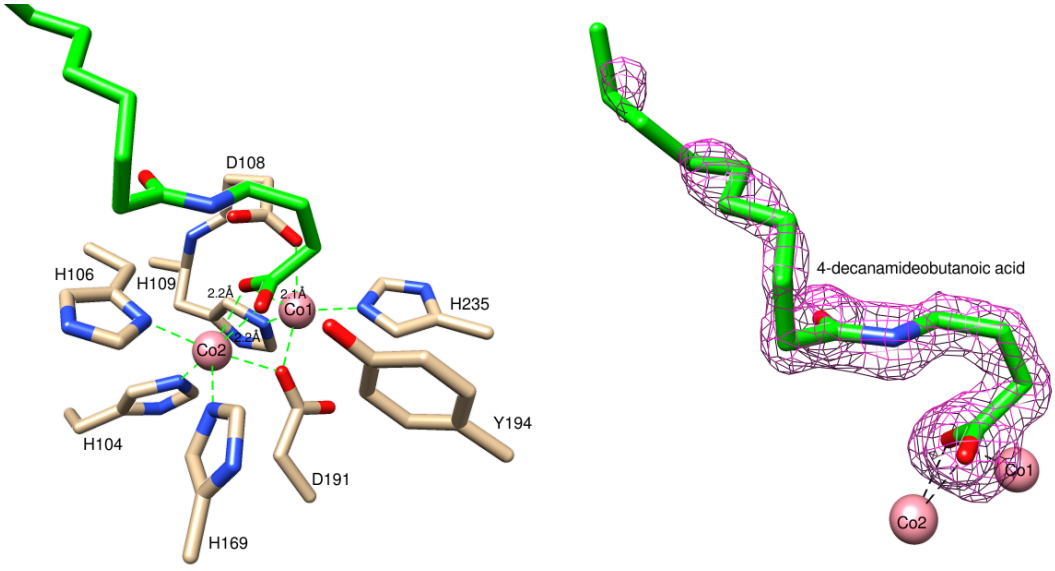

Figure 22: Active site of AiiA-C10CBO. **A.** The atoms representing the protein are shown in tan and the metal atoms (Cobalt) are shown in pink. Heteroatoms oxygen and nitrogen are represented in red and blue, respectively. C10CBO is shown in green. **B.** Represents a *Fo-Fc* map shown as a pink mesh at 2.5σ.

There are no changes in the overall structure of AiiA-C10CBO when compared to that of AiiA. The extra density at the active site after model building and refinement of the protein and solvent molecules was interpreted as 4-decanamideobutanoic acid (**3**) (Figure 22A)**.** Figure 22B shows a *Fo-Fc* map at 2.5σ superimposed with a model of **(3)**. The structure of the active site of AiiA bound to **(3)** shows cleavage of a C-C bond occurred when **(2)** was co-crystallized with AiiA. However, it is uncertain if this ring-opening reaction occurred during catalysis by the enzyme while soaking **(2)** with AiiA crystals, or due to X-ray radiation during data collection. In the crystal structure of AiiA-Zn bound to the product C6 homoserine (PDB:3DHB), a water molecule bridges the two Zn atoms at the active site. This structure is proposed to represent the active site of AiiA during product release and regeneration with the bridging water. In the crystal structure of AiiA-C10CBO we do not see a bridging water in the active site at AiiA. This position is possibly occupied by the oxygen atoms of (**3**) as seen on Figure 22. Therefore the

formation of byproduct **(3)** in the crystal structure of AiiA-C10CBO, possibly depicts one of the intermediates that is formed during the enzyme mechanism of AiiA (Figure 20).

Table 4. Crystallographic Data for AiiA-C10CBO

	AiiA-C10CBO
Data Processing	
Space group	$P2_12_12_1$
Cell dimension	
α, β, γ (deg)	90.0, 90.0, 90.0
a, b, c (Å)	54.7, 55.6, 80.6
Resolution (Å)	1.54
Resolution at I/σ (I) = 2	1.66
R_{merge} [a] (%)	8.0(125.2)[b]
I/σ (I)	17.7(1.05)
R_{pim} [c] (%)	5.5(83.3)
CC ½ [d]	0.998(0.361)
Completeness (%)	98.2(88.0)
Multiplicity	5.5(2.7)
No. Reflections	210994
No. Unique Reflections	38625
Refinement	
R_{work} [e]/R_{free} [f](%)	17.72/20.64
No. of Atoms	
protein	2086
ligand	270
water	18
B factors	
protein	19.3
ligand	20.7
Rmsd [g]	
bond lengths (Å)	0.008
bond angles (deg)	1.045
Ramachandran plot (%)	
most favored	96.0
allowed	3.6
outliers	0.4

[a] **R**merge = **Σ**|**I**obs − **I**avg|/**ΣI**avg.
[b] The values for the highest-resolution bin are in parentheses.
[c] Precision-indicating merging **R**
[d] Pearson correlation coefficient of two "half"data sets.
[e] **R**work = **Σ**|**F**obs − **F**calc|/**ΣF**obs.
[f] Five percent of the reflection data were selected at random as a test set, and only these data were used to calculate

Rfree.
[g]Root-mean square deviation. **h**Not applicable.

HPLC analysis to test formation of ring-opened analog via an enzyme mediated mechanism. (Collaboration with Cory Reidl at Becker Lab)

To determine the rate of formation of the ring opened product (**3**), a discontinuous HPLC assay was carried out using the methods described. HPLC analysis did not reveal any detectable ring-opened by-product (**3)**. The results of this assay suggest the formation of the by-product could occur via a radical mechanism that occured due to x-ray radiation damage during data collection at the synchrotron radiation source.

Chemically induced formation of radicals to test formation of ring-opened analog via a radical mechanism. (Experiments Conducted by Cory Reidl at Becker Lab).

The results of the chemically induced ring-opening experiments were inconclusive due to limitations in generating controlled doses of radicals. The results of these experiments were analyses by HPLC at different time intervals but, there was no detectable formation of (**3**).

General discussion on possible mechanism for the formation of by-product (3)

The detailed mechanism for formation of the ring-opened by-product (**3**) cannot be elucidated based on our current results. However, the experimental data suggests the formation of (**3**) occurred via radiation damage that occurred during data collection. If, AiiA alone catalyzed this ring-opening reaction, the formation of (**3**) would be detectible in the HPLC assay. We can speculate that the mechanism was initiated by formation of a radical during x-ray data collection. The radicals formed could be stabilized by the two cobalt atoms in the active site of AiiA. Tyr 194 in AiiA has been reported [2] as a H-bond donor to stabilize an intermediate during catalysis. Hence, it is reasonable to suggest Tyr194 could participate in this reaction by

stabilizing a radical involved in this mechanism. Our efforts to generate radicals using chemical reactions in solution were inconclusive. HPLC analysis showed the complete degradation of (**2**). This could imply that (**2**) must bind specifically to the active site of AiiA so the cyclobutanone ring is positioned in a conformation that allows only the C-C bond present between C2'and C3' of the ring to be cleaved. Alternately, the natural substrates of AiiA are 5 membered lactone rings. The binding of a 4 membered cyclobutanone ring to the active site of AiiA-Co, coupled with the x-ray radiation damage during data collection could have forced ring opening to form a conformation that has a closer resemblance to a 5 membered lactone ring.

CONCLUSION

N-(2-oxocyclobutyl) decanamide is a competitive inhibitor of AiiA. AiiA along with X-ray radiation caused a ring opening reaction that produced a byproduct 4-decanamideobutanoic acid (**3**). The formation of byproduct **(3)** in the crystal structure of AiiA-C10CBO, possibly depicts one of the intermediates that is formed during the enzyme mechanism of AiiA.

METHODS AND MATERIALS

Inhibition Assay

Rate of decrease of substrate hydrolysis were monitored using a previously described continuous spectrophotometric assay[48] in which the pH indicator phenol red acts as part of the assay buffer [1 mM HEPES (pH 7.5)], which results in a change in the colorimetric signal upon protonation by the net release of a proton upon lactone hydrolysis. Stock solutions of the substrate (C7-HSL) and inhibitor (C10cyclobutanone) were prepared in methanol. Continuous spectrometric kinetic assays were used to determine initial hydrolyses rates by mixing substrate (0.5-2.5mM) and inhibitor (0.015-0.5mM) with assay buffer in a 1mL polystyrene cuvette. Each reaction was initiated by the addition of purified enzyme and the reaction was monitored

continuously at 557nm.

Crystallization

The purified AiiA-Co protein was concentrated to 20mg/mL using an Amicon-Ultra (30000 MWCO), centrifugal filter device (Millipore, MA) and the protein was exchanged into 50mM HEPES buffer pH 7.0. The crystallization was carried out in hanging drops by using previously published conditions[2]. Crystals were obtained from the solution containing 160mM $MgCl_2$.6H20, 80mM Bis-Tris pH8.5, 24% w/v PEG 4000, by using a protein:well solution ration of 1:1. Crystals appeared within a week when incubated at 20°C along with slight precipitation. AiiA-Co crystals with the best morphology were soaked overnight in a well solution containing 25mM C10cyclobutanone and 25% glycerol and cryo-cooled in liquid nitrogen.

Data Collection and Processing

Monochromatic data sets were collected at the 19-BM beamline at SBC, Advanced Photon Source (APS) at Argonne National Laboratory (ANL). Diffraction data was collected at a wavelength of 0.98Å, at 100K using an ADSC Quantum 210r CCD detector. All collected data sets were indexed and integrated using HKL3000. The best data set was processed at a resolution of 1.6Å.

Structure Determination, Model Building and Refinement

The AiiA-C10cyclobutanone structure was solved by molecular replacement using PHASER in the Phenix software suit[71]. The initial search model was based on a previously published structure of AiiA-Zn (PDB Code: 2A7M). Models were rebuilt using COOT[72] and refined using the program Phenix and analyzed using the programs COOT and UCSF Chimera[73]. The inhibitor was build and regularized using the software JLigand and fit into the difference density in COOT. Structural figures were made using UCSF Chimera.

CHAPTER FOUR

SELECTIVE TARGETING BY A MECHANISM-BASED INACTIVATOR AGAINST PLP-DEPENDENT ENZYMES: MECHANISMS OF INACTIVATION AND ALTERNATIVE TURNOVER

Summary

Potent mechanism-based inactivators can be rationally designed against PLP-dependent drug targets, such as ornithine aminotransferase (OAT) or γ-aminobutyric acid aminotransferase (GABA-AT). One of the remaining challenges is the lack of selectivity towards other PLP-dependent off-target enzymes, due to similarities in mechanisms of all PLP-dependent aminotransferase reactions. Based on complex crystal structures, we investigate the inactivation mechanism of OAT, a Hepatocellular Carcinoma (HCC) target, by (1*R*,3*S*,4*S*)-3-amino-4-fluorocyclopentane-1-carboxylic acid (FCP), a known inactivator of GABA-AT. A crystal structure of OAT and FCP showed the formation of a ternary adduct. This adduct is likely derived via an enamine mechanism of inactivation similar to that reported for GABA-AT. On the other hand, the crystal structures of an off-target PLP-dependent enzyme aspartate aminotransferase (Asp-AT) in complex with FCP, along with attempted inhibition assays, suggest that FCP is not an inactivator of Asp-AT, but rather an alternate substrate. Turnover of FCP by Asp-AT is also supported by high resolution mass spectrometry. In comparison to the inactivation mechanisms of FCP against OAT and GABA-AT, the obtained results provided evidence that desired selectivity of inactivation could be achieved, taking advantage of subtle

structural and mechanistic differences between a drug target and an off-target enzyme, despite their largely similar substrate binding sites and catalytic mechanisms.

Introduction

Pyridoxal 5'-phosphate (PLP), the active form of vitamin B_6, is a coenzyme in a variety of enzymatic reactions. Aminotransferases are a class of PLP-dependent enzymes that catalyze myriad biochemical reactions involving amino acid metabolism, amino acid-derived metabolites, and the biosynthesis of amine-containing compounds.[74,20] The importance of these enzymes is further highlighted because some of them have been identified as drug targets. For example, inhibition of γ-aminobutyric acid aminotransferase (GABA-AT) was proven effective in the treatment of many neurological disorders [24], and inhibition of ornithine aminotransferase (OAT) was shown to suppress the growth of hepatocellular carcinoma (HCC)[25]. Although reactions catalyzed by PLP-dependent enzymes appear diverse, they all share a similar catalytic mechanism that makes it challenging to design specific inactivators for each of these enzyme drug targets without effecting one another or other PLP-dependent, off-target enzymes like aspartate aminotransferase (Asp-AT).

Through the general mechanism of aminotransferases, Asp-AT catalyzes a reversible transamination converting *L*-aspartate and *α*-ketoglutarate to oxaloacetate and *L*-glutamate (Scheme 6c).[28] During the catalysis, the cofactor is interconverted between its PLP and pyridoxamine (PMP) forms, facilitating the aminotransferase reaction. The Asp-AT reaction is crucial in both amino acid degradation and biosynthesis.[75] Therefore, when designing an inactivator for PLP-dependent drug targets, any molecule that also inhibits/inactivates Asp-AT or similar off-target enzymes may not be a promising molecule for further pharmacological development due to possible side effects. OAT and GABA-AT are confirmed PLP-dependent

enzyme drug targets.[23] Ornithine aminotransferase, (OAT; EC 2.6.1.13) catalyzes the transfer of the δ-amino group of *L*-ornithine to α-ketoglutarate, forming glutamate γ-semialdehyde and *L*-glutamate (Scheme 6a). OAT is overexpressed in HCC cells, and its inhibition was shown to suppress their growth.[27] GABA-AT (EC 2.6.1.19) catalyzes the transfer of the amino group of GABA to α-ketoglutarate, producing succinic semialdehyde and *L*-glutamate (Scheme 6b). GABA is a principle neurotransmitter in mammalian cells,[76] and abnormally low levels of GABA in the brain have been associated with many neurological disorders including epilepsy, Parkinson's disease, Huntington's disease and Alzheimer's disease.[23] Inhibition of GABA-AT to raise the brain level of GABA has been proven beneficial in the treatment of these neurological disorders. Development of small molecules that selectively target a specific PLP-dependent enzyme is challenging. Much of the effort has focused on the design of mechanism-based inactivators, which are unreactive compounds that require the catalytic activity of the enzyme to convert them into reactive species that then inactivate the enzyme. Because these molecules are not initially reactive, indiscriminate reactions with many off-target proteins, leading to undesired side effects, should be greatly reduced.

Scheme 6**.** General mechanism of A) Aspartate Aminotransferase, B) Ornithine Aminotransferase and C) GABAAminotransferase

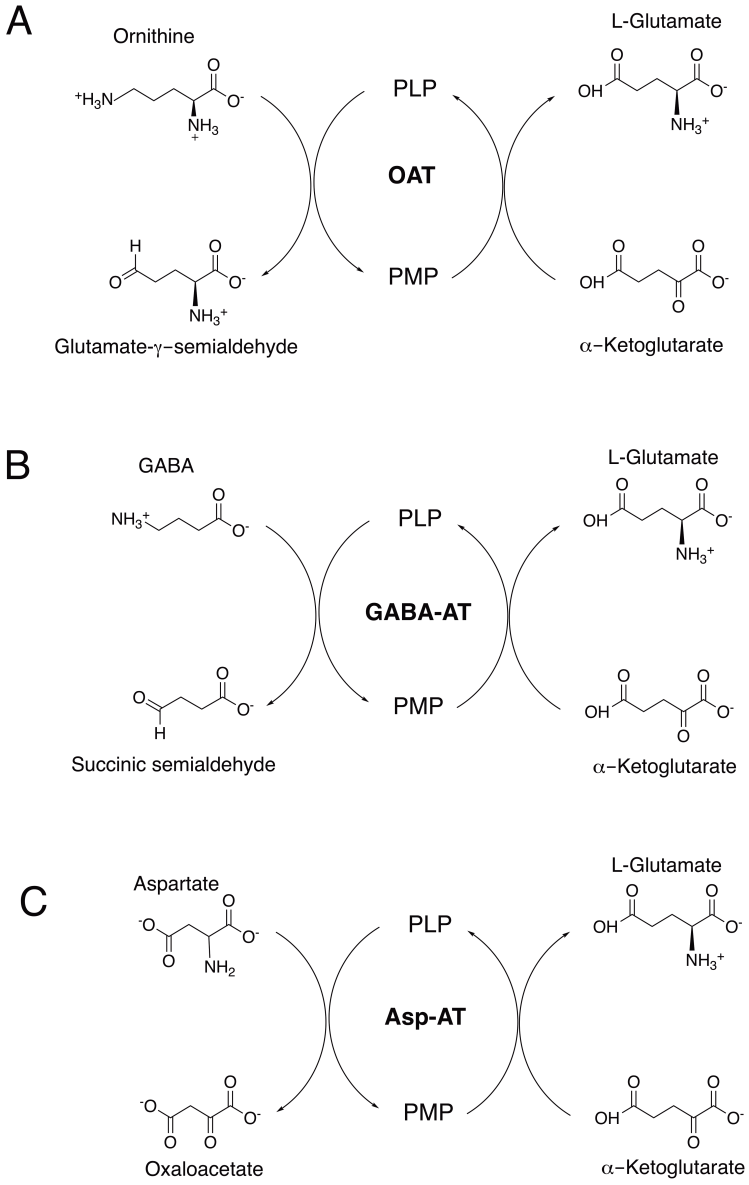

In this study, we investigated the mechanism by which (1*R*,3*S*,4*S*)-3-amino-4-fluorocyclopentane-1-carboxylic acid (FCP) a known inactivator of GABA-AT and OAT[26], inactivates OAT, and the effects of FCP on a PLP-dependent off-target Asp-AT. Our study serves as a proof-of-principle that new OAT inactivators could be developed from GABA analogues, without targeting other off-target PLP-dependent enzymes. Previously Storici *et al*.

studied the inactivation of GABA-AT by FCP.[77] It inactivated GABA-AT through an enamine mechanism (Figure 23A), with the crystal structure of the inactivated enzyme showing the adduct derived from this mechanism (**5**). In this study, we obtained the crystal structure of inactivated OAT by FCP and provide implications about the mechanism. We also report the crystal structures of the off-target Asp-AT in complex with FCP in the presence as well as in the absence of α-ketoglutarate. The crystal structures of Asp-AT in complex with FCP, along with inhibition assays and high resolution mass spectrometry, support the turnover of FCP by Asp-AT and the proposed mechanism.

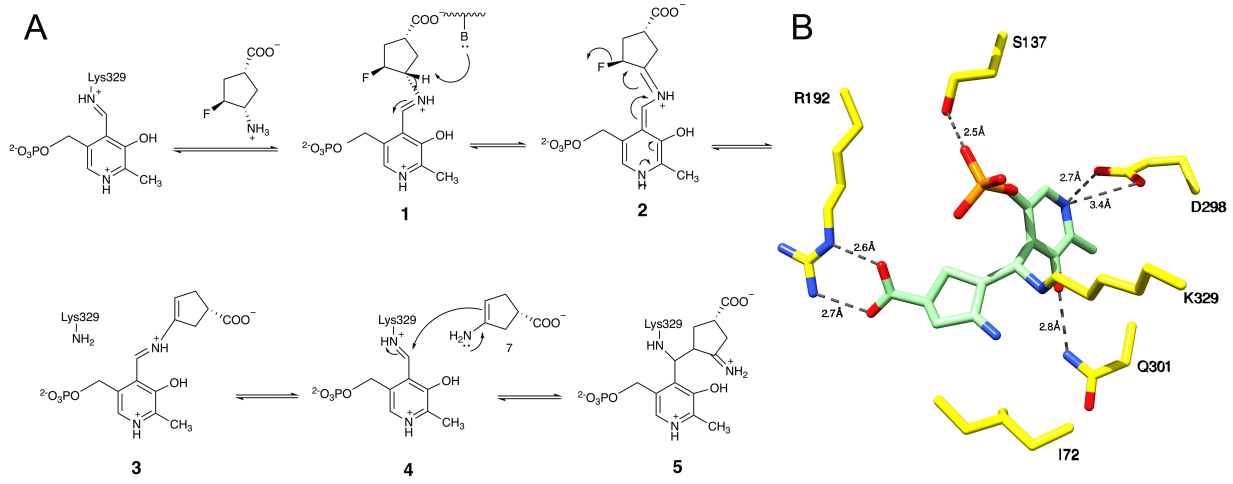

Figure 23. Mechanism of inactivation of GABA-AT by FCP A) Scheme representing the mechanism of inactivation of GABA-AT by FCP. B) Crystal structure of the inactivated GABA-AT showing the adduct derived from an enamine mechanism (**5**)[11]

Results and Discussion

One of the biggest challenges that must be overcome when designing a mechanism based inactivator as a drug is to avoid negative effects caused by possible inactivation of similar off-target enzymes. FCP, a known inactivator of GABA-AT and OAT, is studied for its mechanism

of inactivation of OAT (the drug target) and its effects on Asp-AT (off-target). To compare the effects of FCP on all three enzymes, we cloned, expressed, and purified human OAT and purified Asp-AT for structural and biochemical studies. The cloning results were confirmed by DNA sequencing. Heterologous expression of OAT and Asp-AT in *E. coli* BL21(DE3) cells led to good yields of purified proteins (~ 10 mg/L culture and ~30mg/L culture, respectively). The proteins were characterized and used for biochemical and structural studies as described in Methods and Materials

Inactivation of OAT by FCP

FCP was previously shown to inactivate GABA-AT with a K_I of 49 mM and k_{inact} of 0.18 min^{-1} (k_{inact}/K_I = 0.0013 $mM^{-1}min^{-1}$) and inactivate OAT with a K_I of 3.5 mM and k_{inact} of 0.11 min^{-1} (k_{inact}/K_I = 0.03 $mM^{-1}min^{-1}$)[26]. Due to irreversible inactivation, FCP is a potent inactivator for both GABA-AT and OAT. However, no inactivation studies have been conducted on Asp-AT. Based on a reported complex structure[77], FCP inactivates GABA-AT through an enamine mechanism (Figure 23A).

Here, studies were conducted to gain structural insight into the mechanism of inactivation of OAT by FCP. OAT inactivated by FCP (OAT-FCP) was crystallized and the structure of OAT-FCP was solved by molecular replacement using a monomer of a known OAT structure as a search model (PDB: 1OAT) after deleting all water and ligand molecules. In spacegroup $P32_1$, three monomers were found in one asymmetric unit. Multiple cycles of model building and refinement were conducted, and the final model was refined to a resolution of 1.8Å with R_{free}/R_{work} values of 21.3/18.4. Final refinement statistics are shown in Table 5.

Table 5. Crystallographic Data for OAT_FCP, Asp-AT_FCP and Asp-AT_FCP-KG

	OAT_FCP	ASP-AT_FCP	ASP-AT_FCP_KG
Data Processing			
Space group	P 32 2 $_1$	P1	C 2 2 2_1
Cell dimension			
α, β, γ (deg)	115.3, 115.3, 187.9	118.8,90.1,89.6	84.4, 155.5,77.4
a, b, c (Å)	90, 90, 120	78.9,84.9,88.0	90.0, 90.0, 90.0
Resolution (Å)	1.78	1.80	1.72
Resolution at I/σ (I) = 2	1.84	1.80	1.75
R_{merge} [a] (%)	9.3 (0.0)[b]	6.1(40.0)	4.0(98.0)
R_{pim} [c] (%)	3.9 (79.3)	-	2.7(53.0)
I/σ (I)	26.2 (1.47)	20.0(2.8)	25.3(1.9)
CC ½ [d]	0.998(0.568)	-	0.998(0.701)
Completeness (%)	99.8(99.0)	98.2(83.4)	99.7(99.5)
Multiplicity	9.4 (7.5)	3.8(3.3)	4.3(4.0)
No. Reflections	1315591	676385	240049
No. Unique Reflections	139552	178845	55946
Refinement			
R_{work} [e]/R_{free} [f](%)	17.78/20.99	16.39/18.77	16.7/19.04
No. of Atoms			
protein	9626	13737	3105
ligand	32	63	25
water	1309	1434	366
B factors			
protein	26.4	31.1	25.2
ligand	16.7-32.9	17.7-32.7	35.9
RMSD [g]			
bond lengths (Å)	0.007	0.007	0.007
bond angles (deg)	1.115	1.124	1.138
Ramachandran plot (%)			
most favored	96.41	97.19	95.77
allowed	3.27	2.59	4.23
outliers	0.33	0.22	0.00

[a]Rmerge = Σ|Iobs − Iavg|/ΣIavg

[b]The values for the highest-resolution bin are in parentheses

[c]Precision-indicating merging R

[d]Pearson correlation coefficient of two "half"data sets

[e]Rwork = Σ|Fobs − Fcalc|/ΣFobs

[f]Five percent of the reflection data were selected at random as a test set, and only these data were used to calculate Rfree

[g]Root-mean square deviation

[h]Not applicable

No major conformational changes were observed when the known structure of OAT (PDB:1OAT) was compared to OAT_FCP. The active site of OAT_FCP (Figure 24A) displays a ternary adduct formed between Lys292, PLP and, FCP. The atom C-4 of PLP, at which three parts of the ternary adduct join covalently, are refined with an R-configuration and tetrahedral geometry (Figure 24A). This ternary adduct is similar to the adduct observed in the active site of the crystal structure of inactivated GABA-AT by FCP [77] (Figure 23B).

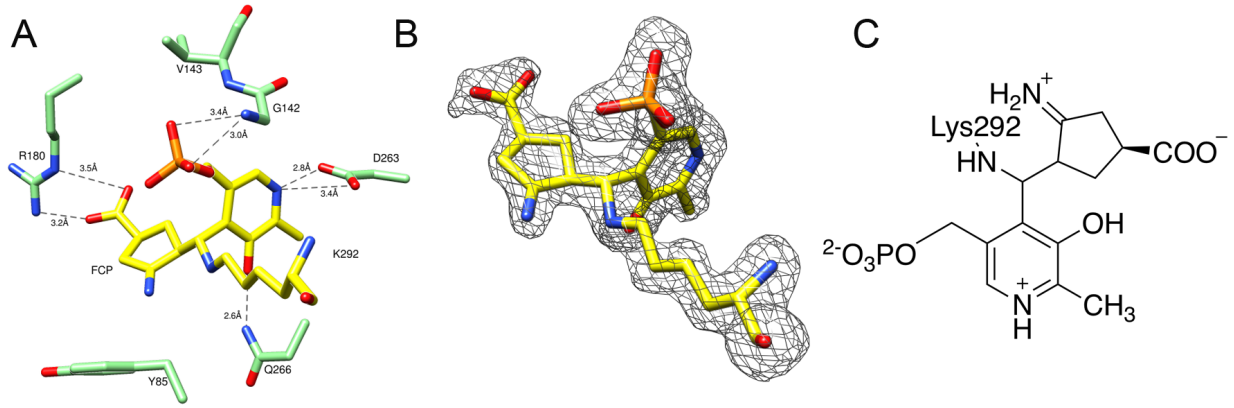

Figure 24. Structure of adduct formed between OAT, PLP and FCP. Protein atoms are shown as sticks, with oxygen colored red, nitrogen blue and phosphorous in orange. A) Active site of OAT showing the ternary adduct formed between K292, FCP and PLP are shown in yellow. The dashed lines represent the electrostatic interactions between active site residues of OAT (green) and the adduct. B) Simulated annealing omit map (Fo-Fc) of the adduct. The omit map is shown as a grey mesh at 3σ. The omit map was generated after omitting FCP, PLP and K292 from the coordinates.

In OAT_FCP, Arg180 forms a salt bridge with the carboxyl group of FCP; this non-covalent interaction has been reported to be important for substrate binding at the active site.[23] Figure 24B shows a simulated annealing omit map (F_o-F_c) superimposed with the ternary adduct. The formation of this adduct implies that the inactivation of OAT by FCP proceeded via an enamine

mechanism, similar to that of the inactivation of GABA-AT by FCP. This mechanism is initiated by a formation of the Schiff base between FCP and PLP (**1**), followed by a γ-proton removal and tautomerization that leads to the release of the fluoride ion and enamine **7** (Scheme 7). Subsequent nucleophilic addition of **7** to the lysine-bound PLP on OAT gives rise to the ternary adduct **8**, which is similar to **5** in the inactivation mechanism of GABA-AT by FCP.

Scheme 7. Proposed mechanism of inactivation of OAT by FCP.

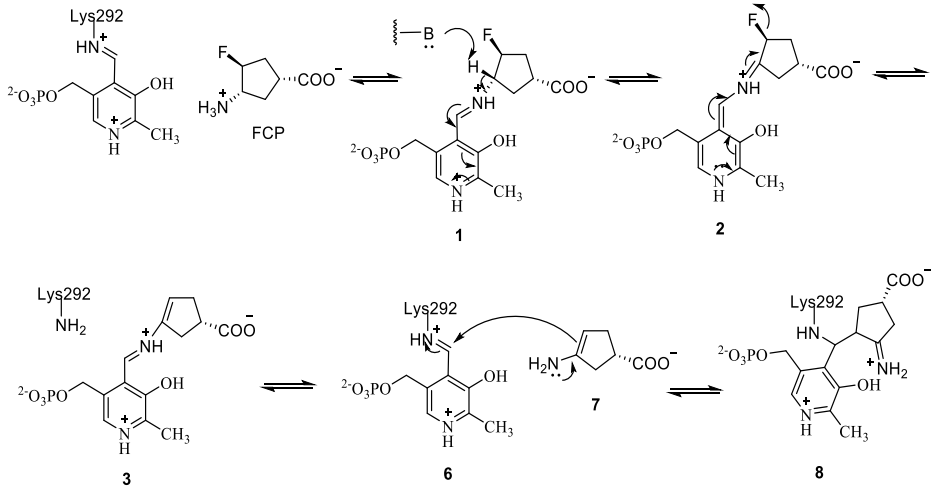

Reaction of FCP and its Effects on Asp-AT

E. coli Asp-AT is similar to *Homo sapiens* (human) Asp-AT with over 40% sequence identity and is a model enzyme among Asp-AT's, which are known to catalyze reactions with the same mechanism [2,28]. Overexpressed and purified *E. coli* Asp-AT has been used as the off-target model enzyme to design inactivators against PLP-dependent enzymes[78,79]. The results showed FCP did not inactivate or inhibit the activity of Asp-AT at up to 10 mM concentration (Figure 25).

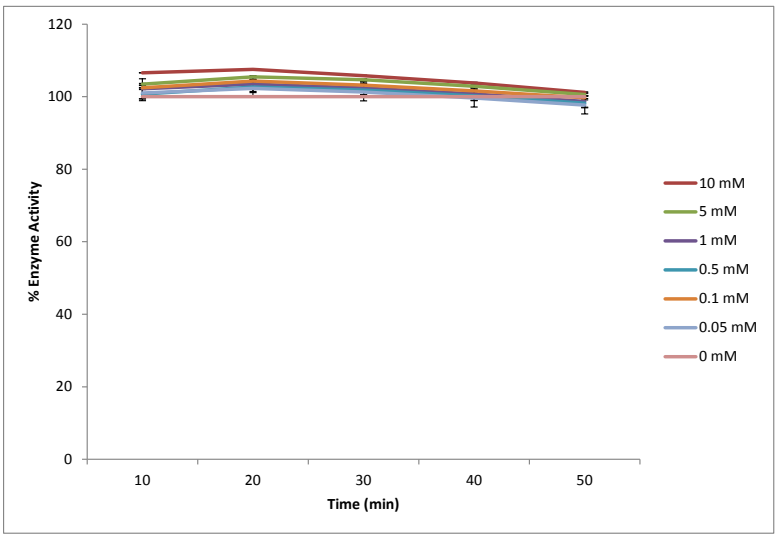

Figure 25. Enzyme activity of Asp-AT at various concentrations of FCP

Cocrystallization of Asp-AT and FCP in the absence of α-ketoglutarate (Asp-AT_FCP) yielded crystals that diffracted to 1.8Å. The data set was processed in space group P1 and the crystal structure was solved by molecular replacement using a known structure of Asp-AT (PDB: 2AAT) as a search model. The resulting structure has 4 monomers per asymmetric unit, and the model was refined with R_{free}/R_{work} values of 18.7/16.4. Final refinement statistics are shown in Table 5.

The active site of Asp-AT_FCP (Figure 26A) contains electron density that is not consistent with the formation of a ternary adduct like observed in the crystal structures of FCP inactivated GABA-AT or OAT. Instead, this electron density is fit well by PMP (Figure 26). The discontinuity in the electron density between Lys246 and the putative pyridoxamine moiety provides evidence for the turnover of PLP to PMP. In addition, the electron density around C7 of the putative PMP fits well with an sp3 hybridized carbon, providing further evidence that the

moiety is in the pyridoxamine rather than the pyridoxal form. Figure 25B shows a simulated annealing omit map (Fo-Fc) superimposed with the atomic model of PMP. The interactions between active site residues and PMP (Figure 25A) in this crystal structure are the same as those in a previously reported structure of the Asp-AT_PMP holoenzyme[80,81]. Observation of PMP bound to Asp-AT in the presence of FCP suggests that Asp-AT catalyzes the conversion of the amine group on FCP to a keto group through the same mechanism it converts aspartate to oxaloacetate and this reaction stops at the generation of PMP after the first half of the "Ping-pong" catalytic cycle.

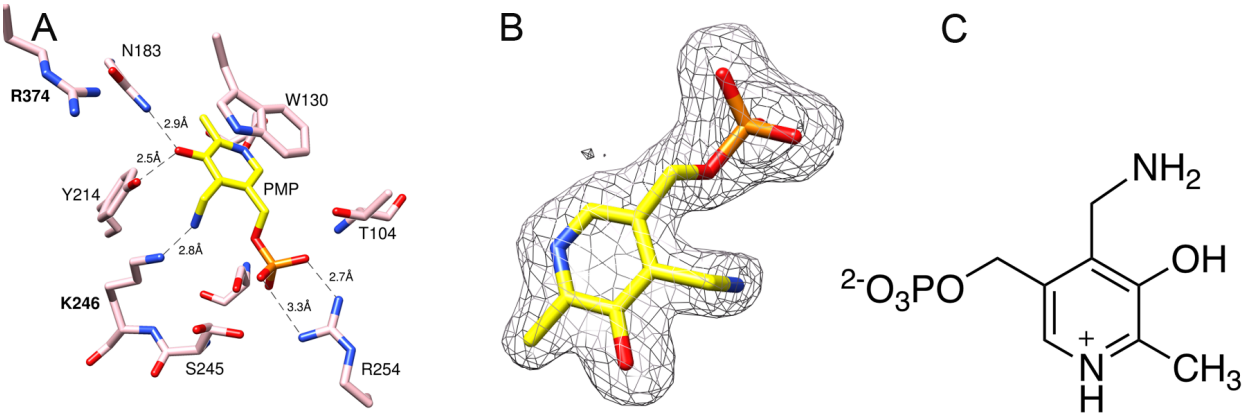

Figure 26. Structure of Asp-AT and PMP. Protein atoms are shown as pink sticks, with oxygen colored red, nitrogen blue and, phosphorous in orange. A) Active site of Asp-AT and PMP The dashed green lines represent the electrostatic interactions between PMP and residues of Asp-AT. B) Simulated annealing omit map (F_o-F_c) of the adduct. The omit map is shown as a grey mesh .The omit map was generated after omitting PMP from the coordinates.

Based on our interpretation of the turnover of FCP by Asp-AT and conversion of PLP to PMP, it is expected that cocrystallization of Asp-AT in the presence of FCP and its second substrate—α-ketoglutarate, should reveal a structure representing regeneration of the enzyme back to the PLP form, as proposed in the second half of the Asp-AT catalytic cycle.

Cocrystallization of Asp-AT and FCP in the presence of α-ketoglutarate yielded crystals that diffracted to 1.7Å. Interestingly, the obtained complex structure (Asp-AT_FCP_α-ketoglutarate) revealed difference density at the active site that fits well with the model of a ketimine intermediate. This ketimine intermediate has long been proposed as a key intermediate in the Asp-AT catalytic mechanism before generating the final product glutamate and regeneration of the cofactor–PLP (Figure 27A). Ketimine intermediates have been previously trapped in the crystal structures of DesV from *Streptococcus pneumonia* (PLP-dependent transaminase)[82] and, ColD from *E.Coli* (dehydratase),[83,84] but to our knowledge not previously reported in Aspartate aminotransferase.

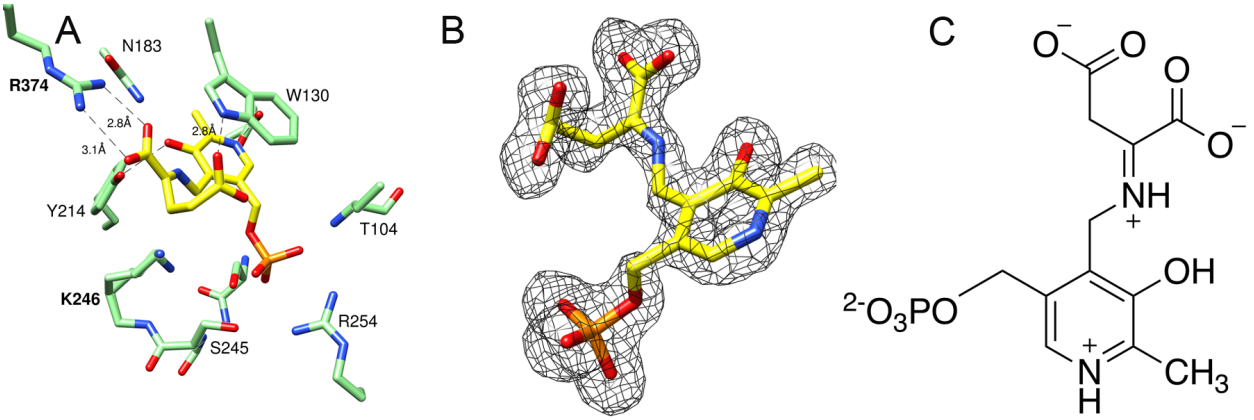

Figure 27**.** Structure of Asp-AT with a ketimine intermediate. Protein atoms are shown as pink sticks, with oxygen colored red, nitrogen blue and, phosphorous in orange. A) Active site of Asp-AT and a ketimine intermediate formed between PMP and α-ketoglutarate are shown in yellow.The dashed green lines represent the electrostatic interactions between ketimine and residues of Asp-AT. B) Simulated annealing omit map (F_o-F_c) of the adduct. The omit map is shown as a grey mesh .The omit map was generated after omitting the ketimine from the coordinates.

Figure 27B shows a simulated annealing omit map (F_o-F_c) superimposed with the atomic model of this ketimine intermediate. The carbon-nitrogen double bond formed between N-2 on

the pyridoxamine moiety and C-2 on α-ketoglutarate provided evidence for this ketimine intermediate. There was no electron density between Lys246 and the pyridoxal moiety, consistent with the measured distance of ~3.2Å. The carboxyl group on the α-ketoglutarate makes a salt bridge with Arg374. The phosphate group on the pyridoxal moiety interacts with Arg254 and Thr104 through hydrogen bonds. These electrostatic interactions are consistent with previous understanding to hold the substrate and cofactor in the active site during the catalytic transformation.[28] Based on both complex crystal structures of Asp-AT, we propose that in the absence of α-ketoglutarate, Asp-AT turns over FCP to a keto product, and PLP is converted to PMP. In the presence of α-ketoglutarate, after the first half of the catalytic cycle occurs, PMP reacts with α-ketoglutarate to form a ketimine intermediate that is then hydrolyzed to *L*-glutamate and PLP. Trapping this ketimine intermediate in the crystal structure is possibly an artifact during cocrystallization. Nonetheless, this ketimine intermediate provides evidence for the occurrence of the second half of the catalytic cycle and further suggests that FCP is an alternate substrate for Asp-AT.

Proposed Mechanism of Alternative Turnover of FCP by Asp-AT

To test for turnover of FCP by Asp-AT and probe its turnover mechanism, we incubated Asp-AT with FCP in the absence of α-ketoglutarate, allowing the putative first half-reaction of FCP turnover to occur in a single turnover fashion. After desalting and deproteinating, FCP turnover samples were analyzed by high mass accuracy HPLC-ESI-MS/MS, using a Q-Exactive mass spectrometer in negative ion mode to detect reaction products. The abundance of ions with molecular formulae corresponding to several putative FCP-turnover products was observed to change significantly when FCP and Asp-AT were incubated together (Table 6, Figure 28).

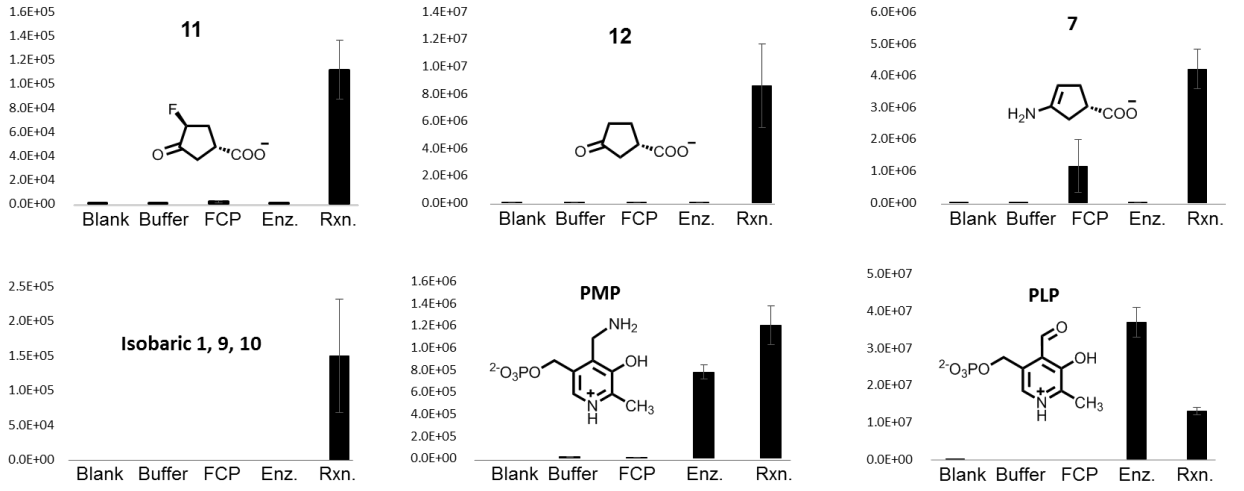

Figure 28. Relative levels of proposed FCP turnover products and intermediates. Relative abundance of each compound was determined by LC-MS. Each compound was increased by incubation of FCP with Asp-AT, except for PLP. Blank = acetonitrile. Buffer = reaction buffer. FCP = FCP at 15.8 mM. Enz = Asp-AT at 39.5 μM. Rxn. = Asp-AT (39.5 μM) + FCP (15.8 mM).

Table 6. Proposed FCP turnover products and intermediates detected by mass spectrometry

Compound	Change	Obs. *m/z*	Theor. *m/z*	Δ ppm	Isotopic envelope supported?	MS^2 Supported?	Synthetic standard supported?
9/10	Increase	375.077	375.076	4	N.D.[a]	N.D.[a]	N.A.[b]
3	Increase	355.072	355.070	5	N.D.[a]	N.D.[a]	N.A.[b]
PLP	Decrease	246.017	246.017	1	Yes	Yes	Yes
PMP	Increase	247.049	247.049	0	Yes	N.D.[a]	Yes
12	Increase	127.039	127.040	-7	Yes	Yes	N.A.[b]
11	Increase	145.030	145.031	-4	N.D.[a]	N.D.[a]	N.A.[b]
7	Increase	126.055	126.056	-7	Yes	Yes	N.A.[b]

[a] compound was below limit of detection for MS^2 or isotopic envelope

[b] synthetic standard not available

Ions were putatively identified based on intact mass and when possible, isotopic envelopes, MS2 fragment assignment, and comparison to synthetic standards. Figure 30-33 present MS2 and/or isotopic envelope evidence for identification of 3-oxocyclopentane-1-carboxylate (12), PLP, PMP, and 7. In some cases, analysis of isotopic envelopes and MS2 was not possible due to low overall abundance (Table 6). The relative level of each of these metabolites is shown in

Figure 28. Notably, each metabolite increased when FCP and enzyme were mixed, relative to negative controls, with the exception of PLP, which decreased. This is consistent with the model proposed in Figure 29, where FCP turnover is partitioned between two separate pathways. The resulting Schiff base from the reaction of FCP and the lysine-bound PLP on Asp-AT is subjected to γ-proton removal, followed by tautomerization that leads to the formation of intermediates 9 and 10 (path a) and the release of the fluoride ion (path b). In path a, hydrolysis of intermediate 10 gives 3-fluoro-4-oxocyclopentane-1-carboxylate 11 and releases PMP. In path b, hydrolysis of 3, the intermediate formed after the release of the fluoride ion, gives enamine 7 and releases PLP; hydrolysis of 7 generates 3-oxocyclopentane-1-carboxylate 12. Pathways a and b occur concurrently. Intermediates 9 and 10, 3-fluoro-4-oxocyclopentane-1-carboxylate (11), 3-oxocyclopentane-1-carboxylate (12), 7, and PMP increased in the incubated solution of FCP and Asp-AT. Only a portion of the PLP pool was reformed, following path b; hence, the level of PLP decreased in the incubated solution.

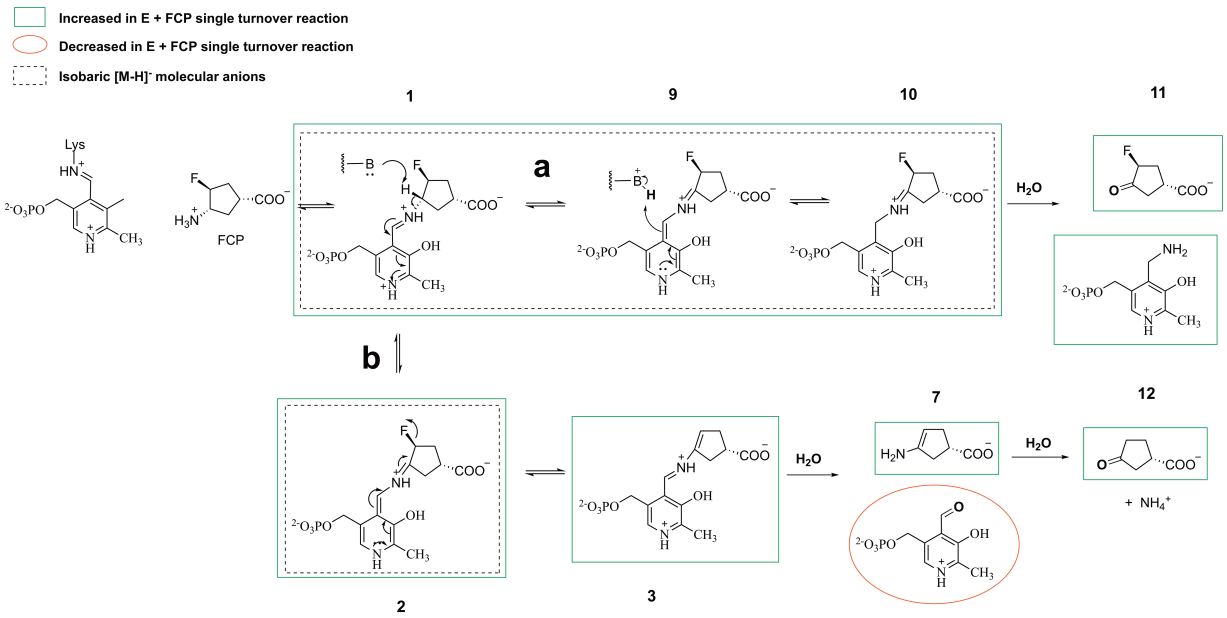

Figure 29: Proposed Turnover Mechanism of FCP by Asp-AT Based on Mass Spectrometry Analysis of Single Turnover of FCP. Species detected to be increased are boxed in green. Species detected to be decreased are circled in red. Isobaric ions are boxed with dashed lines. Both pathways a and b are proposed to occur concurrently. Only a portion of the PLP pool was reformed, following path b; hence, the level of PLP decreased in the incubated solution

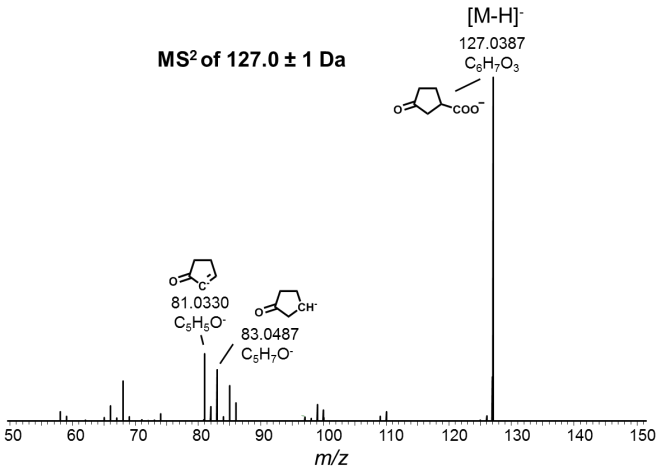

Figure 30. MS^2 fragment assignments for 3-oxocyclopentane-1-carboxylate produced by incubation of FCP with Asp-AT

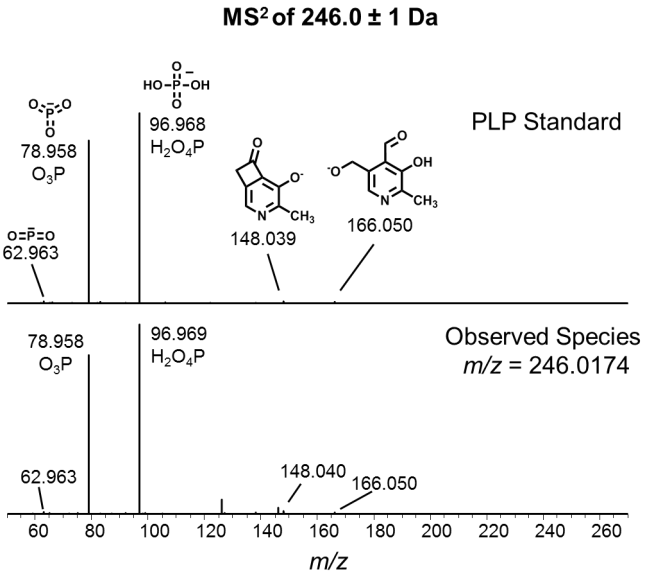

Figure 31. Comparison of MS^2 fragmentation of synthetic PLP standard and observed PLP product of FCP turnover by Asp-AT.

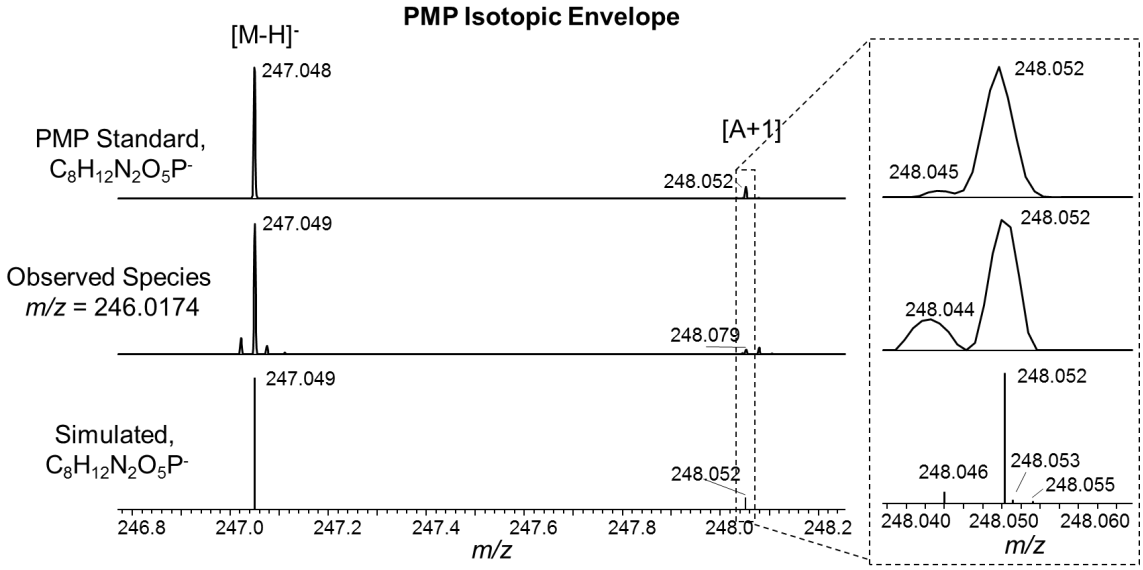

Figure 32. MS1 isotopic envelope of PMP synthetic standard compared to the observed species from incubation of FCP with Asp-AT and the computer simulated isotopic envelope of $C_6H_{12}N_2O_5P^-$.

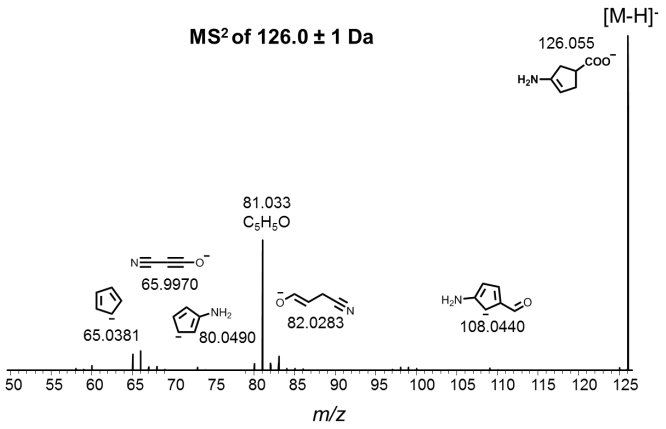

Figure 33. MS^2 fragment assignments for 7, produced by incubation of FCP with Asp-AT.

Comparison of Complex Structures of OAT_FCP, GABA_FCP, and Asp-AT_FCP

OAT, GABA-AT and, Asp-AT (Figure 34) belong to Type-1 fold class of aminotransferases.[85] Within this Type I fold class, Asp-AT belongs to subclass I (AT-I), while OAT and GABA-AT belong to subclass II (AT-II).[33,85] Though these two subclasses are structurally homologous, detailed analysis reported in literature show that the N-terminal domain is not completely conserved and could be a cause for the subtle differences in their mechanisms.[33,86,87] This could explain why FCP inactivates OAT and GABA-AT, but is an alternate substrate for Asp-AT.

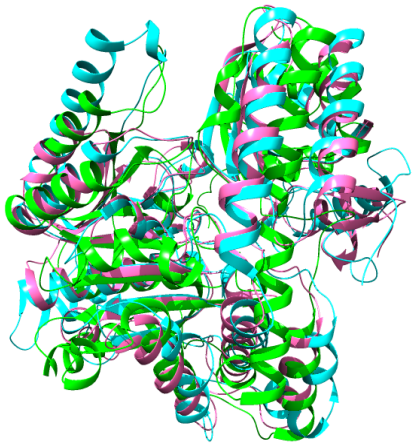

Figure 34. Overlap of the secondary structures of OAT from PDB:1OAT (pink), GABA-AT from PDB:1OHV(cyan), and Asp-AT from PDB:2AAT (green)

The active sites of GABA-AT and OAT are strikingly similar, and an alignment of these two structures showed no major differences in the positions of the conserved key catalytic residues (Figure 35A), including the catalytic Lys and an Arg that is involved in substrate binding. Lee et al.[23] previously proposed that inactivators of GABA-AT could also bind to OAT since the distances between the catalytic Lys residue and the Arg residues are similar (Figure 35A). Therefore, it is reasonable that FCP inactivates both GABA-AT and OAT via a similar enamine mechanism. Despite the presence of the catalytic lysine and PLP, the active site residues in Asp-AT do not align well with those of OAT and GABA-AT (Figure 35B), displaying subtle differences (Tyr 65 from subunit b and position of R254 for substrate recognition)[28] that could contribute to the difference in mechanisms with FCP.

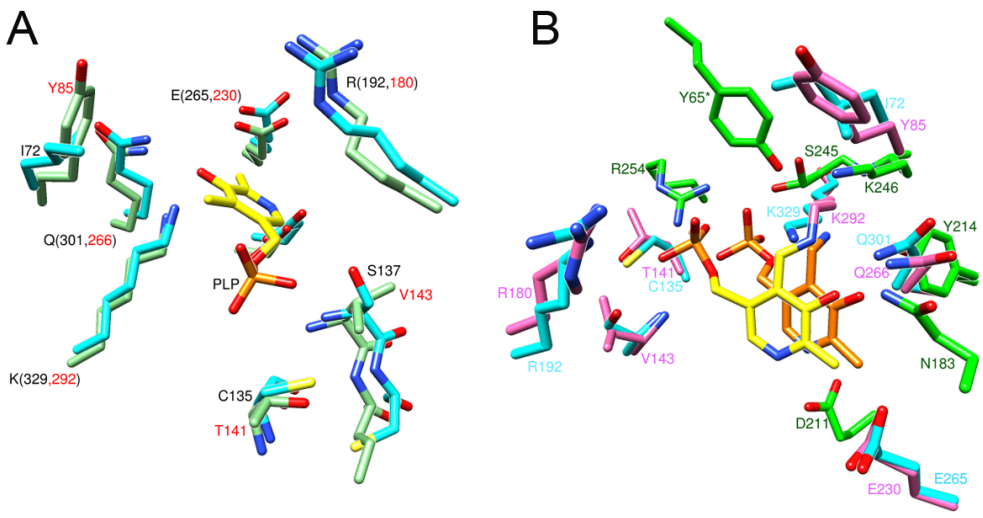

Figure 35. A) Overlap of the active sites of OAT(green) and GABA-AT(cyan) B) Overlap of the active sites of OAT(pink), GABA-AT(blue) and Asp-AT (green)

In the mechanisms of inactivation of OAT and GABA-AT by FCP (Figure 23A; Scheme 7), intermediate **7** is held in position in the active site closed to the Lys-bound PLP via a salt bridge between a conserved Arg and the carboxyl group on FCP, allowing **7** to irreversibly form a covalent adduct with the enzyme and PLP, which leads to the inactivation of the enzyme. In the mechanism of FCP with Asp-AT, this ternary adduct is not formed; instead, FCP is turned over to a keto product, which could be the result of the hydrolysis of **3** that happens before the ternary adduct is formed (Figure 29b). Examination of the active site pockets reveals that in OAT and GABA-AT, the pyridine ring of the cofactor is buried in the enzymes' active sites and is barely exposed to the solvent (Figure 36 A,B), which likely helps to retain intermediates **6** and **4** in the active site cavities long enough for the formation of the final ternary adducts to occur. In Asp-AT (Figure 36C), the pyridine ring of the co-factor is more exposed and closer to the surface of the protein, which may account for the availability of a water molecule for the hydrolysis of **3** to happen fast.

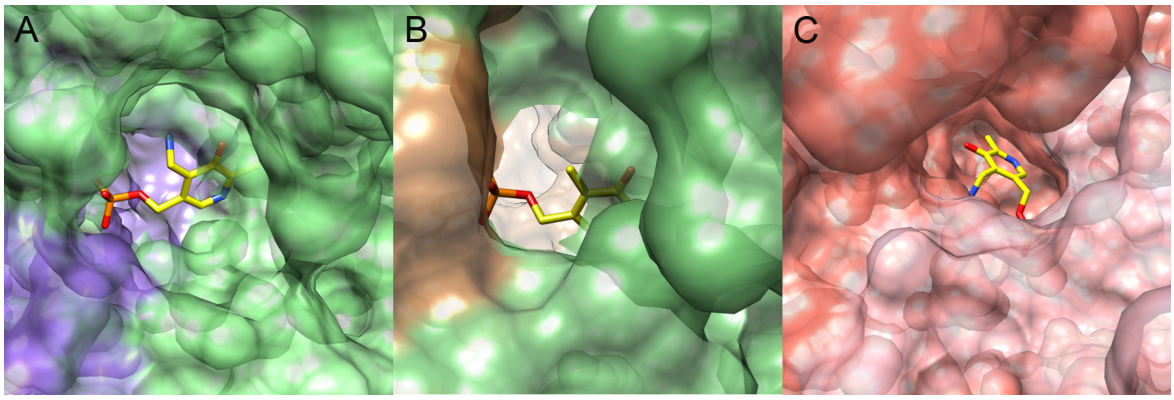

Figure 36. Cofactor binding pockets. A) A surface coated OAT is shown in green and brown. PLP is represented as yellow sticks, with oxygen in red, nitrogen in blue and phosphorous in orange. The PLP pocket is buried in the protein. B) A surface coated GABA-AT is shown in green and purple. PLP is represented as yellow sticks, with oxygen in red, nitrogen in blue and phosphorous in orange. The PLP pocket is buried in the protein. C) A surface coated Asp-AT is shown in pink. PMP is represented as yellow sticks, with oxygen in red, nitrogen in blue and phosphorous in orange.

One difference between the active sites of Asp-AT and OAT is that Asp-AT positions a Tyrosine 214 instead of a threonine close to the PLP (Figure 37). When the two complex structures Asp-AT-PMP and OAT-PLP-FCP are superimposed, Tyrosine would place a water via a hydrogen bound close to the expected binding position of FCP, presenting an estimated distance of 3.3 Å to the point of nucleophilic attack. Thus, this water could be the nucleophile that carries out the hydrolysis to complete the alternative turnover instead of inactivation in Asp-AT.

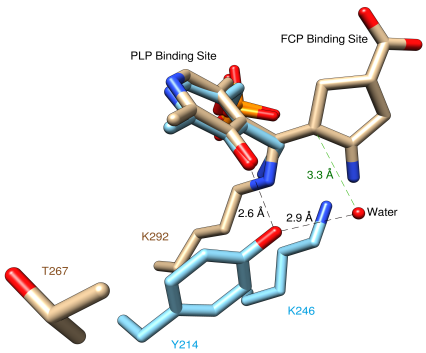

Figure 37. Two complex structures OAT-PLP-FCP and Asp-AT-PMP are superimposed. The carbon atoms in OAT-PLP-FCP are shown in brown. The carbon atoms in Asp-AT-PMP is shown in cyan. The estimated distance of the water to carry out nucleophilic attack is shown in green.

Selectivity of Mechanism-based Inactivators for PLP-dependent Enzymes

Though the active sites and catalytic mechanisms of GABA-AT and OAT are very similar, their substrates, GABA and ornithine, respectively, display certain structural differences. Ornithine is one carbon longer than GABA, and it has an additional amine group at the α-carbon. Previous studies on mechanism-based inactivators of these two enzymes showed that (*S*)-4-amino-5-fluoropentanoic acid (AFPA)[23] is specific for GABA-AT, and (2S,5S)-5-fluoromethylornithine (5FMOrn)[88] is specific for OAT. 5FMOrn is one carbon longer than AFPA, and it has an additional amine group at the α-carbon. An overlap of the active sites of GABA-AT and OAT (Figure 35), though very similar, show differences in a certain amino acids that could account for their selectivity for one substrate. It has been suggested that residues Tyr55 and Tyr85 make the active site of OAT more flexible to accommodate substrates that are larger in size and have an amine group at the α-carbon, when compared to the hydrophobic environment in active site of GABA-AT that is created by residues Ile72 and Phe351.[23] These subtle differences can be exploited when designing mechanism-based inactivators that are specific for either OAT or GABA-AT.

Conclusion

FCP inactivates a drug target OAT via an enamine mechanism similar to that of another drug target GABA-AT, but is an alternative substrate for an apparent PLP-dependent off-target Asp-AT. The proposed mechanisms of inactivation and alternative turnover in all three enzymes are

complex, and all contain multiple reaction pathways. Although FCP is still too toxic to become a drug[89,77] itself, it displays a desirable selectivity in the context of drug development as a mechanism-based inactivator. The reason for this desirable selectivity is due to the subtle differences in the shapes of the active site cavities for retaining an intermediate, as well as the availability of a water molecule for a proposed hydrolysis in a complex mechanism with multiple reaction pathways. In general, the reactive intermediates generated during the complex reactions of these mechanism-based inactivators in active sites could be capable of displaying desirable specificity of inactivation discerning drug targets and off-targets, even with similar structures and reaction mechanisms.

Materials and Methods

Unless otherwise noted, all chemicals were purchased from Sigma-Aldrich (St. Louis, MO), and all enzymes used for cloning were purchased from New England Bio Labs (Beverly, MA).

Cloning, Expression, and Purification of Human OAT.

A shuttle vector (pCMV-SPORT6) carrying the OAT cDNA gene from *Homo sapiens* was purchased from plasmID (Harvard Medical School). The coding sequence for OAT was cloned in a pMAL-C5X vector for expression in *Escherichia coli*. A sequence encoding the cleavage site for tobacco etch virus (TEV) protease (ENLYFQG) was inserted at the 5' end of the OAT coding region using forward primer 5'gcgctcggggaaaacctgtattttcagggcgcctctgctacatctgttgcaac3' and reverse primer 5'gcggaattctcagaaagacaagatggtc3'; restriction sites *Ava*1 and *Eco*R1were added to the 5' and 3' ends, respectively. A commercial protein expression vector, pMAL-C5X (New England Biolabs, Beverly, MA), was digested using restriction enzymes EcoR1 and Ava1, and the resulting PCR insert containing OAT coding region was ligated into the expression

vector using T4 DNA Ligase (New England Biolabs, Beverly, MA) to yield a protein expression plasmid encoding an *N*-terminal maltose binding protein (MBP) linked through a TEV cleavage sequence to the full length OAT enzyme. The resulting vector (pMAL-t-OAT) was used to transform *E.coli* DH5α cells for plasmid storage and amplification. The entire coding region in pMAL-t-OAT was verified by DNA sequencing. (CRC DNA Sequencing, University of Chicago).

For protein production and purification, pMAL-t-OAT was used to transform *E. coli* BL21(DE3) cells. The resulting *E. coli* BL21(DE3) (pMAL-t-OAT) cells were incubated at 37 °C while shaking in Luria-Bertani (LB) medium supplemented with 100 μg/mL ampicillin. When the culture OD_{600} value reached 0.6-0.8 absorbance units, expression of the MBP-t-OAT fusion protein was induced by addition of 0.3 mM IPTG, and the expression was continued for an additional 16-18 h at 25 °C after induction. Cells were harvested by centrifugation at 12400 × *g*, washed with Wash Buffer (20 mM Tris-HCl buffer with 200 mM NaCl, 100μM PLP at pH 7.4), and stored at -80 °C after flash freezing in liquid nitrogen. The frozen cell pellet was thawed, sonicated in Wash Buffer, and centrifuged at 40000 × *g* to pellet cell debris, which was discarded. The resulting supernatant was loaded onto an amylose affinity column (16 × 25 mm Dextrin Sepharose – MBL Trap HP, GE LifeSciences, pre-equilibrated with Wash Buffer). The column was washed with Wash Buffer, and the MBP-t-OAT fusion protein was eluted from the column using Wash Buffer supplemented with maltose (10 mM). Fractions were evaluated using coomassie-stained SDS-PAGE, and those fractions containing MBP-t-OAT were combined and treated batch-wise with TEV protease using previously published protocols[90]. Fractions containing untagged OAT protein were combined, concentrated using a 30,000 molecular weight cut off (MWCO) Amicon-Ultra centrifugal filter device (Millipore, MA), and further purified by

size exclusion chromatography using a HiLoad Superdex-200PG column, 16 × 600 mm (GE Lifesciences, CA). The column was equilibrated and the protein was purified using Size Exclusion Buffer (50 mM HEPES buffer, 300 mM NaCl, pH 7.5). During the purification, fractions were assayed for the presence of MBP-t-OAT or OAT at each step by using 12% SDS-PAGE, followed by staining with EZ-Run Gel Staining Solution (Fisher BioReagents) to detect bands at ~ 92 or ~ 49 kDa, respectively. The final purified untagged OAT protein appeared homogenous when characterized on a Coomassie-stained 12% SDS-PAGE gel. Protein concentrations in solution were measured using bovine serum albumin (BSA) standards and the Bradford assay (BioRad). This purification procedure typically results in a yield of 30 mg of purified untagged OAT/ L culture media.

Purification of E. coli Aspartate aminotransferase

The pJO2 plasmid (provided by Dr. J. F. Kirsch) containing the wild-type aspC gene was transformed into the DH5α *E. coli* strain. The wild-type Asp-AT was overexpressed and purified by following a published protocol[91]. Accordingly, 0.1% of PLP was added to the expression culture. After the harvested cells were broken via sonication and the cell extract was centrifuged at 12400 × *g*, the supernatant was removed and mixed with PEG8000 that was slowly added to a final concentration of 20% of the total volume of the supernatant. The resulting suspension was again centrifuged at 12400 × *g*. The supernatant was diluted in a DEAE running buffer and run through a DEAE column and a hydroxyapatite column on a FPLC consecutively. For crystallization, an additional purification step was added using a HiLoad Superdex-200PG column, 16 × 600 mm (GE Lifesciences, CA). The final yield of the purified Asp-AT was 80-100 mg/L of culture. For crystallization, the purified protein was exchanged into a 25mM potassium phosphate buffer at pH 6.0 and pH 8.0 with a final concentration of 10 mg/mL. A

solution of 1 mM PLP was supplemented to the protein solution to stabilize the enzyme. All purification procedures were carried out at or near 4°C. During the purification, fractions were assayed for the presence of Asp-AT at each step by using 12% SDS-PAGE, followed by staining with EZ-Run Gel Staining Solution (Fisher BioReagents) to detect bands at ~ 47kDa.

Attempted Inhibition Assays of FCP against Asp-AT

Microtiter plate wells were loaded with 90 μL of an assay mixture containing potassium phosphate (100 mM, pH 7.4), *α*-ketoglutarate (5.55 mM), NADH (1.11 mM), *L*-aspartate (5.55 mM), malate dehydrogenase (5.5 units), and various concentrations of FCP. After the mixture was incubated at room temperature for a few min, 10 μL of Asp-AT (2.0 units/mL in 100 mM potassium phosphate at pH 7.4) was added. The plate was shaken at room temperature for 1 min, and the absorbance was measured at 340 nm every 10 s for 60 min. All assays were performed in duplicate.

Crystallization of OAT and FCP

OAT pre-inactivated by FCP was concentrated to 10 mg/mL using a 30,000 MWCO Amicon-Ultra centrifugal filter device (Millipore, MA), and the concentrated protein was exchanged into a crystallization buffer (50mM Tricine HCl, pH 7.8 and 10μM PLP). Crystals were grown using previously published conditions.[32] Crystallization was done in 24-well Cryschem Plates (Hampton Research). Crystals with the best morphology appeared in the well solution containing NaCl (175mM) and 8-10% (v/v) PEG 6000 after incubation at room temperature for a week. OAT crystals with the best morphology were transferred into a cryo-protecting solution (Well Solution supplemented with 25 % (v/v) glycerol) before being flash cooled in liquid nitrogen.

Cocrystallization of Asp-AT and FCP in the Presence and Absence of α-Ketoglutarate

The cocrystallization of Asp-AT and FCP in the absence of α-ketoglutarate was conducted using the hanging-drop method. The well solutions contained 25 mM potassium phosphate and 43% saturated ammonium sulfate. Hanging drops were set up by mixing 4 μL of protein solution (10 mg/mL), 2 μL of FCP (50 mM, stock solution), and 4 μL of well solution. The pH values of the solutions were adjusted to pH 6.5. The crystals appeared overnight. The crystals were then transferred to a cryo-protectant solution that consisted of 48% saturated ammonium sulfate, 25 mM potassium phosphate, 20% glycerol, and 1 mM PLP and was adjusted to the pH value at which the crystals were formed. The crystals were frozen in liquid nitrogen after dipping into the cryo-protectant solution. For the cocrystallization of Asp-AT and FCP in the presence of α-ketoglutarate, the protein buffer was substituted with a solution of α-ketoglutarate (10mM); other crystallization conditions remained the same.

Data Collection and Processing

Monochromatic data sets were collected at the LS-CAT, Advanced Photon Source (APS) at Argonne National Laboratory (ANL). Diffraction data were collected at a wavelength of 0.98 Å at 100 K using a Mar300 Charge Coupled Device (CCD) detector. All collected data sets were indexed and integrated using HKL2000 suite[92]. Data collection statistics are summarized in Table 5.

Model Building and Refinement

The OAT structure and Asp-AT structures were solved by molecular replacement using PHASER in the Phenix software suit[71]. The initial search model was based on a previously published structure of OAT (PDB Code: 1OAT), and Asp-AT (PDB Code: 2AAT). Models were

rebuilt using COOT[72], refined using Phenix[71], and analyzed using COOT[72] and UCSF Chimera[73]. Final refinement statistics are presented in Table 5. Structural Figure were made using UCSF Chimera.

Mass Spectrometry Study of Single Turnover of FCP

Asp-AT (39.5 μM) was incubated in 50 mM ammonium bicarbonate buffer (pH 7.4) containing 15.8 mM FCP in a total volume of 200 μL at room temperature in the dark for 12 h. A similar control solution that did not contain FCP was also incubated. After 12 h, formic acid (5 μL) was added to each solution, and both were centrifuged in a 0.5 mL 10 kDa MWCO centrifuge tube at 13400 x *g* for 20 min or until most of the solution had passed through. Triplicate deproteinated reaction mixtures from incubation of Asp-AT with FCP, or the control, were analyzed by HPLC-ESI-MS. Ten μL of each mixture was injected on a Phenomenex Luna C18(2) column, 2.1 x 150 mm, and analyzed by a linear gradient at 200 μL/min from 10% buffer B to 90% buffer B over 15 minutes, where buffer A was water with 0.1% formic acid and buffer B was acetonitrile with 0.1% formic acid. Eluent from the LC was split 1:4 so that 20% of the eluent (40 μL/min) flowed directly into a Thermo Ion Max ESI source connected to a Thermo Q-Exactive. Data was collected in negative ion mode through a data-dependent top five method where the first duty cycle scan was a global scan from 100 to 1000 Th, followed by MS^2 fragmentation of the five most abundant ions with the higher energy collisional dissociation cell set to a normalized collision energy of 45 arbitrary units. Extracted ion chromatograms for ions of interest were generated and integrated for total peak area. Peak areas from triplicate samples were averaged and error bars were generated based on standard deviation.

CONCLUSION

Structural and biochemical characterization of AidC

Quorum-quenching enzymes are important biochemical tools for probing quorum-sensing pathways in bacteria. They also hold considerable promise as reagents to prevent marine and membrane biofouling, as treatments to prevent costly infections of plants and animals, and as tools to manipulate interactions between microbes[7]. However, the mechanism these enzymes use to recognize and process substrates is not well characterized. An understanding of their selectivity and catalytic mechanism would enable the production of enzymes that can recognize specific quorum-sensing signals to serve as more precise biochemical probes, and as a more promising catalysts for other applications. Several research papers report the characterization of a quorum quenching AHL lactonase from *Bacillus sp*., AiiA, and a general mechanism has been proposed for its catalytic mechanism[13,15,]. AiiA has K_M values in the mM range and displays broad substrate specificity. The research conducted and detailed in the first part of this dissertation has provided information about the catalytic mechanism and selectivity of the quorum-quenching AHL lactonase from the potato root-associated *Chryseobacterium* sp. strain StRB126, AidC.

Steady state enzyme kinetics show AidC has an unusually low K_M value for AHL substrates and displays a stricter substrate selectivity than any other related AHL lactonase characterized to date. To our knowledge, AidC also has the highest reported k_{cat}/K_M value for any characterized wild-type quorum-quenching enzyme, regardless of superfamily. Structural determination of AidC alone, and with bound product, reveals an unusual 'kinked' helix and suggests a structural-

basis for the enhanced selectivity. Intriguingly, AidC shows some structural similarities that more closely match families more distant from AHL lactonases, sharing a dimeric structure similar to an organic phosphotriesterase and an active-site histidine residue similar to that found in related phosphodiesterases. AidC serves as an example for understanding how quorum-quenching enzymes can achieve selectivity between structurally similar AHL substrates, and may serve as an efficient catalytic template amenable to further optimization for a broad array of quorum-quenching applications.

To further probe the catalytic mechanism of AidC, mutation studies can be carried out based on the information reported in this dissertation. The active-site histidine residue in AidC has been proposed to be important for catalysis. The role of histidine can be confirmed by characterizing the histidine to alanine and histidine to tyrosine mutants. A mutation at the proline 203 residue, which creates a 'kink' in one of the alpha helices that surrounds the substrate binding pocket, could provide information about substrate specificity. Further, X-ray crystallography studies using either the wild-type enzyme or newly generated AidC variants, with substrate analogs and transition state mimetics can be used to gain structural insight into the mechanism of AidC.

Selective targeting by a mechanism-based inactivator against PLP-dependent aminotransferases

Ornithine aminotransferase (OAT) and γ-aminobutyric acid aminotransferase (GABA-AT) belong to the same evolutionary subgroup and share similar structural functional and mechanistic features[23]. Therefore, many molecules that bind GABA-AT are also known to bind OAT. Unlike GABA-AT, OAT has only recently been identified as a drug-target and consequently there are only a limited number of therapeutically viable molecules that target OAT. Previous research

efforts have shown that potent mechanism-based inactivators can be rationally designed against these PLP-dependent drugs-targets. However, one the remaining challenges is the lack of selectivity towards other PLP-dependent off-target enzymes like Aspartate aminotransferase (Asp-AT). The second part of this dissertation has provided information on the selectivity of a mechanism-based inactivator–FCP. The results show that FCP inactivates the two drug-targets OAT and GABA-AT via an enamine mechanism, but is an alternative substrate for an apparent PLP-dependent off-target, Asp-AT.

Structural determination revealed a ternary adduct at the active site formed between OAT, FCP and PLP. This data led to the conclusion that OAT is inactivated via an enamine mechanism, similar to the mechanism previously reported for the inactivation of GABA-AT by FCP. Kinetic assays show FCP does not inactivate or inhibit Asp-AT. Structural studies of Asp-AT in complex with FCP and, in the presence and absence of α-ketoglutarate suggested FCP is an alternate substrate for Asp-AT. A model has been proposed, where FCP turnover is partitioned between two separate pathways. High-resolution mass spectrometry studies support both pathways. Therefore, we conclude both pathways occur concurrently.

The proposed mechanisms of inactivation and alternative turnover in all three enzymes are complex, and all contain multiple reaction pathways. Although FCP is still too toxic to become a drug[89,77] itself, it displays a desirable selectivity in the context of drug development as a mechanism-based inactivator. The reason for this desirable selectivity is due to the subtle differences in the shapes of the active site cavities for retaining an intermediate, as well as the availability of a water molecule for a proposed hydrolysis in a complex mechanism with multiple reaction pathways. In general, the reactive intermediates generated during the complex reactions of these mechanism-based inactivators in active sites could be capable of displaying desirable

specificity of inactivation discerning drug targets and off-targets, even with similar structures and reaction mechanisms.

Most of the effort to design mechanism-based inactivators has focused on GABA-AT purified from pig brain. To our knowledge, active GABA-AT cannot be expressed and purified via recombinant methods. However, OAT has be grown and expressed in *E. coli* cells. Future studies could involve mutations in active site residues in OAT. These variants of OAT can provide information about selectivity and reaction mechanisms. This information can be used to design mechanism-based inactivators that are specific for one drug-target.

REFERENCES

1) Walters, C. M., and Bassler, B. L. (2005) Quorum Sensing :Cell-to-Cell Communication in Bacteria. *Annu Rev Cell Dev Biol 21*, 319–46.

(2) Rutherford, S., and Bassler, B. L. (2012) Bacterial Quorum Sensing: Its Role in Virulence and Possibilities for Its Control. *Cold Spring Harb Perspect Med 2*, 11.

(3) Nealson, K., and Hastings, J. (1979) Bacterial bioluminescence: its control and ecological significance. *Microbiol Rev 43*, 145–154.

(4) Engebrecht, J., and Silverman, M. (1983) Bacterial bioluminescence: isolation and genetic analysis of functions from Vibrio fischeri. *Cell 32*, 773–781.

(5) Manefield, M., and Turner, S. . (2002) Quorum sensing in context: out of molecular biology and into microbial ecology. *Microbiology 148*, 3762–64.

(6) Dong, Y., and Zhang, L. (2005) Quorum sensing and quorum-quenching enzymes. *J Microbiol 43*, 101–109.

(7) Hong, K. W., Koh, C. L., Sam, C. K., Yin, W. F., and Chan, K. G. (2012) Quorum quenching revisited--from signal decays to signaling confusion. *Sensors 12*, 4661–96.

(8) Dong, Y., Wang, L., Xu, J., and Zhang, L. . (2001) Quenching quorum-sensing-dependent bacterial infection by an N-acyl homoserine lactonase. *Nature 411*, 813–817.

(9) Dong, Y., and Zhang, L.(2000) AiiA, an enzyme that inactivates the acylhomoserine lactone quorum-sensing signal and attenuates the virulence of Erwinia carotovora. *Proc Natl Acad Sci 97*, 3526–3531.

(10) Lin, Y., and Zhang, L. (2003) Acyl-homoserine lactone acylase from Ralstonia strain XJ12B represents a novel and potent class of quorum-quenching enzymes. *Mol Microbiol 47*, 849–860.

(11) Wang, L. H.; Weng, L. X.; Dong, Y. H.; Zhang, L. H. (2004) Specificity and enzyme kinetics of the quorum-quenching N-Acyl homoserine lactone lactonase (AHL-lactonase). *J Biol Chem 279*, 13645–51.

(12) Thomas, P., and Fast, W. (2005) The quorum-quenching lactonase from Bacillus

thuringiensis is a metalloprotein. *Biochemistry 45*, 13385–93.

(13) Liu, D., Lepore, B. W., Petsko, G. A., Thomas, P. W., Stone, E. M., Fast, W., and Ringe, D. (2005) Three-dimensional structure of the quorum-quenching N-acyl homoserine lactone hydrolase from Bacillus thuringiensis. *Proc Natl Acad Sci U S A 102*, 11882–7.

(14) Liu, D., Momb, J., Thomas, P. W., Moulin, A., Petsko, G. A., Fast, W., and Ringe, D. (2008) Mechanism of the quorum-quenching lactonase (AiiA) from Bacillus thuringiensis. 1. Product-bound structures. *Biochemistry 47*, 7706–7714.

(15) Momb, J., Wang, C., Liu, D., Thomas, P. W., Petsko, G. A., Guo, H., Ringe, D., and Fast, W. (2008) Mechanism of the quorum-quenching lactonase (AiiA) from Bacillus thuringiensis. 2. Substrate modeling and active site mutations. *Biochemistry 47*, 7715–7725.

(16) Liu, C. F., Liu, D., Momb, J., Thomas, P. W., Lajoie, A., Petsko, G. A., Fast, W., and Ringe, D. (2013) A phenylalanine clamp controls substrate specificity in the quorum-quenching metallo-γ-lactonase from Bacillus thuringiensis. *Biochemistry 52*, 1603–10.

(17) Kim, M., and et al. (2005) The molecular structure and catalytic mechanism of a quorum-quenching N-acyl-L-homoserine lactone lactonase. *Proc Natl Acad Sci 102*, 17606–11.

(18) Momb, J., Thomas, P. W., and Fast, W. (2006) The quorum-quenching metallo-gamma-lactonase from Bacillus thuringiensis exhibits a leaving group thio effect. *Biochemistry 45*, 13385–93.

(19) Wang, W. Z., Morohoshi, T., Someya, N., and Ikeda, T. (2012) AidC, novel N-acylhomoserine lactonase from the potato root-associated Cytophaga-Favobacteria-Bacteriodes(CFB) group bacterium, Chryseobacterium sp. StRB126. *Appl Environ Microbiol 78*, 7985–7992.

(20) Eliot, A. C., and Kirsch, J. F. (2004) PYRIDOXAL PHOSPHATE ENZYMES : Mechanistic, Structural and Evolutionary Considerations. *Annu Rev Biochem 73*, 383–415.

(21) Jansonius, J.(1998) Evolutionary relationships among pyridoxal- 5'-phosphate-dependent enzymes. Regio-specific alpha, beta and gamma families. *Curr Opin Struct Biol 8*, 759–769.

(22) Jeremiah, S., and Povey, S. (1981) The biochemical genetics of human gama-aminobutyric acid transaminase. *Ann Hum Genet 45*, 231–236.

(23) Lee, H., Juncosa, J. I., and Silverman, R. B. (2015) Ornithine Aminotransferase versus GABA Aminotransferase: Implications for the Design of New Anticancer Drugs. *Med Res Rev 35*, 286–305.

(24) Herzfeld, A., and Knox, W. E. (1968) The Properties, Developmental Formation, and Estrogen Induction of Ornithine Aminotransferase and Estrogen in Rat Tissues. *J Biol Chem*

243, 3327–3332.

(25) Miyasaka, Y., Enomoto, N., Nagayama, K., Izumi, N., Marumo, F., Watanabe, M., and Sato, C. (2001) Analysis of differentially expressed genes in human hepatocellular carcinoma using suppression subtractive hybridization. *Br J Cancer 85*, 228–234.

(26) Zigmond, E., Ya'acov, A. Ben, Lee, H., Lichtenstein, Y., Shalev, Z., Smith, Y., Zolotarov, L., Ziv, E., Kalman, R., Le, H. V., Lu, H., Silverman, R. B., and Ilan, Y. (2015) Suppression of Hepatocellular Carcinoma by Inhibition of Overexpressed Ornithine Aminotransferase. *ACS Med Chem Lett 6*, 840–844.

(27) Seiler, N. (1997) Ornithine Aminotransferase as a Therapeutic Target in Hyperammonemias, in *Advances in Experimental Medicine and Biology*, pp 113–142.

(28) Kirsch, J. F., Eichel, G., Ford, G., Vincrnt, G., and Jansonius, J. (1984) Mechanism of Action of Aspartate Aminotransferase Proposed on the Basis of its Spatial Structure. *J Mol Biol 174*, 497–525.

(29) Goldberg, J. M., and Kirsch, J. F. (1996) The Reaction Catalyzed by Escherichia coli Aspartate Aminotransferase Has Multiple Partially Rate-Determining Steps, While That Catalyzed by the Y225F Mutant Is Dominated by Ketimine Hydrolysis. *Biochemistry 35*, 5280–5291.

(30) Hayashi, H., Mizuguchi, H., Miyahara, I., Nakajima, Y., Hirotsu, K., and Kagamiyama, H. (2002) Conformational Change in Aspartate Aminotransferase on Substrate Binding Induces Strain in the Catalytic Group and Enhances Catalysis. *J Biol Chem 278*, 9481–9488.

(31) Storici, P., Capitani, G., Biase, D. De, Moser, M., John, R. A., Jansonius, J. N., and Schirmer, T. (1999) Crystal Structure of GABA-Aminotransferase, a Target for Antiepileptic Drug Therapy. *Biochemistry 38*, 8628–8634.

(32) Shen, B. W., Hennig, M., Hohenester, E., Jansonius, J. N., and Schirmer, T. (1998) Crystal Structure of Human Recombinant Ornithine Aminotransferase. *J Mol Biol 277*, 81–102.

(33) Mehta, P. K., Hale, T. I., and Christen, P. (1993) Aminotransferases: demonstration of homology and division into evolutionary subgroups. *Eur J Biochem 214*, 549–561.

(34) Denesyuk, A. ., Denessiouk, K. ., Korpela, T., and Johnson, M. . (2002) Functional attributes of the phosphate group binding cup of pyridoxal phosphate-dependent enzymes. *J Mol Biol 316*, 155–72.

(35) Silverman, R. B. (1995) Mechanism-based enzyme inactivation, in *Methods in Enzymology*, pp 240–283.

(36) Storici, P., Qiu, J., Schirmer, T., and Silverman, R. B. (2004) Mechanistic Crystallography .

Mechanism of Inactivation of γ -Aminobutyric Acid Aminotransferase by (1 R , 3 S , 4 S) -3-Amino-4-fluorocyclopentane-1-carboxylic Acid As Elucidated by Crystallography †. *Biochemistry 43*, 14057–14063.

(37) Schuster, M., Sexton, D. J., Diggle, S. P., and Greenberg, E. P. (2013) Acyl-Homoserine Lactone Quorum Sensing: From Evolution to Application. *Annu Rev Microbiol 67*, 43–63.

(38) Tay, S. ., and Yew, W. . (2013) Development of quorum-based anti-virulence therapeutics targeting Gram-negative bacterial pathogens. *Int J Mol Sci 14*, 16570–16599.

(39) Amara, N., Krom, B. P., Kaufmann, G. F., and Meijler, M. M. (2011) Macromolecular inhibition of quorum sensing: enzymes, antibodies, and beyond. *Chem Rev 111*, 195–208.

(40) Kalia, V. C., and Purohit, H. J. (2011) Quenching the quorum sensing system: potential antibacterial drug targets,. *Crit Rev Microbiol 37*, 121–140.

(41) Romero, M., Acuna, L., and Otero, A. (2012) Patents on quorum quenching: interfering with bacterial communication as a strategy to fight infections. *Recent Pat Biotechnol 6*, 2–12.

(42) Zhu, J., and Kaufmann, G. F. (2103) Quo vadis quorum quenching? *Curr Opin Pharmacol 13*, 688–698.

(43) Fast, W., and Tipton, P. A. (2012) The enzymes of bacterial census and censorship. *Trends Biochem Sci 37*, 7–14.

(44) Pearson, W. R. (1990) Rapid and sensitive sequence comparison with FASTP and FASTA. *Methods Enzym 183*, 63–98.

(45) Carlier, A., Uroz, S., Smadja, B., Fray, R., Latour, X., Dessaux, Y., and Faure, D. (2003) The Ti plasmid of Agrobacterium tumefaciens harbors an attM-paralogous gene, aiiB, also encoding N-Acyl homoserine lactonase activity. *Appl Env Microbiol 69*, 4989–4993.

(46) Liu, D., Thomas, P. W., Momb, J., Hoang, Q. Q., Petsko, G. A., Ringe, D., and Fast, W. (2007) Structure and specificity of a quorum-quenching lactonase (AiiB) from Agrobacterium tumefaciens. *Biochemistry 46*, 11789–11799.

(47) Tang, K., Su, Y., Brackman, G., Cui, F., Zhang, Y., Shi, X., Coenye, T., and Zhang, X. H. (2015) MomL, a novel marine-derived N-acyl homoserine lactonase from Muricauda olearia. *Appl Env Microbiol 81*, 774–782.

(48) Thomas, P. W., and Fast, W. (2011) Heterologous overexpression, purification, and in vitro characterization of AHL lactonases. *Methods Mol Biol 692*, 275–290.

(49) Eisenthal, R., Danson, M. J., and Hough, D. W. (2007) Catalytic efficiency and kcat/KM: a useful comparator? *Trends Biotechnol 25*, 247–249.

(50) Ahlgren, N. A., Harwood, C. S., Schaefer, A. L., Giraud, E., and Greenberg, E. P. (2011) Aryl-homoserine lactone quorum sensing in stem-nodulating photosynthetic bradyrhizobia. *Proc Natl Acad Sci USA 108*, 7183–7188.

(51) Murzin, A. G., Brenner, S. E., Hubbard, T., and Chothia, C. (1995) SCOP: a structural classification of proteins database for the investigation of sequences and structures. *J Mol Biol 247*, 536–540.

(52) Kim, M. K., and Kang, Y. K. (1999) Positional preference of proline in alpha-helices. *Protein Sci 8*, 1492–1499.

(53) Barlow, D. J., and Thornton, J. M. (1988) Helix geometry in proteins. *J Mol Biol 201*, 601–619.

(54) Woolfson, D. N., and Williams, D. H. (1990) The influence of proline residues on alpha-helical structure. *Febs Lett 277*, 185–188.

(55) Krissinel, E., and Henrick, K. (2007) Inference of macromolecular assemblies from crystalline state. *J Mol Biol 372*, 774–797.

(56) Gotthard, G., Hiblot, J., Gonzalez, D., Elias, M., and Chabriere, E. (2013) Structural and enzymatic characterization of the phosphotriesterase OPHC2 from Pseudomonas pseudoalcaligenes. *PLoS One 8*, e77995.

(57) Holm, L., and Rosenstrom, P. (2010) Dali server: conservation mapping in 3D. *Nucleic Acids Res 38*, W545-549.

(58) Crowder, M. W., Spencer, J., and Vila, A. J. (2006) Metallo-beta-lactamases: novel weaponry for antibiotic resistance in bacteria. *Acc Chem Res 39*, 721–728.

(59) Burgi, H. B., and Dunitz, J. D. (1983) From Crystal Statics to Chemical Dynamics. *Acc Chem Res 16*, 153–161.

(60) Minagawa, A., Takaku, H., Ishii, R., Takagi, M., Yokoyama, S., and Nashimoto, M. (2006) Identification by Mn2+ rescue of two residues essential for the proton transfer of tRNase Z catalysis. *Nucleic Acids Res 34*, 3811–3818.

(61) Li de la Sierra-Gallay, I., Pellegrini, O., and Condon, C. (2005) Structural basis for substrate binding, cleavage and allostery in the tRNA maturase RNase Z. *Nature 433*, 657–661.

(62) Clevenger, K. D., Wu, R., Liu, D., and Fast, W. (2014) n-Alkylboronic acid inhibitors reveal determinants of ligand specificity in the quorum-quenching and siderophore biosynthetic enzyme PvdQ. *Biochemistry 53*, 6679–6686.

(63) Von Bodman, S. B., Bauer, W. D., and Coplin, D. L. (2003) Quorum sensing in plant-

pathogenic bacteria. *Annu Rev Phytopathol 41*, 455–482.

(64) Park, S. J., Park, S. Y., Ryu, C. M., Park, S. H., and Lee, J. K. (2008) AiiA, a quorum-quenching enzyme from Bacillus thuringiensis, on the rhizosphere competence. *J Microbiol Biotechnol 18*, 1518–1521.

(65) Afriat, L., Roodveldt, C., Manco, G., and Tawfik, D. S. (2006) The latent promiscuity of newly identified microbial lactonases is linked to a recently diverged phosphotriesterase. *Biochemistry 45*, 13677–13686.

(66) Bar-Rogovsky, H., Hugenmatter, A., and Tawfik, D. S. (2013) The evolutionary origins of detoxifying enzymes: the mammalian serum paraoxonases (PONs) relate to bacterial homoserine lactonases. *J Biol Chem 288*, 23914–23927.

(67) Elias, M., and Tawfik, D. S. (2012) Divergence and convergence in enzyme evolution: parallel evolution of paraoxonases from quorum-quenching lactonases. *J Biol Chem 287*, 11–20.

(68) Thomas, P. W., Zheng, M., Wu, S., Guo, H., Liu, D., Xu, D., and Fast, W. (2011) Characterization of purified New Delhi metallo-beta-lactamase-1. *Biochemistry 50*, 10102–10113.

(69) Battye, T., Kontogiannis, L., Johnson, O., Powell, H. ., and AG., L. (2011) iMOSFLM: a new graphical interface for diffraction-image processing with MOSFLM. *Acta Crystallogr D Biol Crystallogr 67*, 27–81.

(70) Collaborative Computational Project, N. The CCP4 suite: programs for protein crystallography. *Acta Crystallogr D 50 50*, 760–3.

(71) P. D. Adams, P. V. Afonine, G. Bunkóczi, V. B. Chen, I. W. Davis, N. Echols, J. J. Headd, L.-W. Hung, G. J. Kapral, R. W. Grosse-Kunstleve, A. J. McCoy, N. W. Moriarty, R. Oeffner, R. J. Read, D. C. Richardson, J. S. Richardson, T. C. T. and P. H. Z. (2010) PHENIX: a comprehensive Python-based system for macromolecular structure solution. *Acta Cryst D66*, 213–221.

(72) P Emsley, B Lohkamp, W Scott, and K. C. (2010) Features and Development of Coot. *Acta Crystallogr D66*, 486–501.

(73) Huang, C.C., Couch, G.S., Pettersen, E.F., and Ferrin, T. E. (2004) UCSF Chimera: A visulization system for exploratory analysis and reseach. *J Comput Chem 25*, 1605–1612.

(74) Karmen, B. A., Wroblewski, F., and Ladue, J. S. (1955) Transaminase activity in Human blood. *J Clin Invest 34*, 126–133.

(75) Mckenna, M. C., Stevenson, J. H., Huang, X., and Hopkins, I. B. (2000) Differential distribution of the enzymes glutamate dehydrogenase and aspartate aminotransferase in cortical

synaptic mitochondria contributes to metabolic compartmentation in cortical synaptic terminals. *Neurochem Int 37*, 229–241.

(76) Watanabe, M., Maemura, K., Kanbara, K., Tamayama, T., and Hayasaki, H. (2002) GABA and GABA Receptors in the Central Nervous System and Other Organs, in *International Review of Cytology*, pp 1–47.

(77) Storici, P., Qiu, J., Schirmer, T., and Silverman, R. B. (2004) Mechanistic Crystallography. Mechanism of Inactivation of γ-Aminobutyric Acid Aminotransferase by (1R,3S,4S)-3-Amino-4-fluorocyclopentane-1-carboxylic Acid As Elucidated by Crystallography. *Biochemistry 43*, 14057–14063.

(78) Liu, D., Pozharski, E., Lepore, B. W., Fu, M., Silverman, R. B., Petsko, G. a., and Ringe, D. (2007) Inactivation of Escherichia coli L-aspartate aminotransferase by (S)-4-amino-4,5-dihydro-2-thiophenecarboxylic acid reveals "A tale of two mechanisms." *Biochemistry 46*, 10517–10527.

(79) Liu, D., Pozharski, E., Fu, M., Silverman, R. B., and Ringe, D. (2010) Mechanism of inactivation of escherichia coli aspartate aminotransferase by (S)-4-amino-4,5-dihydro-2-furancarboxylic acid. *Biochemistry 49*, 10507–10515.

(80) Smith, D. L., Almo, J. S. C., Toney, M. D., and Ringe, D. (1989) 2.8-A-Resolution Crystal Structure of an Active-Site Mutant of Aspartate Aminotransferase from Escherichia coli. *Biochemistry 28*, 8161–8167.

(81) Metzler, D.E., Christen, P. (1985) Transaminases, pp 133–134.

(82) Burgie, E. S., Thoden, J. B., and Holden, H. M. (2007) Molecular architecture of DesV from Streptomyces venezuelae: a PLP-dependent transaminase involved in the biosynthesis of the unusual sugar desosamine. *Protein Sci 16*, 887–896.

(83) Cook, P. D., and Holden, H. M. (2007) A structural study of GDP-4-keto-6-deoxy-D-mannose-3-dehydratase: Caught in the act of geminal diamine formation. *Biochemistry 46*, 14215–14224.

(84) Cook, P. D., Thoden, J. B., and Holden, H. M. (2006) The structure of GDP-4-keto-6-deoxy- D -mannose-3- dehydratase : A unique coenzyme B 6 -dependent enzyme. *Protein Sci 15*, 2093–2106.

(85) Schneider, G., Käck, H., and Lindqvist, Y. (2000) The manifold of vitamin B6 dependent enzymes. *Structure 8*, R1–R6.

(86) Grishin, N. V., Phillips, M. A., and Goldsmith, E. J. (1995) Modeling of the spatial structure of eukaryotic ornithine decarboxylases. *Protein Sci 4*, 1291–1304.

(87) Schiroli, D., and Peracchi, A. (2015) A subfamily of PLP-dependent enzymes specialized in handling terminal amines. *Biochim Biophys Acta 1854*, 1200–1211.

(88) Storici, P., Capitani, G., Müller, R., Schirmer, T., and Jansonius, J. N. (1999) Crystal structure of Human Ornithine Aminotransferase Complexed with the Highly Specific and Potent Inhibitor 5-Fluoromethylornithine. *J Mol Biol 285*, 297–309.

(89) Mitchell, G. A., Brody, L. C., Looney, J., Steel, G., Suchanek, M., Dowling, C., Der Kaloustian, V., Kaiser-Kupfer, M., and Valle, D. (1988) An Initiator Codon Mutation in Ornithine-5-Aminotransferase Causing Gyrate Atrophy of the Choroid and Retina. *J Clin Invest 81*, 630–633.

(90) Fast, W. (2009) Quorum-quenching N-acyl-homoserine lactonase, in *Springer Handbook of Enzymes* (Chang, A., Ed.), pp 23–38. Springer Berlin Heidelberg, Berlin, Heidelberg.

(91) Onuffer, J. J., and Kirsch, J. F. (1995) Redesign of the substrate specificity of Escherichia coli aspartate aminotransferase to that of Escherichia coli tyrosine aminotransferase by homology modeling and site-directed mutagenesis. *Protein Sci 4*, 1750–1757.

(92) Z. Otwinowski and W. Minor. (1997) " Processing of X-ray Diffraction Data Collected in Oscillation Mode ." *Methods Enzymol 276*, 307–326.

VITA

Romila N. Mascarenhas was born and raised in Bangalore, India. She received her Bachelor of Science in Biotechnology, Chemistry and Botany from Mount Carmel College, Bangalore University in 2009. She received her Master of Science in Chemistry from St. Joseph's College of Arts and Science, Bangalore University in 2011. In 2012, she began the PhD program in Chemistry and Biochemistry at Loyola University Chicago.